JYU DISSERTATIONS 89

Petri Kiuru

Modeling CO_2 Emissions from Boreal Lakes in Present and Future

UNIVERSITY OF JYVÄSKYLÄ
FACULTY OF MATHEMATICS
AND SCIENCE

JYU DISSERTATIONS 89

Petri Kiuru

Modeling CO_2 Emissions from Boreal Lakes in Present and Future

Esitetään Jyväskylän yliopiston matemaattis-luonnontieteellisen tiedekunnan suostumuksella
julkisesti tarkastettavaksi yliopiston Ambiotica-rakennuksen luentosalissa YAA303
kesäkuun 19. päivänä 2019 kello 12.

Academic dissertation to be publicly discussed, by permission of
the Faculty of Mathematics and Science of the University of Jyväskylä,
in building Ambiotica, hall YAA303, on June 19, 2019 at 12 o'clock noon.

JYVÄSKYLÄN YLIOPISTO
UNIVERSITY OF JYVÄSKYLÄ

JYVÄSKYLÄ 2019

Editors
Markku Kataja
Department of Physics, University of Jyväskylä
Ville Korkiakangas
Open Science Centre, University of Jyväskylä

Permanent link to this publication: http://urn.fi/URN:ISBN:978-951-39-7777-1

ISBN 978-951-39-7777-1 (PDF)
URN:ISBN:978-951-39-7777-1
ISSN 2489-9003

Abstract

Kiuru, Petri
Modeling CO_2 emissions from boreal lakes in present and future
Jyväskylä, University of Jyväskylä, 2019, 151 p.
(JYU Dissertations
ISSN 2489-9003; 89;)
ISBN 978-951-39-7777-1 (PDF)
Diss.

In this work, carbon dioxide (CO_2) dynamics in boreal lakes were studied using vertical process-based coupled physical-biogeochemical lake models. Many lakes in the boreal zone are at present supersaturated with the greenhouse gas CO_2 and emit it to the atmosphere. Transport of terrestrially produced organic carbon to boreal lakes and its in-lake degradation is predicted to increase under the ongoing climate change, and lakes may be even greater CO_2 sources to the atmosphere in the future.

Two process-based models of different complexity were developed for the simulation of carbon cycling in lakes. The models are based on a one-dimensional vertical lake model called MyLake, which simulates lake thermal conditions and phosphorus-phytoplankton dynamics. The applications of each model to humic boreal lakes were calibrated and validated with comprehensive measurements of water column CO_2 concentration. The performance of the simpler model was found to be inadequate, partially because of the unusual behavior of the phytoplankton community in the study lake, but the output of the more advanced model agreed well with measurements. Further, the applicability of different parameterizations for the gas exchange velocity for CO_2 incorporated into the more advanced model was assessed. None of the applied parameterizations resulted in an improved lake model performance regarding water column CO_2 concentration or air-water CO_2 flux. The use of more sophisticated and possibly more correct gas exchange models, on the contrary, led to difficulties in obtaining sufficient gain of CO_2 in the water column.

Impacts of warmer air temperature and climate-induced changes in stream inflow on CO_2 dynamics in a boreal lake between the periods 1980–2009 and 2070–2099 were assessed using projections for air temperature from recent-generation global climate models with different radiative forcing scenarios and literature estimates for changes in seasonal stream inflow volume. Also, the effects of additional increases in the inflow concentrations of CO_2 and dissolved organic carbon (DOC) were compared. The results imply that CO_2 concentrations in boreal lakes will be elevated in future climate and, in consequence, the release of CO_2 to the atmosphere will further increase.

Keywords: lakes, gas exchange, carbon dioxide, modelling, biogeochemistry, carbon cycling, climate change

Tiivistelmä

Kiuru, Petri
Pohjoisen havumetsävyöhykkeen järvien nykyisten ja tulevaisuuden CO_2-päästöjen mallintaminen

Työssä tutkittiin pohjoisella havumetsävyöhykkeellä sijaitsevien eli boreaalisten järvien hiilidioksididynamiikkaa vertikaalisten prosessipohjaisten mallien avulla. Monet boreaalisen vyöhykkeen järvet ovat ylikyllästyneitä kasvihuonekaasu hiilidioksidin (CO_2) suhteen ja päästävät sitä ilmakehään. On ennustettu, että meneillään olevan ilmastonmuutoksen vaikutuksesta järviin kulkeutuu yhä enemmän maaekosysteemeissä syntynyttä orgaanista hiiltä ja että sitä myös hajoaa järvissä nykyistä enemmän. Tämän johdosta järvet voivat olla tulevaisuudessa yhä merkittävämpiä ilmakehän CO_2-lähteitä.

Työssä kehitettiin kaksi rakenteeltaan erilaista prosessipohjaista mallia, joilla voidaan simuloida järvien hiilenkiertoa. Mallit pohjautuvat yksiulotteiseen, vertikaaliseen MyLake-järvimalliin, joka simuloi järven lämpöoloja ja fosfori-kasviplanktondynamiikkaa. Humuspitoisille boreaalisille järville tehdyt mallisovellukset kalibroitiin ja niiden toimintakykyä arvioitiin järvien kattavien CO_2-pitoisuusmittausten avulla. Rakenteeltaan yksinkertaisemman mallin suorituskyky oli vaillinainen, mikä johtui osin tutkimusjärven kasviplanktonyhteisön epätavallisesta käyttäytymisestä, mutta kehittyneemmän mallin tulokset vastasivat mittauksia melko hyvin. Työssä selvitettiin myös, kuinka erilaiset CO_2:n kaasunsiirtokertoimelle kehitetyt mallit soveltuvat liitettäväksi kehittyneempään järvimalliin. Mikään näistä malleista ei tuottanut muita selvästi parempia järvimallin tuloksia veden CO_2-pitoisuuden eikä veden ja ilman välisen CO_2-vuon suhteen. Kehittyneempien, mahdollisesti täsmällisempien kaasunsiirtomallien käyttö sitä vastoin jopa huononsi tuloksia, sillä mallinnettu veden CO_2-pitoisuus jäi liian pieneksi.

Työssä arvioitiin myös, kuinka ilman lämpötilan kasvu ja ilmaston aiheuttamat tulovirtaaman muutokset kausien 1980–2009 ja 2070–2099 välillä vaikuttavat boreaalisen järven CO_2-dynamiikkaan. Arviossa hyödynnettiin tuoreimpia globaalien ilmastomallien lämpötilaennusteita eri säteilypakoteskenaarioilla sekä kirjallisuusarvioita tulovirtaaman vuodenaikaismuutoksista. Lisäksi verrattiin CO_2:n ja liuenneen orgaanisen hiilen tulovirtaamapitoisuuden kasvun vaikutuksia. Tulosten mukaan boreaalisen vyöhykkeen järvien hiilidioksidipitoisuus kasvaa ja hiilidioksidia vapautuu ilmakehään yhä enemmän tulevaisuuden ilmasto-oloissa.

Asiasanat: järvet, kaasunvaihto, hiilidioksidi, mallinnus, biogeokemia, hiilenkierto, ilmastonmuutos

Author

Petri Kiuru
Finnish Environment Institute
Jyväskylä
Finland

Department of Physics
University of Jyväskylä
Finland

Supervisors

Prof. Markku Kataja
Department of Physics
University of Jyväskylä
Finland

Dr. Timo Huttula
Finnish Environment Institute
Jyväskylä
Finland

Dr. Anne Ojala
Faculty of Biological and Environmental Sciences
University of Helsinki
Finland

Reviewers

Dr. Tom Jilbert
Faculty of Biological and Environmental Sciences
University of Helsinki
Finland

Dr. Dominic Vachon
Department of Ecology and Environmental Sciences
Umeå University
Sweden

Opponent

Prof. Anna Rutgersson
Department of Earth Sciences
Uppsala University
Sweden

Preface

The work reported in this thesis has been carried out at the Freshwater Centre of the Finnish Environment Institute during the years 2011–2019. Financial support from the Kone Foundation and Maa- ja vesitekniikan tuki ry. is gratefully acknowledged.

First of all, I would like to express my warmest gratitude to my supervisors Professor Markku Kataja, Dr. Anne Ojala, and Professor Timo Huttula for guidance throughout the work. I also gratefully acknowledge the reviewers, Dr. Tom Jilbert and Dr. Dominic Vachon, for their assessment of the thesis.

I am grateful to Professor Timo Vesala and Dr. Ivan Mammarella from the University of Helsinki and Dr. Jouni Heiskanen from ICOS ERIC for cooperation and also for their constructive comments and criticism. I also would like to thank my Heads of Unit, Dr. Olli Malve and Dr. Marko Järvinen, and my co-workers during the years at SYKE in Jyväskylä for support and encouragement.

Special thanks go to my general upper secondary school science teacher Pekka Naumanen for giving me the impulse to study physics. Finally, I wish to thank my parents for their support.

Jyväskylä, May 2019

Petri Kiuru

Related publications

The thesis is partly based on publication I (Chapter 8 and parts of Chapters 4, 5, and 6). The author has also contributed to the publications II and III.

I *Effects of climate change on CO_2 concentration and efflux in a humic boreal lake: A modeling study*
P. Kiuru, A. Ojala, I. Mammarella, J. Heiskanen, M. Kämäräinen, T. Vesala, and T. Huttula
Journal of Geophysical Research: Biogeosciences, 123(7), 2212–2233 (2018).

II *Oxygen dynamics in a boreal lake responds to long-term changes in climate, ice phenology, and DOC inputs*
R.-M. Couture, H. A. de Wit, K. Tominaga, P. Kiuru, and I. Markelov
Journal of Geophysical Research: Biogeosciences, 120(11), 2441–2456 (2015).

III *Effects of changing climate on the hydrology of a boreal catchment and lake DOC—Probabilistic assessment of a dynamic model chain*
M. Holmberg, M. N. Futter, N. Kotamäki, S. Fronzek, M. Forsius, P. Kiuru, N. Pirttioja, K. Rasmus, M. Starr, and J. Vuorenmaa
Boreal Environment Research, 19(suppl.A), 66–82 (2014).

List of symbols

a	Empirical constant [dimensionless]
a_{ice}	Diffusion factor for dissolved gases [dimensionless]
a_{k}	Turbulent diffusion parameter [dimensionless]
$a_{\mathrm{k,ice}}$	Turbulent diffusion parameter under ice-covered conditions [dimensionless]
a_{OD}	Temperature adjustment factor for oxygen demand at $T < 4\,^{\circ}\mathrm{C}$ [dimensionless]
A	Area of the top of a model grid layer [m^2]
A_{s}	Surface area of the lake [m^2]
A_{WS}	Area of the water-sediment interface [m^2]
b	Empirical constant [dimensionless]
c	Empirical constant [dimensionless]
$c_{p\mathrm{a}}$	Specific heat capacity of air at constant pressure [$\mathrm{J/(kg\,K)}$]
$c_{p\mathrm{w}}$	Specific heat capacity of water at constant pressure [$\mathrm{J/(kg\,K)}$]
C_1	Empirical constant [dimensionless]
C_2	Empirical constant [dimensionless]
C_{d}	Drag coefficient [dimensionless]
C_{DI}	Dissolved inorganic carbon (DIC) concentration [$\mathrm{mg/m^3}$]
$C_{\mathrm{DI,IN}}$	DIC inflow concentration scaling factor [dimensionless]
C_{DO}	Dissolved organic carbon (DOC) concentration [$\mathrm{mg/m^3}$]
C_{eq}	Atmospheric equilibrium concentration of a dissolved gas [$\mathrm{mg/m^3}$]
C_{h}	Transfer coefficient of sensible heat [dimensionless]
C_{l}	Transfer coefficient of latent heat [dimensionless]
C_{PO}	Particulate organic carbon (POC) concentration [$\mathrm{mg/m^3}$]
C_{w}	Concentration of a dissolved gas in near-surface water [$\mathrm{mg/m^3}$]
d_{Chl}	Conversion of phytoplankton to POC [$\mathrm{mg/(m^3\,d)}$]
d_{DOC}	Degradation of DOC [$\mathrm{mg/(m^3\,d)}$]
$d_{\mathrm{DOC,b}}$	Bacterial degradation of DOC in FOKEMA [$\mathrm{mg/(m^3\,d)}$]
$d_{\mathrm{DOC},T\mathrm{ref}}$	Bacterial degradation of DOC in a reference temperature in FOKEMA [$\mathrm{mg/(m^3\,d)}$]
d_{POC}	Fragmentation of POC to DOC [$\mathrm{mg/(m^3\,d)}$]
D	Molecular diffusion coefficient [$\mathrm{m^2/s}$]
D_{BO}	Biochemical oxygen demand [$\mathrm{mg/m^3}$]
D_{DOC}	Oxygen consumption through DOC degradation [$\mathrm{mg/(m^3\,d)}$]
D'_{DOC}	Carbon dioxide (CO_2) production through DOC degradation [$\mathrm{mg/(m^3\,d)}$]
D_{g}	Vertical turbulent diffusion coefficient for dissolved gases [$\mathrm{m^2/d}$]
D_{h}	Vertical turbulent diffusion coefficient for heat [$\mathrm{m^2/d}$]
D_{t}	Vertical turbulent diffusion coefficient [$\mathrm{m^2/d}$]
D_{sed}	Oxygen consumption through sedimentary organic carbon degradation [$\mathrm{mg/(m^3\,d)}$]

D'_{sed}	CO_2 production through sedimentary organic carbon degradation [mg/(m^3 d)]
E	Excretion of labile DOC from phytoplankton [mg/(m^3 d)]
E_{k}	Kinetic energy [J]
$f_{\mathrm{DOC,FKM}}$	Temperature correction factor for DOC degradation in FOKEMA [dimensionless]
f_{P}	Photosynthetically active fraction of total shortwave energy [dimensionless]
F	Flocculation of DOC [mg/(m^3 d)]
F_{gas}	Air-water gas flux [mg/(m^2 d)]
g	Gravitational acceleration [m/s^2]
$[\mathrm{H}^+]$	Hydrogen ion concentration ($10^{-\mathrm{pH}}$) [mol/L]
H_{sed}	Thickness of the active sediment layer [m]
I	Light intensity [mol/(m^2 s)]
k	Gas exchange velocity [m/s]
k_{BOD}	Organic decomposition rate at 20 °C [1/d]
$k_{\mathrm{DOC,1}}$	Labile DOC degradation rate at 20 °C [1/d]
$k_{\mathrm{DOC,2}}$	Semilabile DOC degradation rate at 20 °C [1/d]
$k_{\mathrm{DOC,3}}$	Refractory DOC degradation rate at 20 °C [1/d]
$k_{\mathrm{POC,1}}$	Autochthonous POC fragmentation rate at 20 °C [1/d]
$k_{\mathrm{POC,2}}$	Allochthonous POC fragmentation rate at 20 °C [1/d]
$k_{\mathrm{POC,sed}}$	Degradation rate of sedimentary particulate organic matter 20 °C [1/d]
$K_{0,\mathrm{nP}}$	Non-chlorophyll-related attenuation coefficient of photosynthetically nonactive radiation [1/m]
$K_{0,\mathrm{P}}$	Non-chlorophyll-related attenuation coefficient of photosynthetically active radiation [1/m]
$K_{\mathrm{DOC,P}}$	DOC-related attenuation coefficient of photosynthetically active radiation [1/m]
K_{H}	Henry's law constant [mmol/(L atm)]
K_{L}	Total attenuation coefficient of shortwave radiation [1/m]
K_{P}	Attenuation coefficient of photosynthetically active radiation [1/m]
K_{nP}	Attenuation coefficient of photosynthetically nonactive radiation [1/m]
l	Length scale of the smallest eddies [m]
L_{e}	Latent heat of the evaporation of water [J/kg]
m	Specific remineralization/death rate of phytoplankton [1/d]
m_{20}	Phytoplankton remineralization/death rate at 20 °C [1/d]
M	Molar mass [g/mol]
n	Schmidt number exponent [dimensionless]
N^2	Buoyancy frequency [1/s^2]
N^2_{min}	Minimum possible buoyancy frequency [1/s^2]
O_{D}	Dissolved oxygen (DO) concentration [mg/m^3]
$O_{\mathrm{D,T}}$	Threshold concentration of DO [mg/m^3]
p_{a}	Air pressure [atm]

P	DO production in photosynthesis [mg/(m^3 d)]
P'	CO_2 consumption in photosynthesis [mg/(m^3 d)]
P_{B}	Photochemical mineralization of DOC [mg/(m^3 d)]
P_{Chl}	Chlorophyll *a* concentration [mg/m^3]
$P_{\mathrm{Chl,sed}}$	Chlorophyll *a* concentration in total sediment solids [mg/m^3]
P_{D}	Dissolved inorganic phosphorus (phosphate) concentration [mg/m^3]
P_{DO}	Dissolved organic phosphorus concentration [mg/m^3]
P_{IP}	Particle-bound inorganic phosphorus concentration [mg/m^3]
q_{a}	Specific humidity [dimensionless]
q_{s}	Saturation specific humidity at water surface temperature [dimensionless]
q_λ	Spectral scalar photon density per unit irradiance [mol/(W d)]
Q	Local heating rate [J/(m^2 d)]
Q_{eff}	Effective heat flux [W/m^2]
Q_{H}	Sensible heat flux [W/m^2]
Q_{L}	Latent heat flux [W/m^2]
Q_{LW}	Net longwave radiative heat flux [W/m^2]
Q_{p}	Photosynthetic quotient [mol O_2/mol CO_2]
Q_{r}	Respiratory quotient [mol CO_2/mol O_2]
Q_{S}	Surface heat flux [W/m^2]
Q_{SW}	Shortwave radiative heat flux [W/m^2]
R	DO consumption through phytoplankton remineralization/ respiration [mg/(m^3 d)]
R'	CO_2 production through phytoplankton respiration [mg/(m^3 d)]
R_{Chl}	Resuspension of chlorophyll *a* [mg/(m^3 d)]
$s_{\mathrm{Chl,sed}}$	Mass fraction of chlorophyll *a* in sedimentary organic matter (OM) [mg Chl *a*/mg OM]
s_{O2}	Stoichiometric constant [mg O_2/mg Chl *a*]
s_{POM}	Mass fraction of phosphorus in organic matter [mg P/mg OM]
S_{A}	Sum of in-lake sources and sinks of substance A [mg/(m^3 d)]
S_{b}	Sediment oxygen demand [mg/(m^2 d)]
S_{BOD}	Biochemical oxygen consumption [mg/(m^3 d)]
S_{IS}	Particulate inorganic matter concentration [kg/m^3]
S_{OM}	Particulate organic matter concentration [kg/m^3]
$S_{\mathrm{POC,sed}}$	Resuspension of sedimentary POC [mg/(m^3 d)]
S_{SOD}	Sedimentary oxygen consumption [mg/(m^3 d)]
Sc	Schmidt number [dimensionless]
t	Time [d]
Δt	Model time step [d]
T	Water temperature [°C]
T_{a}	Air temperature [°C]
T_{s}	Water surface temperature [°C]
u	Velocity scale of the smallest eddies [m/s]
$u_{*\mathrm{a}}$	Atmospheric friction velocity [m/s]
$u_{*\mathrm{ref}}$	Wind-induced water friction velocity at a reference depth [m/s]

$u_{*\mathrm{w}}$	Water-side friction velocity [m/s]
U	Wind speed [m/s]
U_{10}	Wind speed at 10 m height [m/s]
$U_{\mathrm{res,epi}}$	Resuspension rate of sediment particles in the epilimnion [m/d]
$U_{\mathrm{res,hyp}}$	Resuspension rate of sediment particles in the hypolimnion [m/d]
U_{w}	Total water velocity [m/s]
V	Volume of a model grid layer [m^3]
w_*	Penetrative convection velocity [m/s]
w_{Chl}	Sinking speed of phytoplankton [m/d]
w_{POC}	Sinking speed of POC [m/d]
w_{S}	Sinking speed of particulate inorganic matter [m/d]
W_{str}	Wind sheltering coefficient [dimensionless]
y_{c}	Phytoplankton yield coefficient [mg Chl *a*/mg P]
z	Depth [m]
Δz	Thickness of the model grid layer [m]
$\tilde{z}$	Thickness of the mass boundary layer [m]
z'	Reference depth [m]
z_{AML}	Depth of the actively mixing layer [m]
z_{epi}	Thickness of the epilimnion [m]
α	Air-water CO_2 flux adjustment factor [dimensionless]
α_{i}	Albedo of melting ice [dimensionless]
α_{s}	Albedo of melting snow [dimensionless]
$\alpha_{\mathrm{t,w}}$	Thermal expansion coefficient of water [1/°C]
α_{w}	Water surface albedo [dimensionless]
β	Buoyancy flux [m^2/s^3]
β_{C}	Optical cross section of chlorophyll [m^2/mg]
β_{DOC}	DOC-related specific attenuation coefficient [m^2/mg]
ε	Total turbulent kinetic energy dissipation rate [m^2/s^3]
θ	Temperature adjustment coefficient [dimensionless]
θ_{BOD}	Temperature adjustment coefficient for the organic decomposition rate [dimensionless]
θ_{c}	Temperature adjustment coefficient for organic carbon degradation at $T < 4\,°\mathrm{C}$ [dimensionless]
θ_{SOD}	Temperature adjustment coefficient for sedimentary oxygen consumption [dimensionless]
κ	von Kármán constant [dimensionless]
λ	Wavelength of shortwave radiation [nm]
λ_{max}	Maximum wavelength contributing to photochemical DOC mineralization [nm]
λ_{min}	Minimum wavelength contributing to photochemical DOC mineralization [nm]
μ	Temperature-, phosphate-, and light-dependent specific growth rate of phytoplankton [1/d]
μ'_{20}	Maximal phytoplankton growth rate at 20 °C [1/d]
ν	Kinematic viscosity of water [m^2/s]

ν_{IM}	Volume fraction of inorganic matter in total dry sediment solids [dimensionless]
ρ_{a}	Air density [kg/m^3]
ρ_{org}	Organic matter density [kg/m^3]
ρ_{w}	Water density [kg/m^3]
τ	Wind shear stress [N/m^2]
ϕ_λ	Spectral apparent quantum yield for photochemical DOC mineralization [mol C/(mol quanta nm)]
χ	Mole fraction of a gas in the atmosphere [µmol/mol]

Contents

1 Introduction

Atmospheric carbon dioxide (CO_2) concentration has increased significantly during recent decades because of anthropogenic actions, and the increase is predicted to continue. As a response to increasing radiative forcing due to higher levels of CO_2 and other greenhouse gases (GHGs) in the atmosphere, the global mean surface temperature is estimated to rise by 0.3 to 4.8 °C by the end of the 21st century (IPCC, 2014). The increase will likely be even higher in northern latitudes. In Finland, the annual mean temperature has increased by 0.3 °C per decade during the period of 1961–2010 (Aalto et al., 2016), and it is projected to increase further by 0.8 to 7.7 °C by the end of the 21st century (Ruosteenoja et al., 2016). Increasing atmospheric temperature and other future changes in climate, including, for example, changes in precipitation, will have an impact on the functioning of terrestrial and aquatic ecosystems.

The global carbon cycle describes the complex transformations and exchanges of carbon within and between the major reservoirs in the earth system: the atmosphere; the oceans; land, including inland waters; and fossil fuels (Houghton, 2003). CO_2 is removed from the atmosphere and fixed into terrestrial or aquatic organic matter by photosynthesis. Some of the terrestrial organic carbon is transported through rivers and streams into oceans or transformed back into inorganic form by ecosystem respiration and released to the atmosphere as CO_2. Terrestrial and oceanic ecosystems are global net sinks of atmospheric carbon, compensating for the increase of anthropogenic CO_2 in the atmosphere resulting from burning of the fossil fuels and biomass (Battin et al., 2009).

Even though usually not classified as a separate component in global carbon budgets, lakes are a significant part in carbon cycling and in the net ecosystem exchange of CO_2 both on global (Battin et al., 2009; Tranvik et al., 2009) and regional scales (Cole et al., 2007). The vast majority of inland waters worldwide are found to be supersaturated with CO_2 with concentrations that can exceed the equilibrium concentration by several times, and therefore they are net sources of carbon to the atmosphere (Cole et al., 1994; Sobek et al., 2005). In the boreal zone, small humic lakes are active sites in carbon cycling because of high loading of terrestrially produced organic carbon (Einola et al., 2011; Hanson et al., 2007). Small lakes are abundant in boreal areas (Downing et al., 2006; Verpoorter et al., 2014), and the contribution of small lakes to regional CO_2 effluxes has been found to be

higher than their proportion of the total lake area (Kankaala et al., 2013). In other words, boreal inland waters release significant amounts of CO_2 originally fixed by the surrounding terrestrial system. Atmospheric CO_2 exchange in lakes is one of the key processes to be assessed in attempts to evaluate the role of lakes in carbon processing and to construct carbon budgets of lakes.

Lakes are effective indicators of climate change. Lakes are sensitive to climate, and physical, chemical, and biological lake properties are shown to respond rapidly to climate-related changes (Adrian et al., 2009). The implications of climate warming for lacustrine ecosystems are conspicuous in the boreal zone (Keller, 2007). Higher air temperature shortens the length of the ice season (Gebre et al., 2014), changes the thermal regime of lakes by warming the water column and by altering the thermal stratification (Elo et al., 1998; Huttula et al., 1992; Saloranta et al., 2009), and may accelerate organic matter decomposition processes (Jansson et al., 2008). Climate change may also increase precipitation (Ruosteenoja et al., 2016), which may result in seasonal increases in discharge (Veijalainen, 2012) and elevated annual loading of terrestrial carbon (Pumpanen et al., 2014; Tranvik and Jansson, 2002). Increased nutrient loading due to higher rainfall and a longer ice-free season may increase annual phytoplankton photosynthesis (Jeppesen et al., 2009; Magnuson et al., 1997). Higher primary production may increase the amount of readily degradable organic carbon in lake sediments and, as a consequence, together with higher water column temperature (Gudasz et al., 2010), the internal production of CO_2 in lakes (Sobek et al., 2009). These factors may result in an increase in CO_2 emissions from boreal lakes (Weyhenmeyer et al., 2015). It is of great importance to strive to examine how human-induced climate change affects the functioning of lacustrine ecosystems and consequently the global carbon cycling. There is hence a clear need for simulation tools for judging the impact of the foregoing changes on the physical and biochemical conditions in lakes.

Process-based, coupled physical-biogeochemical modeling is an essential means to understand current lake ecosystem dynamics and to investigate the potential consequences of climate change (Arhonditsis and Brett, 2004). Aquatic ecosystem modeling has advanced considerably in recent decades, but the development of process-based models for carbon cycling in lakes has been hindered by inadequate knowledge on the complex biochemical processes involved (Stepanenko et al., 2016) and the demand for large amounts of input data for parameterization and testing (Robson, 2014). General seasonal patterns and interannual changes in inorganic carbon compound dynamics in boreal lakes have been studied for a long time (e.g., Kelly et al. (2001); Kratz et al. (1997); Rantakari and Kortelainen (2005); Sobek et al. (2003)), but much less is known of the short-term variation and the details of seasonal changes of CO_2. The situation is changing rapidly because continuous monitoring of the water column concentration and air-water flux of CO_2 has become simpler in consequence of the adaptation of modern and increasingly reliable technologies to freshwater ecosystem research (Hari et al., 2008; Mammarella et al., 2015; Provenzale et al., 2018).

The primary aim of this thesis is to assess the implications of warmer atmospheric

temperature for the concentration and air-water flux of CO_2 in small boreal lakes by using a novel vertical process-based lake model for simulation of year-round carbon dynamics. Furthermore, the performance of process-based coupled physical-biogeochemical lake models in the simulation of air-water CO_2 flux was analyzed. Two models of different complexity were developed for these purposes. The specific objectives were:

- To adapt an existing vertical process-based coupled physical-biogeochemical lake model to accommodate simulation of the concentration and air-water flux of CO_2 and to assess the model performance using comprehensive CO_2 measurements in a study lake.
- To utilize a novel lake model in studying the effects of climate change on carbon dynamics in a humic boreal lake, specifically:
  - The impacts of higher atmospheric temperature and changing seasonal inflow patterns on the lake CO_2 concentration and on the role of the lake as a carbon source to the atmosphere.
  - The significance of loading of terrestrially derived organic carbon in lake CO_2 dynamics.
  - The relative importance between the increases in terrestrial loading of inorganic and organic carbon on the lake CO_2 concentration in future climate.
- To assess the applicability of different gas exchange models in a vertical process-based coupled physical-biogeochemical lake model with a daily time step.
- To assess the implications of improved CO_2 efflux estimates for lacustrine carbon budgets.

The outline of this thesis is as follows. In Chapter 2, the inorganic and organic carbon cycle in lake ecosystems and processes affecting it are described. Chapter 3 provides an overview of modeling of biogeochemical processes in lakes, especially methods for the simulation of lake carbon dynamics. Furthermore, it gives a description of the lake model that the models developed in this work are based on and presents different models for air-water gas exchange. In Chapter 4, two models for lake CO_2 dynamics developed in this work are presented. Chapter 5 provides a description of the study lakes and the experimental data used as input to models and for model calibration. Chapter 6 describes the model calibration processes and the forcing data used in the climate impact analysis. Chapter 7 is focused on the application of the first, simpler model for the simulation of CO_2 and dissolved oxygen (DO) concentrations and air-water CO_2 exchange in a small boreal lake. Chapter 8 concerns the application of the more sophisticated model to climate impact analysis. In Chapter 9, the incorporation of different gas exchange models into the more advanced model and the performance of the models regarding the simulation of air-water CO_2 exchange are studied. In the final chapter, the work is summarized and concluded.

2 Aquatic carbon cycle

The lacustrine carbon cycle involves the interactions of gaseous, dissolved, and particulate forms of carbon (Myrbo, 2012). Carbon within boreal lake ecosystems can be separated into three major pools: particulate organic carbon (POC), dissolved organic carbon (DOC), and dissolved inorganic carbon (DIC). DIC, as CO_2, may be fixed into organic form by primary producers, and organic carbon can be mineralized through physical, chemical or biological processes back to CO_2. Interactions between a lake, the surrounding landscape, and the atmosphere are highly important in carbon cycling. Especially small lakes, having a high ratio of shoreline to open water, are strongly influenced by carbon and nutrient inputs from the surrounding catchment (Wetzel, 2001). Lakes that are supersaturated with CO_2 due to the mineralization of terrestrially produced organic carbon emit CO_2 to the atmosphere.

The variability of inorganic carbon in lakes is strongly scale-dependent and related to different drivers depending on the time scale of the analysis (Hanson et al., 2006). Metabolic and physical factors control both short-term and long-term variations in CO_2 concentration. Metabolism is a governing factor in the diel pattern of CO_2 concentration, along with gas exchange with the atmosphere. In addition, physical processes, such as water temperature, stratification, wind-induced water column mixing, and hydrological events causing changes in inputs of surface water, groundwater, and degradable organic matter, have an effect on the amount and distribution of CO_2 in the water column particularly on longer time scales (Weyhenmeyer et al., 2012). On seasonal and yearly scales, metabolism is an influential factor, but physical processes related to spring and autumn mixing together with carbon loading from the catchment may have significant effects (Ojala et al., 2011; Striegl and Michmerhuizen, 1998). On decadal and even longer scales, climate-related changes in weather conditions and hydrologic carbon inputs change the physicobiogeochemical conditions of lakes, thus affecting the overall annual patterns of CO_2 concentration (Tranvik et al., 2009; Weyhenmeyer et al., 2015).

Effects of physical processes on seasonal CO_2 dynamics

Physical lake processes, such as seasonal thermal stratification of the water column and a seasonal ice cover, have a profound impact on CO_2 dynamics in boreal lakes. Many boreal lakes are dimictic; that is, they are mixed in spring and autumn

and thermally stratified in summertime and during the ice-covered period (Wetzel, 2001). In winter the lakes are inversely stratified, the surface water under ice being close to the freezing point and the densest and warmest water being located near the bottom. As the radiative heating of the surface water is gradually increased in spring, the surface water reaches maximum density at 4 °C, and the water column is readily mixed. The spring mixing is usually dampened rather quickly because the surface water becomes less dense as it warms further, impeding further mixing. Thermally driven density differences eventually separate the warmer, circulating, and rather turbulent upper layer, the epilimnion, from the colder and more stagnant bottom layer, the hypolimnion. The epilimnion and the hypolimnion, which are characterized by rather uniform temperatures, are separated by a layer with a strong density gradient, the metalimnion. The thermocline, the plane of maximum temperature gradient, is located in the metalimnion. During the course of summer, the thermocline starts to deepen because of heat losses from the epilimnion to the atmosphere and wind-induced and convective heat transfer to the hypolimnion. Eventually, the water column reaches uniform temperature and the autumn turnover occurs. The autumnal mixing period usually lasts until the lake freezes and is often longer than the spring mixing period.

Lakes in the boreal zone are ice-covered part of the year, typically from November to April–May (Bengtsson, 2012). The ice cover excludes the release of gases to the atmosphere, which results in CO_2 accumulation in lake water until ice melt (Ducharme-Riel et al., 2015; Karlsson et al., 2013). The highest CO_2 efflux is often found to occur immediately after ice breakup as the accumulated CO_2 degasses to the atmosphere in a short time (Anderson et al., 1999; Striegl et al., 2001). In contrast, the CO_2 produced near the bottom of a lake or entering the hypolimnion via groundwater inflow during summer stratification is trapped in the hypolimnion and released not until the autumnal mixing (Kortelainen et al., 2006; Weyhenmeyer et al., 2012). In small boreal lakes the spring mixing may be incomplete, which may lead to insufficient ventilation of the water column and a rapid development of anoxia (Salonen et al., 1984). The hypolimnion often becomes anoxic also in productive lakes during summer stratification, which may lead to a significant level of methanogenesis (Huttunen et al., 2006). Methane (CH_4) is mostly oxidized to CO_2 above the oxic-anoxic interface in the metalimnion (Bastviken et al., 2003).

Lake carbon processes

Lakes contain carbon in organic and inorganic forms. Organic matter is produced in a lake by primary producers (autochthonous organic matter) or imported from the catchment (allochthonous organic matter). Particulate organic matter (POM) and dissolved organic matter (DOM) are usually quantified by measuring their organic carbon concentration. Generally, the dry weights of POM and DOM are equal to two times the dry weights of POC and DOC, respectively (Thurman, 1985). The operational distinction between particulate and dissolved organic carbon is based on particle size, organic matter compounds smaller than 0.2 to 1.0 µm being classified as DOC (Benner, 2002). The upper size limit of DOC is generally 0.45 µm (Thurman, 1985). POC, also referred to as suspended organic carbon

(SOC), exists in lake water in living and dead forms. Photosynthetic and heterotrophic organisms belong to the living fraction of POC. Dead POC is also known as detritus. The majority (90% or more) of organic carbon within the water column of a lake is generally in a dissolved form (Wetzel, 2001). Allochthonous organic matter is generally rather recalcitrant; that is, it is slowly, if at all, degradable because it has passed through many degradation stages on its way to a lake (Wetzel, 2001). Autochthonous DOC is usually more labile, and it is produced through fragmentation of dead POC by, for example, zooplankton grazing (Kragh and Søndergaard, 2004) or through excretion by phytoplankton (Baines and Pace, 1991).

Some of the DOC is degraded, primarily by microbial processes, in the water column (Jansson et al., 2000), and carbon is transformed into an inorganic form, CO_2, through microbial respiration. DOC can also be degraded via photochemical reactions through exposure to solar radiation in the surface water (Granéli et al., 1996). Terrestrially derived DOC may also be transformed into POC via the process of flocculation (von Wachenfeldt et al., 2009). Both autochthonous and allochthonous POC eventually settle to the lake bottom. The sedimentary POC is gradually degraded and transformed into CO_2 or CH_4 or buried permanently in the sediments.

The CO_2 produced via in-lake respiration or entering a lake from the atmosphere reacts with water to form carbonic acid (H_2CO_3), which dissociates into bicarbonate ions (HCO_3^-) and carbonate ions (CO_3^{2-}). The vast majority of undissociated CO_2, however, remains as CO_2 molecules, and the combined concentration of CO_2 and H_2CO_2 is denoted as the concentration of CO_2 (Stumm and Morgan, 1981). The sum of these three dissolved species of inorganic carbon in the aqueous solution is denoted as dissolved inorganic carbon (DIC). The relative abundance of the dissolved species of inorganic carbon is dependent on the temperature and the pH of lake water. The dominant species is CO_2 under acidic conditions, HCO_3^- under conditions close to neutral, and CO_3^{2-} under alkaline conditions. The molar concentrations of CO_2 and HCO_3^- in nonsaline water at 20 °C are equal at pH 6.4 (Millero, 1995).

Temperature-driven DIC equilibria changes and lake metabolism affect mainly the CO_2 fraction of DIC (Hanson et al., 2006). Many lakes are intense sites of organic carbon mineralization. Production of CO_2 through in-lake heterotrophic respiration fueled primarily by allochthonous organic matter and through phytoplankton respiration exceeds the gross CO_2 consumption by primary production in most lakes (del Giorgio et al., 1999), which results in CO_2 supersaturation in the water column and an efflux of CO_2 from lakes to the atmosphere (Sobek et al., 2005). The relative importance between water column respiration and sediment respiration as contributors to CO_2 supersaturation is shown to vary significantly among boreal lakes (Algesten et al., 2005; Kortelainen et al., 2006). CO_2 dissolves less in warm water, which increases the CO_2 efflux from the supersaturated epilimnion in summer. The air-water CO_2 flux may also be downward at the time of vigorous photosynthesis in productive humic lakes (Huotari et al., 2009; Ojala et al., 2011).

Diurnal fluctuation in the epilimnetic CO_2 concentration and the resulting CO_2 flux is induced by the interplay between ecosystem respiration and net primary production. Photosynthetic primary production consumes CO_2 from the water during daytime, whereas the CO_2 concentration increase through respiration is not attenuated by primary production in the absence of photosynthesis in dark conditions.

Terrestrial carbon loading

Terrestrially produced organic and inorganic carbon enter lakes via surface water and groundwater inflow. The concentration of DOC is high in many lakes in the boreal zone because of large inputs of humic matter from the catchment. The median organic carbon concentrations in boreal lakes fall within the range of 10 to 13 mg/l depending on the land cover types of their catchments (Sobek et al., 2007). In Finland, the DOC concentration is found to be higher than 10 mg/l in about 60% of lakes (Kortelainen, 1993). Especially small, shallow lakes with a high ratio of catchment area to lake volume and a high proportion of peatland in their catchments tend to have high organic carbon concentrations (Kortelainen, 1999). Terrestrially produced DOC is often highly colored (Meili, 1992); thus, a high concentration of allochthonous DOC reduces water column transparency, which affects, for example, lake thermal regime and phytoplankton photosynthesis through increased attenuation of shortwave radiation (Kirk, 2011). The degradation of allochthonous carbon is a major source of CO_2 in humic lakes (Jonsson et al., 2001; Sobek et al., 2003). Direct external loading of DIC to lakes may also be substantial (Weyhenmeyer et al., 2015).

The contribution of groundwater discharge to the total terrestrial loads of DOC and DIC has shown to be important in some boreal lakes (Einarsdóttir et al., 2017). The concentration of CO_2 in groundwater is generally around an order of magnitude higher than the atmospheric equilibrium concentration (Lahermo et al., 1990). Groundwater–lake water interactions have been found to affect lake water chemistry (Rautio and Korkka-Niemi, 2015), but the extent of the effect depends on the landscape position of the lake (Ala-aho et al., 2013). In the riparian zone, commonly from a few meters to a few tens of meters wide area adjacent to a water body (Ledesma et al., 2015), the groundwater table is shallow and the soils are often rich in organic matter, which may further increase the CO_2 concentration of the groundwater entering streams and lakes (Leith et al., 2015).

Atmospheric CO_2 exchange

Along with carbon inputs from the terrestrial catchment and outputs through lake outflow, the exchange of CO_2 with the atmosphere is an important external source or sink of carbon in lakes, depending on the surface water CO_2 concentration with respect to the atmospheric equilibrium concentration. The exchange occurs, driven by a combination of molecular diffusive and turbulent diffusive processes at the air-water boundary layer, through molecular diffusion at the air-water interface (MacIntyre et al., 1995). The flux is proportional to the CO_2 concentration gradi-

ent near the interface, the proportionality factor being known as the gas exchange velocity, the gas transfer velocity or the gas exchange coefficient. In addition, the flux of CO_2 can be enhanced by hydration reactions near the air-water interface (Wanninkhof and Knox, 1996). However, the chemical enhancement is negligible in nonalkaline waters (Portielje and Lijklema, 1995). Diffusive gas exchange is a rather slow process, which results in CO_2 supersaturation in the mixed surface water in heterotrophic lakes as the biochemically produced CO_2 accumulates below the air-water interface.

For the quantification of CO_2 exchange between a lake and the atmosphere, knowledge of the gas exchange velocity is required. In many widely used, empirically derived gas exchange models the parameterization of the gas exchange velocity is based solely on wind speed (Cole and Caraco, 1998; Wanninkhof, 1992). However, recent CO_2 exchange measurements over lakes using eddy covariance (EC) techniques (e.g., Heiskanen et al., 2014; Jonsson et al., 2008; MacIntyre et al., 2010) have yielded higher predictions of the gas exchange velocity compared to the wind-based models. For slightly soluble gases, such as CO_2, air-water transfer is mainly driven by turbulence in near-surface water, which is not a function of wind alone (MacIntyre et al., 1995).

Near-surface turbulence is generated principally by shear and thermal convection, also referred to as penetrative convection (Imberger, 1985). Shear is caused by wind forcing at the air-water interface. Thermal convection in the mixed surface water is induced by heat loss from the surface. The increasing density of cooling near-surface water causes it to sink and penetrate through the mixed layer. The relative contribution of wind and convection to turbulence in the surface water is shown to vary with lake size (Read et al., 2012). Thermal convection is a relatively more important factor in small, wind-sheltered lakes, which are abundant in the boreal zone. Water-side shear stress and surface heat flux can either be determined through direct atmospheric measurements with the EC method and radiation measurements (Mammarella et al., 2015) or calculated using meteorological variables (Fairall et al., 1996). Turbulence-based gas exchange models have been shown to agree well with direct field measurements of gas exchange over lakes of different sizes (e.g., Mammarella et al., 2015; Vachon et al., 2010; Zappa et al., 2007). Improved estimates of CO_2 flux between lake water and the atmosphere can provide a more accurate insight on other processes occurring in the carbon cycle in lakes and on the role of lakes in the global carbon cycle.

3 Modeling of biogeochemical processes in lakes

Mechanistic, process-based biogeochemical models have had an essential role in the research of lakes and other aquatic ecosystems as they illustrate aspects and patterns of system dynamics that are difficult to attain by other means and are able to address issues that are related to potential changes in ecosystem functioning (Arhonditsis et al., 2006). In Finland, the use and development of water quality models integrated with flow and transport models has been ongoing for several decades (see Virtanen, 2009). With regard to spatial dimensions, the range of process-based models for the simulation of lakes extends from zero-dimensional mass balance models to fully three-dimensional hydrodynamic models (Martin and McCutcheon, 1999). One-dimensional models are either vertically layered and horizontally integrated or sectioned in the longitudinal direction. In two-dimensional models, the integration can be performed in the vertical or in the lateral direction. Three-dimensional and vertically integrated two-dimensional models include horizontal water flow and substance transport, whereas vertical one-dimensional models describe the lake water column as horizontally stagnant.

Process-based models are deterministic: the evolution of the system is described by mathematical equations, and the output of the model is fully determined by the initial conditions and parameter values. Deterministic models are usually dynamic; that is, they simulate the development of the system over time and the effect of different drivers on the system functioning. A substantial drawback of process-based models of complex systems is the requirement of substantial amount of detailed data for input and calibration together with independent data for performance assessment or, in other words, validation. Models of natural systems may even be too complex to be accurately evaluated (Oreskes et al., 1994). However, process-based models may still outperform other approaches, such as statistical modeling, when the aim is to make prognoses for the future development of the system and to study outcomes of changes within the system or to quantify underlying processes instead of only the final conditions (Robson, 2014).

Because many essential processes in aquatic ecosystems can only be comprehended through the interaction between physical and biochemical processes, coupled models that integrate physical and biogeochemical models are an appropriate foun-

dation for theoretical studies (Fennel and Neumann, 2001). However, coupled aquatic physical-biogeochemical models perform less well in simulating biological and chemical components of aquatic systems than physical processes within the systems (Arhonditsis and Brett, 2004). Models of physical systems can be built largely from recognized physical theories and their approximations, whereas models of biogeochemical processes consist mainly of simple statistical models integrated into a mechanistic framework (Robson, 2014). Many biogeochemical processes are inadequately understood to develop rigorous mathematical description (Stepanenko et al., 2016). Processes are also difficult to quantify because of the complex interplay between physical and biochemical driving factors in a lake. Hence, more assumptions and simplifications are needed in biogeochemical models than in physical models, and biogeochemical models tend to have more parameters.

The application of a process-based model is subject to many sources of uncertainties, including technical uncertainties concerning the inexactness of model parameters and the quality of input data; methodological uncertainties related to model structure and, for example, coarse spatiotemporal scales or simplifications in process descriptions and inadequacies in functional relationships; and epistemological uncertainties concerning incomplete conceptual understanding of natural systems (Saloranta et al., 2003). Technical uncertainties can be quantified by sensitivity and uncertainty analysis, but methodological and especially epistemological uncertainties are more difficult to assess. Errors caused by incorrect or inconsistent process descriptions can often be partly compensated for by finding not necessarily totally correct but optimal model parameter values by calibration (Stepanenko et al., 2016). In regard to model structure, balancing between realism and generality is an essential issue (Clark, 2005). General dependencies attained by simple models may not be scalable to different settings or be able to account for the range of influences operating within the system. Thus, it is important that the model is structured to reflect the natural system dynamics more realistically if it is intended for making predictions and studying potential system dynamics outside of its calibration domain (Arhonditsis et al., 2007). However, specifying many effects with associated parameters in complex and more realistic models may lead to the problem of parameter unidentifiability or equifinality meaning that many different parameter sets can produce similar results (Beven, 2006). In addition, complex models may be overparameterized relative to the amount of independent information in experimental data, so that the parameters cannot be properly determined through calibration. Also, small defects in each parameter and in the formulation of each process may accumulate the error and uncertainty in a complex model, and proper calibration and uncertainty analysis may be difficult to perform (Doherty and Christensen, 2011). Thus, a careful selection of only the most important processes is essential for mechanistic modeling.

An effective means to improve the calibration of a process-based model and the uncertainty analysis of its parameters and predictions is to make use of statistical inference techniques, such as the Markov chain Monte Carlo (MCMC) simulation method based on Bayesian inference (Saloranta et al., 2009). Instead of trying to find a single optimal value for each parameter, the purpose is to find a joint

distribution of parameter sets that optimally fit the model results to observations (Arhonditsis et al., 2007). The integration of mechanistic models with Bayesian analysis thus provides a way to represent and resolve the parameter equifinality problem. The uncertainty of the model results can further be assessed using the resultant parameter sets: the uncertainty bounds can be generated by conducting simulations with parameter sets resampled from the joint distribution.

3.1 Vertical models for aquatic carbon cycling

Because of the large amount of inadequately known processes and complex interactions within the aquatic carbon cycle, there are currently rather few mechanistic models for simulating CO_2 or other GHGs in lakes or other natural water bodies that include the descriptions of both physical and biogeochemical processes. The existing models are mainly vertical; that is, they simulate the concentration and the vertical distribution of carbon species in the water column. Vertical dynamic models can be classified into three types according to the spatial structure (Stepanenko et al., 2013). In zero-dimensional or bulk models the water column is completely mixed and the temperature profile is homogeneous. In two-layer models a distinction is made between a mixed top layer and a bottom layer with either homogeneous profiles of temperature and substance concentrations or a parameterized temperature-depth dependence. In one-dimensional models the temperature and substance concentration profiles are explicitly calculated on a vertical grid. The spectrum of vertical process-based models of varying levels of detail for carbon cycling in lakes extends from zero-dimensional steady-state mass balance models (e.g., McDonald et al., 2013) to complex coupled one-dimensional hydrodynamic and biogeochemical models. Because the uncertainty of a single model is often rather high, constructing and developing new models of different complexity enables the assessment of uncertainties within and between models (Doherty and Christensen, 2011).

The spatiotemporal dynamic processes of CO_2 are closely related to those of DO, and sophisticated water quality models are available for simulating DO conditions in lakes (see Stefan and Fang, 1994; Virtanen, 2009). Stefan and Fang (1994) formulated a deterministic, one-dimensional DO model based on the morphometry and trophic status of a lake to simulate summer conditions. The model formulation is guided by a lake water quality model MINLAKE (Riley and Stefan, 1988), which has been successfully applied for a long time to simulate hydrothermal and kinetic processes in a variety of lakes and meteorological conditions.

The simplest process-based models for carbon cycling in lakes are bulk or two-layer models that include biochemical processes between different carbon species within a lake and the external sources and sinks of carbon but do not include the simulation of lake thermal structure or the vertical distribution of carbon. The level of complexity regarding the distinction between species of organic carbon varies between models. A dynamic bulk model by Cole et al. (2002) simulates the fates of

allochthonous and autochthonous organic matter in the surface mixed layer. The model includes DIC, DOC, dead POC, bacteria, phytoplankton, and zooplankton as the carbon compartments. A two-layer, dynamic steady-state model by Hanson et al. (2004) accounts for internal organic and inorganic carbon cycling together with carbon fluxes with terrestrial and atmospheric systems. Organic carbon is divided into DOC, living POC, and dead POC in the model.

One-dimensional process-based models with varying complexity regarding the description of biochemical processes have been developed for the simulation of CO_2 in natural waters. Stepanenko et al. (2016) presented a one-dimensional process-based model for lake CO_2 and CH_4 dynamics based on a vertical hydro-thermodynamic model LAKE (Stepanenko et al., 2011). The descriptions of biochemical processes in the model are mostly based on the DO model by Stefan and Fang (1994), in which the biochemical in-lake source of DO (and thus the sink of CO_2) is photosynthesis, which is regulated by chlorophyll *a* (Chl *a*) concentration, and the biochemical in-lake sinks of DO (and sources of CO_2) are biological oxygen demand (BOD) and sediment oxygen demand (SOD). Chl *a* concentration, SOD, and BOD are given as input parameters in the model by Stepanenko et al. (2016). Omstedt et al. (2009) developed an advanced one-dimensional physical-biogeochemical model for the uptake and release of CO_2 in the Baltic Sea. The model uses the PROBE lake model (Svensson, 1998) to specify the physical behavior, allowing the effective modeling of fully coupled physical and biogeochemical processes. However, a significant deficiency in the models by Stepanenko et al. (2016) and Omstedt et al. (2009) is that they lack the simulation of lake ice cover, which greatly impacts the seasonal dynamics of dissolved gases. Also, the spatiotemporal dynamics of organic carbon species are not simulated in these models.

There are advanced one-dimensional process-based lake models that can be used for simulation of inorganic and organic carbon also in lakes with seasonal ice cover. These include, for example, a coupled hydrodynamic and water quality model DYRESM-CAEDYM (Hamilton and Schladow, 1997) containing comprehensive modules for carbon cycling (Bruce et al., 2006) and ice cover (e.g., Oveisy and Boegman, 2014); a hydrodynamic model GLM (Hipsey et al., 2014) coupled with the biogeochemical AED modeling library (Hipsey et al., 2013); and the recent Arctic Lake Biogeochemistry Model (ALBM) by Tan et al. (2017), which has been specifically designed to have a comprehensive description of the carbon cycle in permafrost lakes. However, the description of biogeochemical processes is rather complex in these models, containing, for example, the simulation of zooplankton or nitrogen.

3.2 Lake model MyLake v.1.2

In this work, a one-dimensional process-based lake model MyLake (Multi-year Lake simulation model) v.1.2 (Saloranta and Andersen, 2007) was extended to include descriptions of DO and organic and inorganic carbon. MyLake v.1.2, developed

in MATLAB, simulates the vertical distribution of lake water temperature, the evolution of lake ice and snow cover, phosphorus-phytoplankton and DOC dynamics, and the exchanges of heat and substances between the lake water column and bottom sediment. The microbial and photochemical degradation of DOC is simulated in a FOKEMA submodel (Holmberg et al., 2014). MyLake v.1.2 has been developed to contain only the most important physical, chemical, and biological processes in a balanced and robust way. MyLake shares many characteristics with other existing one-dimensional models, such as MINLAKE and PROBE. In addition, the model aims to combine good simulation efficiency with relatively short execution time as well as easy utilization of numerical calibration, uncertainty analysis, and sensitivity analysis techniques. Because of the fast execution, it is well suited for simulation over long periods. Because of the inclusion of an ice and snow cover submodel, MyLake is also applicable for lakes in colder climatic conditions. MyLake v.1.2 has been applied to several boreal lakes for the simulation of lake stratification and ice cover characteristics (e.g., Dibike et al., 2012; Gebre et al., 2014; Saloranta et al., 2009), phosphorus and phytoplankton concentrations (e.g., Couture et al., 2018, 2014; Romarheim et al., 2015), and DOC concentration (Holmberg et al., 2014).

It is assumed in MyLake that a lake is a horizontally mixed water basin with heat and mass flow occurring only in the vertical direction. External substance loads are taken into account by means of stream inflow. The volume of the lake is fixed: neither inflow nor outflow changes the lake volume. Furthermore, groundwater exchange and water level changes due to precipitation or evaporation are omitted in MyLake. The model time step is set to 24 h except for the calculation of the water column heating rate and convection, which are calculated separately for daytime and nighttime. The vertical grid length can be defined by the user. MyLake v.1.2 can be divided functionally into two submodels: a thermal submodel and a biochemical (phosphorus-phytoplankton) submodel. The main model state variables in MyLake v.1.2 are temperature T, particulate inorganic matter (or suspended inorganic particulate matter, such as clay particles) S_{IS}, dissolved inorganic phosphorus (phosphate) P_{D}, particle-bound inorganic phosphorus P_{IP}, dissolved organic phosphorus P_{DO}, and chlorophyll a P_{Chl}. In addition, dissolved organic carbon C_{DO} has been introduced as a model state variable into MyLake v.1.2 via the FOKEMA submodule.

The data needed for setting up a MyLake v.1.2 application are: (1) daily time series of meteorological data, inflow volume, inflow temperature, and the inflow concentrations of particulate inorganic matter, total phosphorus, dissolved organic phosphorus, and Chl a; (2) lake depth-area data and the initial vertical profiles of water column temperature and the concentrations of particulate inorganic matter, total phosphorus, dissolved organic phosphorus, and Chl a; and (3) the user-adjustable parameter values. The meteorological variables include global radiation, cloud cover fraction, air temperature, relative humidity, air pressure, wind speed, and precipitation.

3.2.1 Thermal submodel

In MyLake, the horizontally homogeneous and vertically stratified lake is partitioned into N mixed horizontal layers with a constant thickness Δz and a top area $A_i, i = 1, \ldots, N$. A conservation equation of the form

$$A\frac{\partial T}{\partial t} = \frac{\partial}{\partial z}\Big(D_{\mathrm{t}} A \frac{\partial T}{\partial z}\Big) + A\frac{Q}{\rho_{\mathrm{w}} c_{p\mathrm{w}}} \tag{3.1}$$

is solved to obtain the vertical transport of heat in the water column. A is the horizontal area of the lake at depth z, t is time, D_{t} is the vertical turbulent diffusion coefficient, Q is the local heating rate, ρ_{w} is the water density, and $c_{p\mathrm{w}}$ is the specific heat capacity of water at constant pressure. The first term on the right-hand side of Eq. (3.1) represents mixing processes due to turbulent diffusion, and the second term represents water column heating due to sensible, latent, and radiative heat fluxes and diffusive heat exchange between the water column and the lake bottom. The vertical turbulent diffusion coefficient is calculated as

$$D_{\mathrm{t}} = a_{\mathrm{k}}(N^2)^{-0.43}, \tag{3.2}$$

where a_{k} is the turbulent diffusion parameter and N^2 is the buoyancy frequency

$$N^2 = \frac{g}{\rho_{\mathrm{w}}}\frac{\partial \rho_{\mathrm{w}}}{\partial z}, \tag{3.3}$$

where g is the gravitational acceleration. An upper limit for D_{t} is set through a minimum possible buoyancy frequency N^2_{min}. The turbulent diffusion parameter applied under open water conditions is determined by default by the lake surface area A_{s} (km^2) as (Hondzo and Stefan, 1992)

$$a_k = 0.00706(A_{\mathrm{s}}^{0.56}). \tag{3.4}$$

An area-invariant value of a_{k} is used during the ice-covered period.

All heat fluxes are defined positive when directed towards the water column. The net surface heat flux Q_{S} consists of sensible heat flux Q_{H}, latent heat flux Q_{L}, and net longwave radiative heat flux Q_{LW}:

$$Q_{\mathrm{S}} = Q_{\mathrm{H}} + Q_{\mathrm{L}} + Q_{\mathrm{LW}}. \tag{3.5}$$

The attenuation of shortwave radiation in the water column is separated into two wavelength bands: photosynthetically active radiation (PAR) and photosynthetically nonactive radiation (non-PAR). The shortwave radiative heat flux Q_{SW} at the surface of layer i is calculated as

$$Q_{\mathrm{SW},i} = Q_{\mathrm{SW},0}(1-\alpha_{\mathrm{w}})\big(f_{\mathrm{P}} e^{-\overline{K}_{\mathrm{P},i} z_i} + (1-f_{\mathrm{P}}) e^{-\overline{K}_{\mathrm{nP},i} z_i}\big), \tag{3.6}$$

where $Q_{\mathrm{SW},0}$ is the incident shortwave radiative heat flux at the surface, α_{w} is the average daily albedo, f_{P} is the PAR fraction of the total shortwave energy, and

$\overline{K}_{\mathrm{P},i}$ and $\overline{K}_{\mathrm{nP},i}$ are the PAR and non-PAR attenuation coefficients, respectively, averaged down to the top of layer i, taking into account both chlorophyll-related and non-chlorophyll-related attenuation. The integrated attenuation coefficients are of the form

$$\overline{K}(z) = K_0 + \beta_{\mathrm{C}}\overline{P}_{\mathrm{Chl}}(z), \tag{3.7}$$

where K_0 is the non-chlorophyll-related attenuation coefficient, β_{C} is the optical cross section of chlorophyll, and $\overline{P}_{\mathrm{Chl}}(z)$ is the average Chl a concentration from the surface to depth z. Separate values, $K_{0,\mathrm{P}}$ and $K_{0,\mathrm{nP}}$, are applied for PAR and non-PAR radiation, respectively. The value of β_{C} is generally of the order of $0.01\,\mathrm{m}^2/\mathrm{mg}$ (Kirk, 2011).

MyLake v.1.2 utilizes the Air-Sea Toolbox (Pawlowicz and Bearsley, 1999) to calculate most of the atmospheric forcing, including surface wind stress and the components of surface heat flux, and the water surface albedo. Aerodynamic bulk formulas are used for sensible heat flux Q_{H}, latent heat flux Q_{L}, and wind shear stress τ, and they are calculated according to the parameterizations and algorithms in Fairall et al. (1996). Simplified, conceptual equations for the quantities can be written as

$$Q_{\mathrm{H}} = \rho_{\mathrm{a}} c_{p\mathrm{a}} C_{\mathrm{h}} U (T_{\mathrm{a}} - T_{\mathrm{s}}) \tag{3.8}$$

$$Q_{\mathrm{L}} = \rho_{\mathrm{a}} L_{\mathrm{e}} C_{\mathrm{l}} U (q_{\mathrm{a}} - q_{\mathrm{s}}) \tag{3.9}$$

$$\tau = \rho_{\mathrm{a}} C_{\mathrm{d}} U^2, \tag{3.10}$$

where ρ_{a} is the air density, $c_{p\mathrm{a}}$ is the specific heat capacity of air, C_{h} and C_{l} are the transfer coefficients of sensible and latent heat, respectively, C_{d} is the drag coefficient, U is the wind speed, T_{a} is the air temperature, T_{s} is the water surface temperature, L_{e} is the latent heat of evaporation of water, q_{a} is the specific humidity, and q_{s} is the saturation specific humidity at the water surface temperature.

Differing from the daily time step approach, the change in water temperature due to heat fluxes is calculated twice a day. The daily heat fluxes are multiplied by the fractions of day when the solar angle is above and below 15° and then applied for daytime and nighttime, respectively. The solar heat flux is applied only in daytime. The heat flux between the water column and the lake bottom and the longwave radiative heat flux penetrating through snow and ice are the only sources of local heating during the ice-covered period. The albedos of snow and ice, α_{s} and α_{i}, respectively, differ from the albedo of the water surface. In addition, in the case of an unstable density profile, natural convection is allowed to mix the unstable layers with a layer below them until a stable density profile is achieved.

Wind-induced mixing in the water column under open water conditions is calculated by balancing the total kinetic energy supplied by wind shear and the change in the potential energy of the water column due to mixing. The kinetic energy is calculated as

$$E_{\mathrm{k}} = W_{\mathrm{str}} A_{\mathrm{s}} \Big(\frac{\tau^3}{\rho_{\mathrm{w}}}\Big)^{0.5} \Delta t, \tag{3.11}$$

where Δt is the model time step and W_{str} is the wind sheltering coefficient, which can be parameterized by the lake surface area (km^2) as (Hondzo and Stefan, 1992)

$$W_{\mathrm{str}} = 1 - e^{-0.3A_{\mathrm{s}}}. \tag{3.12}$$

3.2.2 Biochemical submodel

The biochemical submodel of MyLake v.1.2 simulates the temporal evolution of the vertical distributions of particulate inorganic matter, phytoplankton biomass, and three species of phosphorus. The phytoplankton biomass is represented by Chl *a* concentration. A conservation equation based on Eq. (3.1), including turbulent diffusion and the local sources and sinks, together with an additional advective term that describes the sinking of the particles is applied to the particulate, sedimenting substances S_{IS}, P_{IP}, and P_{Chl}:

$$A\frac{\partial Y}{\partial t} = \frac{\partial}{\partial z}\Big(D_{\mathrm{t}}A\frac{\partial Y}{\partial z}\Big) - A\frac{\partial (wY)}{\partial z} + AS, \tag{3.13}$$

where Y is the concentration of the substance, w is the downward vertical sinking speed, and S is the sum of all the internal sources and sinks of the substance. For the dissolved substances, P_{D} and P_{DO}, $w = 0$ and the equation is structurally similar to Eq. (3.1). Sinking particulate matter eventually settles to the lake bottom from which it can be resuspended into the water column. In addition to the processes in Eq. (3.13), the external substance loads via stream inflow are taken separately into account. The daily stream inflow is inserted on the top of the first layer that has a higher density than the inflow, and a volume of surface water equaling the amount of inflow is considered as outflow and is lost from the lake.

The dynamics of phytoplankton are described through phosphate and Chl *a* concentrations. Phosphate is consumed during phytoplankton growth and released within the degradation of phytoplankton. The elemental composition of phytoplankton is assumed to be fixed, and the phosphorus content of phytoplankton, which is also the representation of particulate organic phosphorus in the model, is given by $P_{\mathrm{Chl}}/y_{\mathrm{c}}$, where y_{c} is a constant yield coefficient. The yield coefficient is defined here as the stoichiometric ratio of biomass formation to nutrient consumption expressed using the mass units of Chl *a* and phosphorus. If the phytoplankton composition is assumed to follow the Redfield mass ratio of carbon to phosphorus of 40 to 1 and if the mass ratio of carbon to Chl *a* in phytoplankton is assumed to be of similar magnitude, y_{c} will be approximately 1. All phytoplankton-related processes are contained in r, the net specific rate of change in Chl *a* concentration, which can be separated into the difference between the specific growth rate μ and the specific loss rate m. The in-lake source and sink term for Chl *a* is thus

$$S_{\mathrm{Chl}} = (\mu - m)P_{\mathrm{Chl}} + R_{\mathrm{Chl,sed}}, \tag{3.14}$$

where $R_{\mathrm{Chl,sed}}$ is the change in water column Chl *a* concentration due to resus-

pension of sedimentary phytoplankton.

The loss of phytoplankton biomass is described as a first-order kinetic processes, meaning that it is linearly proportional to the Chl *a* concentration. Dead phytoplankton is directly remineralized, that is, converted into inorganic substances. The specific loss rate or remineralization rate of phytoplankton depends exponentially on temperature as

$$m = m_{20}\theta^{T-20}, \tag{3.15}$$

where m_{20} is the phytoplankton remineralization rate at 20 °C and the base θ, denoted as the temperature adjustment coefficient, has a value of 1.072 if it is assumed that the rates of biological processes are doubled when temperature increases by 10 °C. The growth of algal biomass is limited by temperature, phosphate concentration, and light intensity $I(z)$, and the temperature-, phosphate-, and light-dependent specific growth rate of phytoplankton is

$$\mu = \mu'_{20}\theta^{T-20} f(P_{\mathrm{D}}(z))g(I(z)), \tag{3.16}$$

where μ'_{20} is the maximal phytoplankton growth rate at 20 °C. The exact functional forms of phosphate and light limitation, $f(P_{\mathrm{D}}(z))$ and $g(I(z))$, are presented in Saloranta and Andersen (2007).

The exchange of particulate inorganic matter and Chl *a* between the water column and the bottom sediment through sedimentation and resuspension is calculated as follows. At the lake bottom, there is an active, mixed sediment layer of thickness $H_{\mathrm{sed}} = 3\,\mathrm{cm}$. The active sediment layer consists of inorganic and organic particles settling from the water column to the bottom of the lake and resuspending back to the water column. The organic sedimenting particles are represented by Chl *a*, and the conversion from the concentration of Chl *a* to the concentration of particulate organic matter in the water column S_{OM} is given by $S_{\mathrm{OM}} = P_{\mathrm{Chl}}/(y_{\mathrm{c}} s_{\mathrm{POM}})$, where s_{POM} is the mass fraction of phosphorus in organic matter. Assuming that the phosphorus fraction follows the Redfield ratio and that the carbon mass content in phytoplankton is 50%, $s_{\mathrm{POM}} = 12\,\mathrm{g/kg}$.

The relative abundances of inorganic and organic particles in the active sediment layer are given by the volume fraction of inorganic matter in the total dry sediment solids ν_{IM}. The concentration of Chl *a* in the sediment solids $P_{\mathrm{Chl,sed}}$ is then calculated as

$$P_{\mathrm{Chl,sed}} = s_{\mathrm{Chl,sed}}\rho_{\mathrm{org}}(1 - \nu_{\mathrm{IM}}), \tag{3.17}$$

where ρ_{org} is the density of organic matter, set to be $1000\,\mathrm{kg/m^3}$ in MyLake, and $s_{\mathrm{Chl,sed}}$ is the mass fraction of Chl *a* in organic sediment particles, which is calculated from the vertical profile of Chl *a* concentration in wet sediment given as initial data.

The change in the Chl *a* concentration in the sediment is calculated through a thickness-weighted average of the Chl *a* concentrations in the old active sediment layer and in the new layer of net sedimented matter. Old sediment equal to the thickness of the daily net sedimentation is buried below the active layer. The

resuspension rate of sediment particles U_{res}, given as an input parameter, is the thickness of the sediment layer that is resuspended in the water column within a day. The change in water column Chl a concentration due to resuspension in layer i in Eq. (3.14) is calculated as

$$R_{\mathrm{Chl},i} = U_{\mathrm{res}} P_{\mathrm{Chl,sed},i} \frac{A_{\mathrm{WS},i}}{V_i}, \tag{3.18}$$

where $A_{\mathrm{WS},i}$, approximated by $A_i - A_{i+1}$, is the area of the water-sediment interface in layer i and V_i is the volume of layer i.

3.2.3 DOC submodule

The degradation of DOC is simulated in a separate submodule FOKEMA incorporated into MyLake v.1.2 (Holmberg et al., 2014). The submodule is based on a three-pool first-order kinetic model for bacterial degradation of DOC by Vähätalo et al. (2010) and on a model for photochemical mineralization by Vähätalo et al. (2000). The additional input data include the initial DOC concentration profile and the time series of the daily inflow concentration of DOC.

In FOKEMA, the total DOC concentration C_{DO} is expressed as a sum of three conceptual, discrete compound classes, also called pools, with concentrations of $C_{\mathrm{DO},i}$:

$$C_{\mathrm{DO}} = C_{\mathrm{DO},1} + C_{\mathrm{DO},2} + C_{\mathrm{DO},3}. \tag{3.19}$$

Each DOC compound class has its own bacterial degradability. The pool with the highest degradability, that is, the labile pool DOC_1, has the highest degradation rate $k_{\mathrm{DOC},1}$. The semilabile pool DOC_2 is degraded at a slower rate $k_{\mathrm{DOC},2}$, and the refractory pool DOC_3 is not affected by bacterial degradation at all ($k_{\mathrm{DOC},3} = 0/\mathrm{d}$). The degradation rates of labile and semilabile DOC are typically of the order of 0.1/d and 0.01/d, respectively (Hopkinson et al., 2002).

The only source of DOC is stream inflow. The inflow of DOC consists of the three pools with constant fractions. The in-lake sinks of DOC are bacterial degradation $d_{\mathrm{DOC,b}}$ and photochemical mineralization P_{B}. Thus, the in-lake source and sink term for DOC is given as

$$S_{\mathrm{DOC,FOKEMA}} = -d_{\mathrm{DOC,b}} - P_{\mathrm{B}}. \tag{3.20}$$

The bacterial degradation of DOC is calculated as

$$d_{\mathrm{DOC,b}} = f_{\mathrm{DOC,FKM}} d_{\mathrm{DOC},T\mathrm{ref}}, \tag{3.21}$$

where $d_{\mathrm{DOC},T\mathrm{ref}}$ is the degradation at a reference temperature, given as

$$d_{\mathrm{DOC},T\mathrm{ref}} = \frac{1}{\Delta t} \sum_{i=1}^{3} (1 - e^{-k_{\mathrm{DOC},i}\Delta t}) C_{\mathrm{DO},i}, \tag{3.22}$$

and $f_{\mathrm{DOC,FKM}}$ is the temperature correction factor based on Tulonen (1993) and defined as

$$f_{\mathrm{DOC,FKM}} = \begin{cases} 1 & T > 5°\mathrm{C} \\ \frac{T}{5} & T \leq 5°\mathrm{C}. \end{cases} \tag{3.23}$$

Photochemical mineralization is largely induced by ultraviolet (UV) radiation located in the high-energy region of the solar radiation spectrum (Vähätalo et al., 2000). UV radiation is attenuated rapidly in the water column, especially in humic lakes (Huovinen et al., 2003). In FOKEMA, all shortwave radiation contributing to photochemical mineralization is assumed to be absorbed in near-surface water, and photochemical mineralization is thus applied only to the topmost grid layer. It is calculated in units of mg/(m^3 d) as

$$P_{\mathrm{B}} = \frac{M(\mathrm{C}) Q_{\mathrm{SW},0}(1-\alpha_{\mathrm{w}})}{\Delta z} \int_{\lambda_{\min}}^{\lambda_{\max}} \phi_\lambda q_\lambda d\lambda, \tag{3.24}$$

where $M(\mathrm{C})$ is the molar mass of carbon, $Q_{\mathrm{SW},0}$ is the incident shortwave radiative heat flux, α_{w} is the water surface albedo, $\lambda_{\min} = 300$ nm and $\lambda_{\max} = 800$ nm are the minimum and maximum wavelengths contributing to photochemical mineralization, ϕ_λ is the spectrum of apparent quantum yield for photochemical DOC mineralization, and q_λ is the monthly spectral scalar photon density above the water surface normalized to an irradiance of 1 W/m^2.

3.3 Air-water gas exchange

The air-water exchange of sparingly soluble gases such as CO_2 and oxygen is controlled by the transport of the gas from or to the air-water interface across a very thin (less than 1 mm) water-side mass boundary layer (MacIntyre et al., 1995). At the surface of the boundary layer, the gases are at equilibrium with the atmosphere and their concentrations are determined by their solubilities. In the mixed surface layer below the boundary layer, dissolved gases are transported by turbulent eddies. The relative effectiveness between diffusive momentum transport and diffusive mass transport near the air-water interface is expressed by the Schmidt number $Sc = \nu/D$, where ν is the kinematic viscosity of water and D is the molecular diffusion coefficient of the gas. With Sc's of around 1000 (Jähne and Haußecker, 1998), the molecular diffusion of a dissolved gas is much slower than the diffusion of momentum in water, and the water-side mass boundary layer is much thinner than the water-side velocity boundary layer. The mass boundary layer is thus relatively stagnant, and gas transfer through it occurs mainly by molecular diffusion. However, also turbulent eddies transport gases within the mass boundary layer and from the mixed layer to the mass boundary layer, and pure molecular diffusion is restricted to a thin laminar layer near the air-water interface.

The flux of a sparingly soluble gas between water and the atmosphere, F_{gas}, can

be parameterized as the product of the concentration gradient between the surface water and the atmosphere and the gas exchange velocity k (Cole and Caraco, 1998) as

$$F_{\mathrm{gas}} = \alpha k(C_{\mathrm{w}} - C_{\mathrm{eq}}), \tag{3.25}$$

where C_{w} is the concentration of the gas in the surface water below the mass boundary layer, C_{eq} is the equilibrium concentration of the gas, and α is the chemical enhancement factor applicable for reactive gases, such as CO_2. However, if a lake is supersaturated with CO_2 and surface water pH in less than 7, the chemical enhancement of CO_2 exchange is negligible, and α can be assumed to be 1 (Portielje and Lijklema, 1995). The equilibrium concentration is calculated by Henry's law as

$$C_{\mathrm{eq}} = MK_{\mathrm{H}}\chi p_{\mathrm{a}}, \tag{3.26}$$

where M is the molar mass of the gas, K_{H} is the Henry's law constant for the gas at surface water temperature, χ is the mole fraction of the gas in the atmosphere, and p_{a} is the atmospheric pressure. The temperature dependence of solubility applied in this work is given in Weiss (1970) for oxygen and Weiss (1974) for CO_2. Here, the flux from water to the atmosphere is defined to be positive. Also, the chemical enhancement of CO_2 flux is omitted hereinafter and α is set to 1. The magnitude of k depends on turbulence in the mass boundary layer. Turbulence is mediated predominantly by wind shear and thermal convection promoted by heat loss from the surface (MacIntyre et al., 2010).

The most simple models for k consider wind shear as the only factor causing turbulence in the near-surface water. In the long used experimental regression formula by Cole and Caraco (1998) k is parameterized by wind speed, and it is given in units of cm/h as

$$k_{\mathrm{CC}} = (2.07 + 0.215U_{10}^{1.7})\Big(\frac{Sc}{600}\Big)^{n}, \tag{3.27}$$

where U_{10} is the wind speed at 10 m. The parameterization is based on k values normalized to a Sc of 600, which is the Sc of CO_2 at 20 °C. For a smooth air-water interface k is proportional to $Sc^{-2/3}$, whereas for an interface with waves k is predicted to be proportional to $Sc^{-0.5}$ (Jähne et al., 1987; Wanninkhof, 1992). The Schmidt number depends significantly on the temperature in the water phase. Although widely applied, the formula has been found to have limitations, especially on a half-hour scale (Åberg et al., 2010; Heiskanen et al., 2014; Mammarella et al., 2015). Thus, more sophisticated models for the gas exchange velocity with physically derived parameterizations have been developed.

3.3.1 Boundary layer and surface renewal models

In addition to purely experimental parameterizations of the gas exchange velocity, many kinds of theoretical formulations have been made (see, e.g., Kraus and Businger, 1994; MacIntyre et al., 1995). More sophisticated modeling of near-

surface turbulence gives further insight into the processes occurring in the mass boundary layer. Gas exchange models that assume that water in the mass boundary layer is intermittently replaced by water from the turbulent layers are called surface renewal models.

If the gas flux is assumed to be maintained only by molecular diffusion in the mass boundary layer, the flux is given by Fick's law (Jähne and Haußecker, 1998):

$$F_{\text{gas}} = D\frac{C_{\text{w}} - C_{\text{eq}}}{\tilde{z}}, \tag{3.28}$$

where $\tilde{z}$ is the thickness of the mass boundary layer, given by Kraus and Businger (1994)

$$\tilde{z} = b\frac{\nu}{u_{*\text{w}}}Sc^{-0.5}, \tag{3.29}$$

where b is an empirical coefficient and $u_{*\text{w}}$ is the water-side friction velocity. Combining Eqs. (3.25), (3.28), and (3.29) yields an equation for the gas exchange velocity obtained by the boundary layer theory:

$$k = bu_{*\text{w}}Sc^{-0.5}. \tag{3.30}$$

The gas exchange velocity is now dependent on the water-side friction velocity, which is a measure for the turbulent velocity fluctuations in the surface water. Heiskanen et al. (2014) developed a model that take into account both wind shear and water-side convection as the generators of turbulence. Thus, the wind-generated $u_{*\text{w}}$ in Eq. (3.30) is replaced by another velocity scale, the total water velocity U_{w}, which can be divided into wind-induced and convection-induced components as

$$U_{\text{w}} = (u_{*\text{ref}}^2 + (C_2 w_*)^2)^{0.5}, \tag{3.31}$$

where w_* is the penetrative convection velocity, C_2 is an empirical coefficient, and $u_{*\text{ref}} = C_1 U$ is the wind-induced water friction velocity at a reference depth, where U is the wind speed at 1.5 m and C_1 is an empirical constant. The penetrative convection velocity, a scale for heat-induced turbulent fluctuations, is defined as (Imberger, 1985)

$$w_* = \begin{cases} (-\beta z_{\text{AML}})^{1/3} & \text{if } \beta < 0, \\ 0 & \text{if } \beta \geq 0, \end{cases} \tag{3.32}$$

where z_{AML} is the depth of the actively mixing layer and β is the buoyancy flux. The actively mixing layer (AML) is defined as the near-surface layer in which the water temperature is within a certain range, usually 0.02 °C, of the temperature at the air-water interface (MacIntyre et al., 2001). Finally, the equation for k by Heiskanen et al. (2014) in units of m/s is

$$k_{\text{HE}} = ((C_1 U)^2 + (C_2 w_*)^2)^{0.5} Sc^{-0.5}, \tag{3.33}$$

where $C_1 = 1.5 \times 10^{-4}$ and $C_2 = 0.07$ were determined experimentally for the study lake. The impacts of wind shear and buoyancy flux were parameterized to

be roughly of the same order of magnitude.

Buoyancy flux is generated by the heat exchange between the AML and the atmosphere. If the buoyancy flux is positive, that is, the AML is gaining heat, the turbulence in the AML is suppressed. If there is heat loss from the AML to the atmosphere and the buoyancy flux is negative, turbulence is generated in the AML through gravitational convection. The buoyancy flux is defined as (Imberger, 1985)

$$\beta = \frac{g\alpha_{\mathrm{t,w}} Q_{\mathrm{eff}}}{\rho_{\mathrm{w}} c_{p\mathrm{w}}}, \tag{3.34}$$

where $\alpha_{\mathrm{t,w}}$ is the thermal expansion coefficient of water and Q_{eff} is the effective heat flux. The effective heat flux is defined as the sum of the net surface heat flux Q_{S} defined in Eq. (3.5) and the fraction of net shortwave radiative heat flux that is trapped in the AML, $Q_{\mathrm{SW,AML}}$:

$$Q_{\mathrm{eff}} = Q_{\mathrm{S}} + Q_{\mathrm{SW,AML}}. \tag{3.35}$$

The penetration of shortwave radiation into the water can be parameterized by the Beer–Lambert law

$$Q_{\mathrm{SW}}(z) = Q_{\mathrm{SW}}(0) e^{-K_{\mathrm{L}} z}, \tag{3.36}$$

where K_{L} is the total attenuation coefficient of shortwave radiation. The net shortwave radiative heat flux trapped in the AML is calculated as

$$Q_{\mathrm{SW,AML}} = Q_{\mathrm{SW}}(0) + Q_{\mathrm{SW}}(z_{\mathrm{AML}}) - \frac{2}{z_{\mathrm{AML}}} \int_0^{z_{\mathrm{AML}}} Q_{\mathrm{SW}}(z) dz. \tag{3.37}$$

In the small eddy version of the surface renewal model, the turbulence generating the mass transfer near the air-water interface is quantified by the dissipation of turbulent kinetic energy of small-scale eddies (MacIntyre et al., 1995). The flow within the smallest eddies is dominated by viscous effects. Mass transfer is considered to occur via molecular diffusion between the interface and the smallest eddies of a length scale l and a velocity scale u. The expression for the mass transfer velocity under these conditions is given as (Banerjee et al., 1968)

$$k = a\Big(\frac{Du}{l}\Big)^{0.5}, \tag{3.38}$$

where a is a dimensionless constant. At the smallest scale in turbulent flow, the length and velocity scales of eddies are dependent only on kinematic viscosity and the kinetic energy dissipation rate ε, and the scales can be obtained by dimensional analysis as

$$l = \Big(\frac{\nu}{\varepsilon}\Big)^{0.25}, \qquad u = (\nu\varepsilon)^{0.25}. \tag{3.39}$$

Equation (3.38) can now be written in the form

$$k = c(\nu\varepsilon)^{0.25} Sc^{-0.5}, \tag{3.40}$$

where c is a dimensionless constant.

The measured dissipation of turbulent kinetic energy can be related to the production of turbulent kinetic energy by wind shear and convection by similarity scaling. Tedford et al. (2014) obtained the total turbulent kinetic energy dissipation rate in terms of shear production $\varepsilon_\mathrm{s} = u_{*\mathrm{w}}^3/\kappa z'$, where κ is the von Kármán constant and z' is a reference depth, and convective production $\varepsilon_\mathrm{c} = \beta$ as

$$\varepsilon_\mathrm{TE} = \begin{cases} \frac{0.56u_{*\mathrm{w}}^3}{\kappa z'} + 0.77\,|\beta| & \text{if } \beta < 0, \\ \frac{0.6u_{*\mathrm{w}}^3}{\kappa z'} & \text{if } \beta \geq 0. \end{cases} \tag{3.41}$$

The wind-induced water friction velocity $u_{*\mathrm{w}}$ can be calculated from the atmospheric friction velocity $u_{*\mathrm{a}}$ as (MacIntyre et al., 1995)

$$u_{*\mathrm{w}} = u_{*\mathrm{a}} \left(\frac{\rho_\mathrm{a}}{\rho_\mathrm{w}} \right)^{0.5}. \tag{3.42}$$

The atmospheric friction velocity can be measured directly (Mammarella et al., 2015) or calculated with the bulk formula Eq. (3.10) using the definition $u_{*\mathrm{a}} = (\tau/\rho_\mathrm{a})^{0.5}$. Thus, the formula for the gas exchange velocity by Tedford et al. (2014), in units of m/s, is

$$k_\mathrm{TE} = c(\nu\varepsilon_\mathrm{TE})^{0.25} Sc^{-0.5}. \tag{3.43}$$

In this work, the constants are defined as $c = 0.5$ and $z' = 0.15\,\mathrm{m}$ as in Erkkilä et al. (2018).

In a regression model by MacIntyre et al. (2010), the gas exchange velocity, in units of cm/h, is parameterized by wind speed depending on the direction of buoyancy flux, that is, separately during the heating and during the cooling of near-surface water:

$$k_\mathrm{MI} = \begin{cases} (2.04U_{10} + 2.0)\left(\frac{Sc}{600}\right)^{-0.5} & \text{if } \beta < 0, \\ (1.74U_{10} - 0.15)\left(\frac{Sc}{600}\right)^{-0.5} & \text{if } \beta \geq 0. \end{cases} \tag{3.44}$$

4 New models for carbon dynamics in lakes

In this chapter, two new models for simulating CO_2 dynamics and carbon cycling in lakes are presented. The first model, hereinafter referred to as MyLake DO-DIC, is essentially a submodel extension added to MyLake v.1.2, and it includes the simulation of DO and DIC. The lake model MyLake v.2 (Couture et al., 2015; de Wit et al., 2018) simulating coupled DO and organic carbon dynamics is partially based on Mylake DO-DIC. The second model, MyLake C (Kiuru et al., 2018), is an extended and more widely upgraded version of MyLake. In MyLake C, lake carbon cycling involves the interplay between physical (temperature, stratification, ice cover, terrestrial hydrologic loading), chemical (pH and inorganic carbon system) and biological (photosynthetic primary production and organic carbon degradation within the water column and in bottom sediments) processes. DIC, dead POC, and DO are additionally incorporated into MyLake C in comparison with MyLake v.1.2. In addition, lake water pH is simulated through hydrogen ion concentration. Some descriptions of phytoplankton and sedimentary processes related to carbon cycling have also been modified compared to the biochemical submodel in MyLake v.1.2.

4.1 MyLake DO-DIC

MyLake DO-DIC includes dissolved oxygen O_{D} and dissolved inorganic carbon C_{DI} as additional model state variables compared to MyLake v.1.2. The processes included in the DO-DIC submodel are illustrated in Fig. 4.1. The formulation of the submodel follows the procedures used in Stefan and Fang (1994) and Omstedt et al. (2009) and the terminology used in Stefan and Fang (1994) in many ways. Biochemical oxygen demand (BOD) within the water column, sediment oxygen demand (SOD), and phytoplankton remineralization are the internal DO sinks and DIC sources, and photosynthesis is the only internal DO source and DIC sink. The production of DIC is thus coupled to the consumption of DO and vice versa, and no other biochemical oxygen-related processes are included. The exchanges of oxygen and DIC between a lake and the terrestrial system and the atmosphere

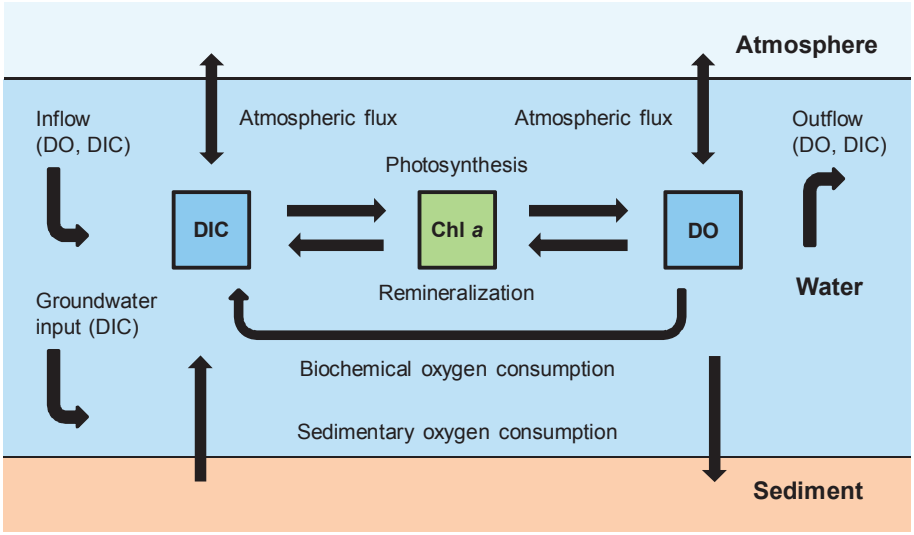

Figure 4.1: Schematic illustration of the lacustrine processes related to the new model state variables (DO and DIC) introduced to MyLake DO-DIC. The state variables related to CO_2 dynamics include gaseous substances (blue boxes) and living organic matter (green box). Biochemical oxygen consumption is related to the microbial degradation of non-phytoplankton-related organic matter within the water column, and sedimentary oxygen consumption is related to the degradation of sedimentary organic matter.

occur through stream inflow, lake outflow and the atmospheric exchange of oxygen and CO_2. Water column pH is set constant in the submodel. The formulas applied for the temperature dependence of the fractionation of DIC are presented in Kiuru et al. (2018). In addition to the input data requirements in MyLake v.1.2, the initial vertical profiles and the daily inflow concentrations of DO and DIC are needed in MyLake DO-DIC.

The evolution of the distributions of DO and DIC is calculated using Eq. (3.13) with $w = 0$. However, a distinction is made between the vertical diffusion coefficient for heat D_h and the vertical diffusion coefficient of dissolved gases D_g, differing from MyLake v.1.2, in which only turbulent diffusion is applied and the same vertical turbulent diffusion coefficient, D_t, is used for thermal energy and all substances. The vertical diffusion mechanics for heat and dissolved gases are commonly assumed to be similar during the open water season (Stefan and Fang, 1994), but the effect of other diffusion mechanisms than molecular diffusion is smaller when a lake is ice-covered. The molecular diffusivities of DO and CO_2 in water at 20 °C, $1.1 \times 10^{-3}\,\mathrm{mm^2/s}$ (Han and Bartels, 1996) and $1.2 \times 10^{-3}\,\mathrm{mm^2/s}$ (Maharajh and Walkley, 1973), respectively, are considerably lower than the thermal diffusivity of water, $0.14\,\mathrm{mm^2/s}$ (Bergman et al., 2011). Hence, turbulence drives diffusion and $D_\mathrm{g} = D_\mathrm{h}$ in MyLake DO-DIC during the open water season,

and a constant factor $a_{\mathrm{ice}} = 0.01$ is used in order to take into account the difference between the diffusion rates of heat and dissolved gases during the ice-covered period as $D_{\mathrm{g}} = a_{\mathrm{ice}} D_{\mathrm{h}}$.

The in-lake source and sink term for DO is given as

$$S_{\mathrm{O2}} = P - R - S_{\mathrm{BOD}} - S_{\mathrm{SOD}} - \frac{F_{\mathrm{O2}}}{\Delta z}, \tag{4.1}$$

where P is the DO production by photosynthesis; R is the DO consumption by phytoplankton remineralization; S_{BOD} is the non-phytoplankton-related biochemical DO consumption in the water column, referred to shortly as biochemical oxygen consumption; S_{SOD} is the sedimentary oxygen consumption; and F_{O2} is the air-water flux of oxygen. The DO flux is applied only to the topmost grid layer. Accordingly, the term for CO_2 is

$$S_{\mathrm{CO2}} = -\frac{M(\mathrm{CO_2})}{M(\mathrm{O_2})} Q_{\mathrm{r}} (P - R - S_{\mathrm{BOD}} - S_{\mathrm{SOD}}) - \frac{F_{\mathrm{CO2}}}{\Delta z}, \tag{4.2}$$

where F_{CO2} is the air-water flux of CO_2, $M(CO_2)$ and $M(O_2)$ are the molar masses of CO_2 and oxygen, respectively, and Q_{r} is the respiratory quotient, that is, the molar ratio of CO_2 production to DO consumption. The air-water exchange of DO and CO_2 is calculated with Eq. (3.25) using the gas exchange velocity formula by Cole and Caraco (1998), Eq. (3.27), with $n = -2/3$ and the dependence of Sc on water temperature given by Wanninkhof (1992). In addition, the effect of sheltering on wind speed is taken into account by multiplying the observed wind speed by $W_{\mathrm{str}}^{1/3}$, where W_{str} (Eq. (3.12)) is the wind sheltering coefficient. Also, the chemical enhancement factor α is applied as a calibration parameter referred to as the air-water CO_2 flux adjustment factor, and it is not restricted to values greater than or equal to 1. The external inputs of DO and DIC through inflow are included in the model similarly to the substances in MyLake v.1.2. The effect of groundwater DIC load is taken into account by multiplying the DIC inflow concentration by a scaling factor $C_{\mathrm{DI,IN}}$. The extra inflowing DIC is then mixed with the bottommost layer of the lake.

The production and loss of DO through photosynthesis and remineralization, respectively, are proportional to the growth and loss rates of phytoplankton biomass. The DO production by photosynthesis is

$$P = s_{\mathrm{O2}} \mu P_{\mathrm{Chl}}, \tag{4.3}$$

where μ is the specific growth rate of phytoplankton defined in Eq. (3.16), and the DO consumption by phytoplankton remineralization is

$$R = s_{\mathrm{O2}} m P_{\mathrm{Chl}}, \tag{4.4}$$

where m is the remineralization rate of phytoplankton (Eq. (3.15)). The value of the stoichiometric constant s_{O2} derived from the Redfield ratio is 110 assuming

that $y_c = 1$.

The descriptions of biochemical and sedimentary oxygen consumption follow the DO model presented by Stefan and Fang (1994). The temperature dependence of the consumption processes is assumed to be similar to that of phytoplankton processes, and consumption is assumed to slow down substantially at temperatures below 4 °C during the ice-covered period. Biochemical oxygen demand originates from microbial decomposition of organic matter in the water column. The biochemical oxygen consumption S_{BOD} is a function of the mass of dead organic matter expressed in oxygen equivalents:

$$S_{\mathrm{BOD}} = \begin{cases} k_{\mathrm{BOD}} \theta_{\mathrm{BOD}}^{T-20} D_{\mathrm{BO}} & \text{during the open water season,} \\ k_{\mathrm{BOD}} e^{-a_{\mathrm{OD}}(4-T)} \theta_{\mathrm{BOD}}^{-16} D_{\mathrm{BO}} & \text{during the ice-covered period,} \end{cases} \tag{4.5}$$

where D_{BO} is the biochemical oxygen demand (BOD), that is, non-phytoplankton-related dead organic matter in oxygen equivalents, k_{BOD} is the organic decomposition rate at 20 °C, θ_{BOD} is the temperature adjustment coefficient for k_{BOD} in the open water season, and a_{OD} is the temperature adjustment factor for temperatures below 4°C during the ice-covered period. A depth- and time-independent value for BOD is employed in the model, and there is no external inflow of BOD. A value of 0.1/d is applied for k_{BOD} (Stefan and Fang, 1994). A value of 1.047 is commonly used for the temperature adjustment coefficient (Bowie et al., 1985). Organic decomposition rate possibly approaches zero at lower temperatures; thus, two values for θ_{BOD} are used: $\theta_{\mathrm{BOD}} = 1.047$ as $T \geq 10$ °C and $\theta_{\mathrm{BOD}} = 1.13$ as $T < 10$ °C.

The rate of sedimentary oxygen consumption in grid layer i depends on the area of bottom sediments in contact with water and is given by

$$S_{\mathrm{SOD},i} = \begin{cases} S_{\mathrm{b}} \theta_{\mathrm{SOD}}^{T_i-20} \frac{A_{\mathrm{WS},i}}{V_i} & \text{during the open water season,} \\ S_{\mathrm{b}} e^{-a_{\mathrm{OD}}(4-T_i)} \theta_{\mathrm{SOD}}^{-16} \frac{A_{\mathrm{WS},i}}{V_i} & \text{during the ice-covered period,} \end{cases} \tag{4.6}$$

where S_{b} is the sediment oxygen demand (SOD) at 20 °C and θ_{SOD} is the temperature adjustment coefficient for SOD in the open water season. The sediment oxygen demand is independent of both depth and time. The temperature adjustment coefficient has a reported range of 1.04 to 1.13, and a value of 1.065 is generally applied (Bowie et al., 1985). Below 10 °C the sediment oxygen demand decreases fast and comes close to zero when the temperature is less than 4 °C. Therefore, two different values for θ_{SOD} are applied in the model: $\theta_{\mathrm{SOD}} = 1.065$ as $T \geq 10$ °C and $\theta_{\mathrm{SOD}} = 1.13$ as $T < 10$ °C (Stefan and Fang, 1994).

The consumption of DO is possibly limited by the supply of oxygen below the concentration of 30–90 mmol/m^3 in wintertime (Mathias and Barica, 1980; Meding and Jackson, 2001). This effect is incorporated into the model by the linear suppression of both k_{BOD} and S_{b} when the DO concentration is below a threshold concentration $O_{\mathrm{D,T}} = 93.75$ mmol/m^3. It is applied both in the ice-covered period and in the open water season. The modified organic decomposition rate and

sediment oxygen demand are hence

$$k'_{\mathrm{BOD}} = \frac{O_{\mathrm{D}}}{O_{\mathrm{D,T}}} k_{\mathrm{BOD}} \qquad \text{when } O_{\mathrm{D}} < O_{\mathrm{D,T}}, \tag{4.7}$$

$$S'_{\mathrm{b}} = \frac{O_{\mathrm{D}}}{O_{\mathrm{D,T}}} S_{\mathrm{b}} \qquad \text{when } O_{\mathrm{D}} < O_{\mathrm{D,T}}. \tag{4.8}$$

4.2 MyLake C

The new state variables in MyLake C in comparison with MyLake v.1.2 are the three fractions of DIC, including CO_2; dead POC, hereafter referred to as POC, C_{PO}; hydrogen ion H^+; and DO. The hydrogen ion concentration is related to lake water pH as $[H^+] = 10^{-\mathrm{pH}}$. In addition, MyLake C uses an upgraded version of FOKEMA for the description of DOC degradation. The carbon-related in-lake processes included in MyLake C are illustrated in Fig. 4.2. The exchanges of oxygen, DIC, POC, and H^+ between a lake and the terrestrial system occur through stream inflow and lake outflow, and the atmospheric exchanges of oxygen and CO_2 is described similarly to MyLake DO-DIC. Groundwater exchange is not included in MyLake C. The additional input data compared to MyLake v.1.2 consists of the initial concentration profiles and the daily time series of the inflow concentrations of DO, DIC, POC, and H^+.

The spatiotemporal evolution of the new state variables is calculated using Eq. (3.1) with $w = 0$ for the dissolved substances (DO, DIC, and H^+) and with $w = w_{\mathrm{POC}}$ equal to the sinking speed of phytoplankton, w_{Chl}, for POC. For simplicity, contrary to MyLake DO-DIC, MyLake C uses the vertical turbulent diffusion coefficient D_{t} for both heat and dissolved gases. The description of the fractionation of DIC is similar to that in MyLake DO-DIC with the additional inclusion of changes in alkalinity due to biochemical processes (see Kiuru et al., 2018). Unlike in MyLake v.1.2., the attenuation of light in the water column is explicitly dependent on the concentrations of both phytoplankton and DOC because DOC dynamics are fully integrated into MyLake C instead of being simulated in a separate submodule. The non-chlorophyll-related PAR attenuation coefficient $K_{0,\mathrm{P}}$ in Eq. (3.7) has been replaced by a coefficient dependent on DOC concentration:

$$\overline{K}_{\mathrm{DOC,P}}(z) = \beta_{\mathrm{DOC}} \overline{C}_{\mathrm{DO}}(z), \tag{4.9}$$

where β_{DOC} is the DOC-related specific PAR attenuation coefficient of water and $\overline{C}_{\mathrm{DO}}(z)$ is the average DOC concentration from the surface to depth z.

The organic carbon in the water column is composed of three classes: living particulate organic carbon $\mathrm{POC_L}$, represented by the carbon content in phytoplankton; POC; and DOC. $\mathrm{POC_L}$ transforms into POC that further transforms into DOC through fragmentation. POC is divided into two pools according to its origin. Dead phytoplankton is classified as autochthonous POC, which converts to DOC relatively fast. The other pool, allochthonous POC, enters the lake through

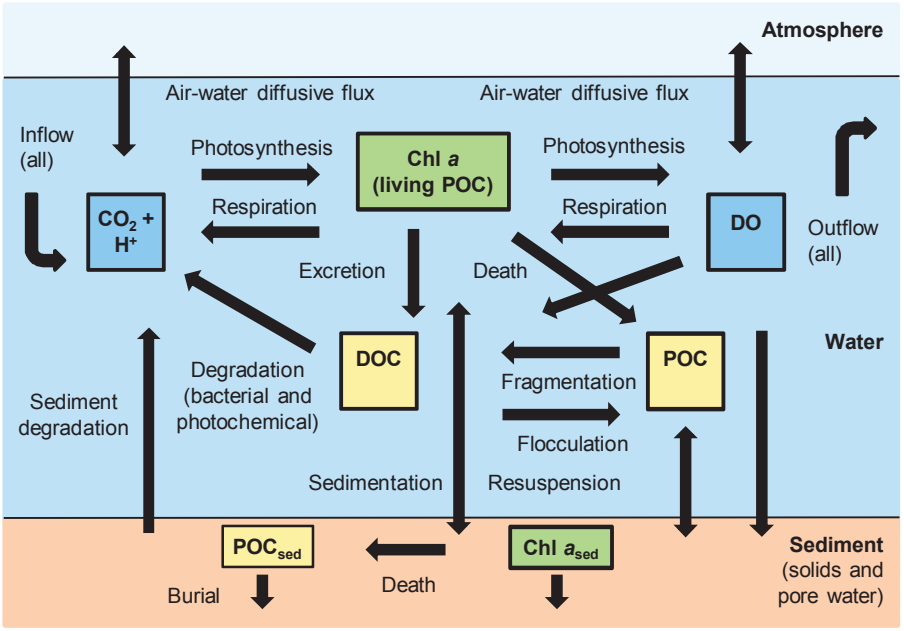

Figure 4.2: Schematic illustration of the lacustrine carbon processes related to the new model state variables (CO_2, H^+, DO, and POC) in MyLake C. The state variables included in carbon cycling consist of gaseous substances (blue boxes) and species of living organic carbon (green boxes) and dead organic carbon (yellow boxes). [Modified from Kiuru et al. (2018).]

stream inflow and has a slower fragmentation rate. MyLake C uses an upgraded version of FOKEMA for the description of DOC degradation. The labile pool DOC_1 is formed through fragmentation of autochthonous POC. Fragmentation of allochthonous POC produces DOC_2 and DOC_3 in equal proportions because allochthonous POC is assumed to be generally rather weakly degradable but not completely refractory, similarly to allochthonous DOC. Finally, organic carbon in the water column is mineralized to CO_2 through the degradation of DOC.

The description of sedimentary organic carbon degradation is integrated with the slightly modified sediment-water interaction procedures in the biochemical submodel of MyLake v.1.2. Living sedimentary particulate organic carbon POC_{Lsed} corresponds to sedimentary organic matter in MyLake v.1.2, and its concentration is expressed through $P_{Chl,sed}$. In addition, dead sedimentary particulate organic carbon POC_{sed} is introduced into the model. POC_L and POC in the water column settle to the bottom sediment, and POC_{Lsed} and POC_{sed} are resuspended into the water column. Both POC_{Lsed} and POC_{sed} degrade directly into CO_2 without a dissolved phase. The in-lake source and sink term for POC in the water column is given as

$$S_{POC} = d_{Chl} + F - d_{POC} + S_{POC,sed}, \tag{4.10}$$

where d_{Chl} is the conversion of phytoplankton to POC, F is the loss of allochthonous DOC due to flocculation (von Wachenfeldt and Tranvik, 2008), d_{POC} is the fragmentation of POC to DOC, and $S_{POC,sed}$ is the resuspension of POC_{sed}. The corresponding term for DOC is

$$S_{DOC} = d_{POC} + E - F - d_{DOC}, \tag{4.11}$$

where E is the amount of excretion of labile DOC from phytoplankton (Baines and Pace, 1991) and d_{DOC} is the degradation of DOC to CO_2.

The in-lake source and sink term for DO is given as

$$S_{DO} = P - R - D_{DOC} - D_{sed} - \frac{F_{O2}}{\Delta z}, \tag{4.12}$$

where P is oxygen production through photosynthesis, R is oxygen consumption through phytoplankton respiration, D_{DOC} is oxygen consumption via DOC degradation, D_{sed} is oxygen consumption via sedimentary organic carbon degradation, and F_{O2} is the air-water flux of oxygen. The in-lake source and sink term for CO_2 is

$$S_{CO2} = D'_{DOC} + D'_{sed} + R' - P' - \frac{F_{CO2}}{\Delta z}, \tag{4.13}$$

where D'_{DOC} is CO_2 production through DOC degradation, D'_{sed} is CO_2 production through sedimentary POC degradation, R' is CO_2 production through phytoplankton respiration, P' is CO_2 consumption in photosynthesis, and F_{CO2} is the air-water flux of CO_2. The air-water fluxes are calculated using Eq. (3.25) and Eq. (3.27) with $n = -2/3$ and the dependence of Sc on water temperature by Wanninkhof (1992). All the equations applied in Eqs. (4.10) to (4.13) are described

in detail in Appendix A.

4.2.1 Alternative gas exchange models

In this work, three alternative models for the gas exchange velocity in addition to the widely used default model by Cole and Caraco (1998) (Eq. (3.27)) were incorporated into MyLake C and their performance was assessed. The additional models were the boundary layer model by Heiskanen et al. (2014) (Eq. (3.33)), the surface renewal model by Tedford et al. (2014) (Eq. (3.43)), and the regression model by MacIntyre et al. (2010) (Eq. (3.44)). In contrast to the original parameterization in MyLake C, a value of -0.5 was used for n in Eq. (3.27) to make the results comparable with experimental studies, in which $n = -0.5$ has been used. The depth of the actively mixing layer z_{AML} in Eq. (3.32), applied in the model by Heiskanen et al. (2014), and in Eq. (3.37), applied in all models but the one by Cole and Caraco (1998), was specified as the thickness of the layer in which the water column temperature is within 0.02 °C of the temperature in the topmost grid layer before the wind-induced mixing of the epilimnion.

5 Experimental data

In this work, the presented carbon models are applied for the simulation of DO and CO_2 dynamics and air-water CO_2 flux in two study lakes. An application of MyLake DO-DIC is built for Lake Valkea-Kotinen. MyLake C is applied to Lake Kuivajärvi for comparing different models for air-water CO_2 exchange and for climate impact analysis. In this chapter, the characteristics of the lakes and the observational data used as model forcing and in model calibration and performance assessment are described.

5.1 Study lakes

Lake Valkea-Kotinen and Lake Kuivajärvi are humic, dimictic lakes in southern Finland (see Fig. 5.1). Characteristics of the lakes and their catchments are listed in Table 5.1. The depth-area graphs, or the hypsometric curves, for the lakes are presented in Fig. 5.2.

Lake Valkea-Kotinen is a small, acidic, and mesotrophic headwater lake situated in the Kotinen nature reserve area in Evo in southern Finland. The lake is sheltered by the surrounding forest, which prevents high winds from mixing the water. The lake has no inlet, but it has a small outlet stream in the southeast end. Lake Valkea-Kotinen can be regarded as a seepage lake tightly connected with the groundwater in the surrounding catchment area (Rasilo et al., 2012). The catchment area of the lake consists of old pristine forest and a small area of peatland (Vuorenmaa et al., 2014). The catchment has been a site of intensive, multidisciplinary ecosystem monitoring. Lake Valkea-Kotinen, as well as the catchment, is an International Cooperative Programme on Integrated Monitoring of Air Pollution Effects on Ecosystems (ICP IM) monitoring site.

Lake Valkea-Kotinen is strongly stratified both thermally and chemically. Stratification begins to develop early in spring, and the spring turnover is short or incomplete (Salonen et al., 1984). In summer, the thermocline depth is usually 2–2.5 m and the hypolimnion is anoxic because of the incomplete spring turnover. The lake is very productive for a humic lake, but the primary production is restricted to the uppermost 1.5–2 m because of a dark water color and low water transparency (Keskitalo et al., 1998). The dark water color is due to high DOC

Figure 5.1: Locations of the study lakes.

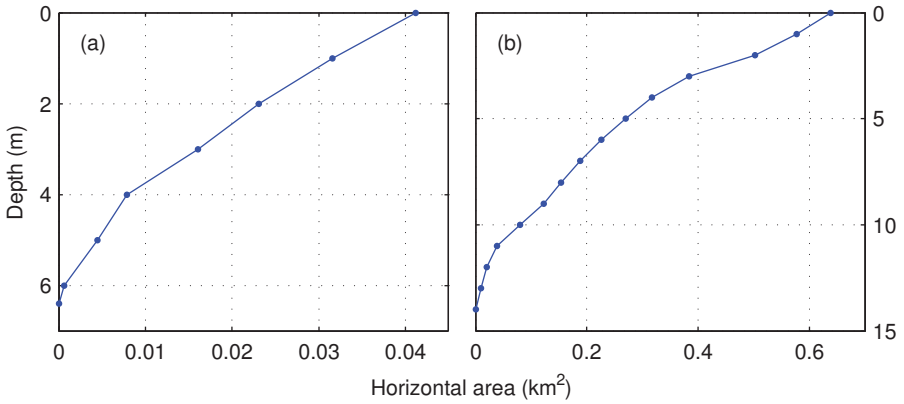

Figure 5.2: Hypsometric curves of (a) Lake Valkea-Kotinen and (b) Lake Kuivajärvi.

Table 5.1: Characteristics of the study lakes.

	Valkea-Kotinen	Kuivajärvi
Location		
Latitude/Longitude	61°14′N, 25°3′E	61°50′N, 24°16′E
Elevation (m.a.s.l.)	156	141
Morphometry		
Surface area (km^2)	0.041	0.64
Maximum length (km)	0.46	2.6
Maximum width (km)	0.13	0.3
Maximum depth (m)	6.4	13.2
Mean depth (m)	2.5	5.0
Volume (10^6 m^3)	0.10	3.2
Residence time (yr)	1.0[a]	0.65
Chemistry		
Mean pH	5.4[a]	6.3
Mean alkalinity (mmol/l)	0.02[a]	N/A
Mean DOC concentration (mg/l)	12–13[a]	12–14[b]
Mean inlet pH	N/A	6.5[c]
Catchment characteristics		
Area (km^2)	0.22[a]	9.4[b]
Primary soil type	Dystric Cambisol[a]	Haplic Podsol[b]
Climate characteristics[d]		
Mean annual temperature (°C)	4.2	3.5
Mean annual precipitation (mm)	645	711

[a]Vuorenmaa et al. (2014), [b]Miettinen et al. (2015), [c]Dinsmore et al. (2013b), [d]Pirinen et al. (2012)

loading from the catchment. Degradation of organic carbon of terrestrial origin may also be a significant source of the high CO_2 concentration in the water column. The CO_2-rich hypolimnion is separated from the epilimnion during summer because of steep stratification, which results in surface water being depleted in CO_2 by primary producers under bright conditions in daytime. The possible deficit can only be replaced from the atmosphere (Vesala et al., 2006).

Lake Kuivajärvi is an elongated, mesotrophic two-basin lake in Hyytiälä in southern Finland. The catchment area of Lake Kuivajärvi is mainly flat and consists of managed pine forests together with small amounts of peatland and agricultural land (Miettinen et al., 2015). The main inlet stream drains four upstream lakes, which are smaller in area than Lake Kuivajärvi. Similarly to Lake Valkea-Kotinen, the lake is characterized by a rather high DOM content, mainly originated from the catchment. The spring turnover usually happens quickly in the lake, and stratification develops soon after ice-off. The thermocline is located at around 4–6 m depth during summertime. The hypolimnion usually becomes anoxic in late summer but not during wintertime (Miettinen et al., 2015).

Lake Kuivajärvi is located in the vicinity of the Station for Measuring Ecosystem–Atmosphere Relations (SMEAR II) (Hari and Kulmala, 2005). The station is used for continuous, comprehensive measurements of meteorology and material and energy exchange in the land ecosystem–atmosphere continuum. SMEAR II is also a part of the pan-European research infrastructure Integrated Carbon Observation System (ICOS) measuring network (Heiskanen et al., 2014). There is a measuring platform called Lake-SMEAR for continuous lake measurements at the center of the deeper south basin of Lake Kuivajärvi, forming an ICOS Associate Ecosystem Station (Miettinen et al., 2015). An EC measurement system on the platform measures the turbulent fluxes of momentum, heat, CO_2, and water vapor over the lake. In addition, automatic high-frequency water column temperature and CO_2 concentration measurements are performed on the platform. Shortwave and longwave radiation components and many meteorological variables, including air temperature, wind speed, and relative humidity, are also measured directly on the platform. All measurement data are presented as half-hour averages. A detailed description of the meteorological and EC measurements and of the postprocessing of the EC data used in this work is given in Mammarella et al. (2015), and the water column measurements are described in Heiskanen et al. (2014).

5.2 Model forcing and calibration data

5.2.1 Lake Valkea-Kotinen

Meteorological forcing data
The daily or subdaily observations of global radiation, cloud cover, air temperature, relative humidity, air pressure, wind speed, and precipitation from the Jokioinen weather station (Finnish Meteorological institute, FMI), located about 95 km to

the south-west from Lake Valkea-Kotinen, in 2001–2005 were used as meteorological forcing of the model. All the subdaily time series were integrated to daily values. The atmospheric CO_2 mixing ratio was set to 380 ppm (IPCC, 2007).

Hydrological loading data

Because Lake Valkea-Kotinen is a headwater lake, inflow measurements were not available. Instead, discharge estimates from catchment models were used. The daily time series of surface discharge was obtained from the application of the hydrological model HBV (Bergström, 1992; Sælthun, 1996) to the catchment of Lake Valkea-Kotinen by Holmberg et al. (2014). The daily concentrations of total phosphorus and particulate inorganic matter in the surface discharge were obtained from the Watershed Simulation and Forecasting System (WSFS-VEMALA) (Finnish Environment Institute, SYKE). The WSFS-VEMALA model (Huttunen et al., 2016) simulates hydrology and water quality for all river basins in Finland. The hydrological part of the model is based on the HBV model, and it simulates the hydrological cycle on a one-day time step using standard meteorological data. The water quality component of the model simulates the erosion and leaching of total phosphorus, total nitrogen, suspended solids, and total organic carbon from terrestrial areas and the concentrations of these substances in rivers and lakes on a daily time step.

The concentration of dissolved organic phosphorus in the surface discharge was not known, and it was assumed to be 20% of total phosphorus, which is a conservative estimate of the proportion of the dissolved fraction of organic phosphorus from unmanaged forested catchments (Mattsson, 2010). The concentration of DIC was also unknown, and it was set to a constant value of $20\,g/m^3$, which is roughly in the range of the measurements from small forested headwater catchments in the boreal zone (Rantakari et al., 2010). The atmospheric equilibrium concentration was used for the discharge concentration of DO.

Initial profile data

The definitions of the initial water column concentration profiles of total phosphorus, Chl *a*, and DO were based on the measurements performed on 10 May 2001 available in the HERTTA database (SYKE). Chl *a* concentration was measured at the surface layer (0–2 m), total phosphorus concentration at depths of 1, 3, and 5.7 m, and DO concentration at depths of 1, 3, 4, and 5.7 m. The initial profiles of total phosphorus and DO were obtained by linearly interpolating these values to the model depth levels. For Chl *a*, a nearly homogeneous concentration profile in the epilimnion and a negligible concentration in the hypolimnion was estimated. The initial water temperature profile was interpolated from the measurements at depths of 0.1, 0.5, 1, 1.5, 2, 2.5, 3, 3.5, and 4.5 m on 5 May 2001 obtained from Holmberg et al. (2014). Homogeneous initial profiles were estimated for particulate inorganic matter and dissolved organic phosphorus. The initial DIC concentration was estimated on the basis of the DO concentration profile. The pH value of the lake was set to 5.3.

Calibration data
The daily averages of the measured lake water temperature profiles in 2001–2003 and the lake water temperature observations in 2004–2005 were obtained from Holmberg et al. (2014). The measurements in 2001 and 2002 covered almost the whole respective open water seasons, whereas in 2003 the measurement period was extended from March to the end of December, thus containing also periods under ice-covered conditions. The observations in 2004–2005 were temporally irregular, and they were conducted on average twice a week during the open water seasons. The temperature measurements were performed at depths of 0.1, 0.5, 1, 1.5, 2, 2.5, 3, 3.5, and 4.5 m in 2001–2003 and at depths of 0, 1, 2, 2.5, 3, 4, 5, and 6 m in 2004–2005.

The measurements of the in-lake concentrations of total phosphorus at 1 m, Chl *a* at 0–2 m, and DO at 1, 3, and 5 m in 2001–2005 were obtained from HERTTA. The measurements of total phosphorus and Chl *a* concentrations were conducted approximately once a month during the open water seasons. The DO measurements were carried out about once a month from March to December in 2001, 2002, and 2004 and from March to October in 2003 and 2005. The determination of CO_2 concentration profiles was carried out once a month from October 2002 to October 2003. The manual measurements were performed at 1 m intervals from the surface to the depth of 6 m. In April 2005 to October 2006, automatic CO_2 concentration measurements were performed at the depths of 0.1, 0.5, and 1.5 m (Huotari et al., 2009).

5.2.2 Lake Kuivajärvi

The MyLake C application to Lake Kuivajärvi was calibrated in two stages. The first calibration was performed for the use of the model in climate impact analysis (Chapter 8). The second calibration stage consisted of recalibrations of the application with the same input data and initial data but with alternative gas exchange models (Chapter 9). The two stages are hereafter referred to as the initial calibration and the recalibrations, respectively.

Meteorological forcing data
The daily averages of incoming shortwave radiation and wind speed during the period for model calibration and validation, years 2013–2014, were obtained from the platform measurements. However, the incoming shortwave radiation was altered by a factor of 0.9, which resulted in a better correspondence between the simulated and the observation-based water column heat volume development in preliminary model calibration. The better correspondence may be explained by the fact that the north-south-oriented oblong lake is partly shaded by the surrounding forests especially during seasons in which the maximum solar angle is low. SMEAR II data were used for air temperature, relative humidity, and atmospheric pressure. In addition, SMEAR data on wind speed were used on days with missing platform data. Cloud cover data were obtained from the Hyytiälä weather station (FMI),

and precipitation data were obtained from the nearest available weather station in Tikkakoski, located about 95 km to the north-east from the lake. The CO_2 mixing ratio in the atmosphere was assumed to be 380 ppm (IPCC, 2007) in the first model calibration. It was increased to a value of 395 ppm, which was better in accordance with the rather sporadic in situ measurements during the calibration period, in the recalibrations.

Hydrological loading data

Continuous measurements of the discharges at the main inlet and at the outlet of Lake Kuivajärvi in 2013 and 2014 (see Dinsmore et al., 2013b) were used as the basis for the inflow volume time series. The daily inlet discharge volumes were multiplied by 2 in order to take into account the discharge from smaller inlets and to be better in accordance with the measured outlet discharge volume. Water temperature at the main inlet was measured approximately two times a month in 2013 and continuously in 2014. DOC and CO_2 concentrations and pH at the main inlet were measured two times a month in 2013 but mostly at intervals of 2 to 3 days in late April and early May. Daily time series for DOC and CO_2 concentrations and pH were obtained through interpolation. Inflow POC concentration was set to be 5% of the inflow DOC concentration, which is close to the average ratio in Finnish catchments (Kortelainen et al., 2006; Mattsson et al., 2005). The inflowing DOC was divided in semilabile (19%) and refractory (81%) pools (Søndergaard and Middelboe, 1995). Inflow total phosphorus concentration had a constant value of $20\,mg/m^3$. The proportion of dissolved organic phosphorus of total phosphorus was estimated to be 45% on the basis of Mattsson (2010). An estimate of the DO saturation percentage in rivers in southern Finland based on Niemi and Raateland (2007), 90%, was applied in calculating the inflow DO concentration.

Initial profile data

The initial water column temperature profile was obtained from the daily averages of the automatic high-frequency measurements at 16 depths between 0.2 and 12 m. The initial vertical profiles of pH and DO, CO_2, and DOC concentrations were obtained by linearly interpolating the values from manual measurements to the model depth levels. The measurements were performed on the day before the first day of the calibration period, and they include DOC concentration and pH at the surface and near the bottom, DO concentration at 0.5 m intervals from the surface to 9 m and at 10, 11, and 12 m, and CO_2 concentration at 0.2 m, at 2 m intervals from 1 m to 11 m, and at 12 m. The refractory fraction of DOC was set to be 85% (Søndergaard and Middelboe, 1995; Tulonen, 2004). The initial POC concentration was estimated to be 10% of DOC concentration (Wetzel, 2001), and 98% of it was set to be allochthonous. The initial total phosphorus concentration profile was obtained by interpolation from the yearly median concentrations in the surface water and at 12 m given in Miettinen et al. (2015). The initial concentration profile of particulate inorganic matter was estimated to be homogeneous. The initial volume fraction of inorganic matter in sediment was assumed to be 60%, which is close to the median value for small lakes located nearby (Pajunen, 2004).

Calibration and performance assessment data

Automatic high-frequency water column temperature and CO_2 concentration measurement data during the years 2013–2014 were used in both stages of the calibration and performance assessment of the Lake Kuivajärvi application. In addition, manual water column CO_2 and DO concentration measurement data from January 2013 to October 2014 were used in the first model calibration and validation. The automatic CO_2 concentration measurements were performed at 0.2, 1.5, 2.5, and 7 m. Manual CO_2 and DO concentration profile measurements were made once a week during the open water seasons and twice a month during the ice-covered period (see Miettinen et al., 2015). Measurements of pH near the surface and near the bottom were performed about twice a month in January–October 2013.

Additional meteorological measurement data were applied in assessing the performance of different gas exchange models incorporated into MyLake C during May–October 2013. The simulated longwave radiative heat flux and sensible and latent heat fluxes were compared to the observations, and the simulated gas exchange velocities for CO_2 were compared to those calculated with the gas exchange models using measurement data as input (hereafter referred as to calculated gas exchange velocities). The measurements included on-lake measurements of net surface longwave radiation and EC measurements of sensible heat flux, water vapor flux, and momentum flux. In EC data postprocessing, latent heat flux was calculated from the water vapor flux, and the atmospheric friction velocity was derived from the momentum flux.

Contrary to the model forcing data, air temperatures used in the calculation of the gas exchange velocities were obtained from the platform measurements instead of SMEAR II on 44 days mainly in May–July, and only days on which platform measurements of wind speed were available were included in the calculation. The average difference between the applied platform temperature measurements and the corresponding SMEAR II measurements during the whole period was only 0.02 °C, but the variation in the half-hour values was higher in the SMEAR II measurements (daily values: coefficient of determination $R^2 = 0.80$, root-mean-square error (RMSE) = 1.57 °C, $n = 44$; half-hour values: $R^2 = 0.84$, RMSE = 1.88 °C, $n = 2112$). On average, SMEAR II temperatures were lower than platform temperatures in May (difference −0.96 °C, 15 days) and June (−0.33 °C, 9 days) and higher in July (0.74 °C, 15 days). However, the resultant discrepancies in the calculated gas exchange velocities were minor or negligible, depending on the gas exchange model. In addition, the rather intermittent relative humidity data from the platform were used. Missing humidity values were replaced by a value of 75% in the calculation of air density needed for the determination of water-side friction velocity.

There were gaps in the heat flux data due to short-term system malfunction and a longer gap on 14–27 June, and some of the existing heat flux data were left out through the application of EC data quality screening criteria similar to those described in Erkkilä et al. (2018). The monthly proportion of accepted half-hour data varied from 43 to 69% for sensible heat flux and from 32 to 70% for latent

heat flux. Gap-filled half-hour time series for sensible and latent heat fluxes were constructed using regression models depending on wind speed multiplied by the difference between air and surface water temperatures for sensible heat flux and on wind speed multiplied by the vapor pressure difference for latent heat flux. Only the vapor pressures based on the measured values of relative humidity were used in the regression. The regression coefficients were determined through a linear fit according to Mammarella et al. (2015). The fitting was made separately for each month.

The daily average of the depth of the actively mixing layer was estimated from the daily averaged temperature profiles as the depth at which the temperature was within 0.25 °C of the surface temperature, similarly to Erkkilä et al. (2018), because of the precision of the temperature probes. A constant value of $2\,\mathrm{m}^{-1}$ was used for the shortwave radiation attenuation coefficient K_L in the calculation of the net shortwave radiation trapped in the actively mixing layer $Q_{\mathrm{SW,AML}}$ in Eq. (3.37) as in Mammarella et al. (2015). The calculated CO_2 exchange velocities for each gas exchange model were obtained using the daily averages of measured variables, and the calculated air-water CO_2 fluxes were obtained as the product of the calculated CO_2 exchange velocities and the daily average of the measured CO_2 concentration gradient. The atmospheric equilibrium concentration was calculated from the measured atmospheric CO_2 mixing ratio.

6 Model calibration and climate impact analysis

In this chapter, the procedures used in the calibration of the MyLake DO-DIC application to Lake Valkea-Kotinen and in the two calibration stages of the MyLake C application to Lake Kuivajärvi are described. In addition, forcing data for climate impact analysis performed with the Lake Kuivajärvi application is presented.

The goodness-of-fit metrics applied in all calibrations were the coefficient of determination (R^2), the root-mean-square error (RMSE), the Nash–Sutcliffe efficiency (NS), the normalized bias (B^*), and the normalized unbiased root-mean-square difference (RMSD$'^*$). NS gives a relative model evaluation assessment, determining the relative magnitude of the residual variance compared to the variance of measurement data (Moriasi et al., 2007). The value of B^* describes a systematic overestimation ($B^* > 0$) or underestimation ($B^* < 0$) of the state variables in the simulation, whereas RMSD$'^*$ contains information about whether the standard deviation of the simulated values is higher (RMSD$'^* > 0$) or smaller (RMSD$'^* < 0$) than the standard deviation of the measurements (Los and Blaas, 2010).

6.1 Lake Valkea-Kotinen application

Because only little feedback occurs in the conceptual submodel chain from the thermal submodel to the biochemical submodel and further to the DO-DIC submodel in MyLake DO-DIC, the submodels were not calibrated simultaneously but one at a time. The total simulation period was 5 May 2001 to 31 December 2005. The vertical grid length of the model was set to 0.5 m. The biogeochemical submodels needed some spin-up time before they reached a dynamic equilibrium because some of the initial concentration profiles were merely approximations. Therefore, the model was run in the calibrations from 5 May 2001 to 31 December 2003, and the calibration period was 1 January 2002 to 31 December 2003 in all of the individual submodel calibrations. The remaining observations in 1 January 2004 to 31 December 2005 were used to validate the calibrated model against independent data using fixed parameters obtained through the calibration. A semiautomatic optimization method was employed in the calibrations. The aim was to minimize

the sum of the squares of the differences between the calculated and the measured values.

We used the temperature calibration made for Lake Valkea-Kotinen in Saloranta et al. (2009) as a basis in the calibration of the thermal submodel. The parameters selected for calibration were the effective lake surface area A_{eff}, the non-chlorophyll-related PAR attenuation coefficient $K_{0,\mathrm{P}}$, the minimum allowed buoyancy frequency N^2_{min}, and the albedos of melting snow α_{s} and melting ice α_{i}. The open water season turbulent diffusion parameter a_{k} and the wind sheltering coefficient W_{str} are parameterized in MyLake by default by the lake surface area A_{s} (see Eqs. (3.4) and (3.12)). By defining A_{eff}, which is a fraction of A_{s}, the parameters W_{str} and a_{k} could be calibrated simultaneously. In addition, we used the non-chlorophyll-related non-PAR attenuation coefficient $K_{0,\mathrm{nP}}$ as a calibration parameter, setting it equal to $K_{0,\mathrm{P}}$. The turbulent diffusion parameter for the ice-covered period $a_{\mathrm{k,ice}}$ was also modified manually in order to get better wintertime simulation results. The thermal submodel was calibrated against water temperature measurements at depths of 1, 3, and 4.5 m in May 2002 to December 2003 and validated with measurements at depths of 1, 3, and 5 m in May 2004 to October 2005. Every fifth daily value in the temperature time series for each depth was chosen in the calibration period 2002–2003 in order to reduce the autocovariance in the time series. Every observation in the more sparse temperature time series was used in the validation period 2004–2005. This resulted in an approximately similar number of observations in both periods.

The calibration of the biochemical submodel was founded on the sensitivity analyses by Saloranta (2006) and Saloranta and Andersen (2007) who studied model sensitivity to changes in its parameter values by a global sensitivity analysis method. According to those results the most influential parameters for Chl *a* concentration were the sinking speed of phytoplankton w_{Chl}, the maximal phytoplankton growth rate μ'_{20}, and the phytoplankton remineralization rate m_{20}. For total phosphorus concentration, the most influential parameters included w_{Chl}, the resuspension rate of sediment particles U_{res}, and the scaling factor of the inflow total phosphorus concentration. Thus, the parameters w_{Chl}, μ'_{20}, m_{20}, and the settling speed of inorganic sediment particles w_{s} were included in the calibration of the biochemical submodel. The phytoplankton yield coefficient y_{c} was also altered slightly. In addition, the resuspension rates of sediment particles in the epilimnion $U_{\mathrm{res,epi}}$ and in the hypolimnion $U_{\mathrm{res,hypo}}$ and the initial concentration profile of total phosphorus in sediment were manually adjusted so that the sedimentary phosphorus load remained stable. The remaining parameter values in the biochemical submodel were the same as in Saloranta et al. (2009). The submodel was calibrated simultaneously against the observed total phosphorus concentration at 1 m and Chl *a* concentration in the 0–1 m layer during the open water seasons of 2002 and 2003 and validated with the corresponding measurements during the open water seasons of 2004 and 2005.

After the model was calibrated for phosphorus and Chl *a*, the DO-DIC submodel was calibrated using the sediment oxygen demand S_{b}, the biological oxygen de-

mand D_{BO}, the low temperature adjustment factor for oxygen demand a_{OD}, the respiratory quotient Q_{r}, and the air-water CO_2 flux adjustment factor α as calibration parameters. The organic decomposition rate was set to be 0.1/d (Stefan and Fang, 1994). The submodel was calibrated against the observed DO concentrations at the depths of 1, 3, and 5 m in 2002–2003 and the observed CO_2 concentrations at the depths of 0, 3, and 5 m measured in October 2002 to October 2003. The submodel validation for DO was performed against the measurements at depths of 1, 3, and 5 m in 2004–2005. The CO_2 validation was performed over the period of the continuous measurements from April to November 2005. Because the vertical model resolution was 0.5 m, the validation depths were chosen to be 0.5 and 1.5 m.

6.2 Lake Kuivajärvi application

The MyLake C application to Lake Kuivajärvi was calibrated separately for the use of the application in climate impact analysis (initial calibration) and for the comparison the performance of different gas exchange models for CO_2 (recalibrations). All the calibrations were performed by using a Markov chain Monte Carlo (MCMC) simulation method. An adaptive Metropolis MCMC technique (Haario et al., 2001) was used in the parameter estimation. The method is based on a Bayesian inference algorithm. Starting from prior distributions for the parameters, the MCMC simulation produces a chain of parameter sets that finally converges to an acceptable, stationary distribution, the posterior joint distribution. The MCMC method used in this work is described in Saloranta et al. (2009).

In the calibrations, the vertical grid length of the model was set to 0.5 m. Because the temperature profile and the concentration profiles at the initial state were known, no spin-up time was applied in either calibration stage. Therefore, the total simulation period was 8 January 2013 to 31 December 2014, of which the calibration period extended from 8 January to 31 December 2013. The measurements in 2014 were applied for model validation, in which fixed model parameters obtained through the respective calibrations were used. The details of the initial calibration procedure are described in Kiuru et al. (2018). The calibration and validation periods in the recalibrations were the same as in the initial calibration.

Initial calibration

The metalimnion often extends to 7 m, which was the lowest depth of automatic water column CO_2 concentration measurements, in Lake Kuivajärvi in late summer. In order to include the hypolimnion in the parameter estimation to as large extent as possible, the manual CO_2 concentration measurements were used in the initial calibration and validation. The model was thus calibrated against the manual CO_2 and DO concentration measurements at 1, 5, and 9 m depths.

The 14 parameters used in the initial calibration contained parameters included in the thermal and biochemical submodels as well as some of the new parameters

introduced in Mylake C, many of which cannot be properly obtained from the literature. The statistical prior distributions of the parameters were defined through preliminary manual calibration or estimated from the literature or from prior MyLake applications. The calibrated parameters were the open water season turbulent diffusion parameter a_{k}, the wind sheltering coefficient W_{str}, the DOC-related specific PAR attenuation coefficient of water β_{DOC}, the maximal phytoplankton growth rate μ'_{20}, the phytoplankton death rate m_{20}, the phytoplankton yield coefficient y_{c}, the degradation rates of labile DOC $k_{\mathrm{DOC},1}$ and semilabile DOC $k_{\mathrm{DOC},2}$, the fragmentation rates of autochthonous POC $k_{\mathrm{POC},1}$ and allochthonous POC $k_{\mathrm{POC},2}$, the degradation rate of sedimentary POC $k_{\mathrm{POC,sed}}$, the photosynthetic quotient Q_{p}, the respiratory quotient Q_{r}, and the temperature adjustment coefficient for organic carbon degradation θ_{c}. In the calibration, two parallel parameter chains were produced, of which the final posterior parameter chain with 3000 parameter sets was formed. The median of each posterior parameter distribution was defined to be the calibrated value of the parameter. In addition, the albedos of melting snow α_{s} and melting ice α_{i} were calibrated manually against the observed ice-off date.

Recalibrations

The recalibrations were based on the initial calibration and followed its procedures. The recalibrations were performed against the daily averages of the automatic CO_2 concentration measurements at the depths of 0.2, 2.5, and 7 m. Automatic measurements were used in order to make the simulation results comparable to the calculated CO_2 fluxes because the flux calculation using the measurement data was based on the automatic CO_2 concentration measurements at 0.2 m. Although the CO_2 concentration near the surface was the most significant variable considering CO_2 exchange, two other depths were included in the calibration in order for the calibration not to yield unreasonable results for CO_2 concentration at deeper levels.

Because DOC and Chl *a* affect light attenuation in the water column and hence the simulation of epilimnetic temperature, the parameters affecting thermal dynamics were included also in the recalibrations. Because DO concentration was not used in the calibration, the parameters related to interactions between DO and CO_2, Q_{p} and Q_{r}, were excluded from the recalibrations and kept at their original values. The DIC inflow concentration scaling factor $C_{\mathrm{DI,IN}}$ was introduced as a new calibration parameter. It was applied only during open water seasons. The calibrated 11 parameters were thus a_{k}, W_{str}, β_{DOC}, μ'_{20}, m_{20}, $k_{\mathrm{DOC},1}$, $k_{\mathrm{DOC},2}$, $k_{\mathrm{POC},1}$, $k_{\mathrm{POC},2}$, $k_{\mathrm{POC,sed}}$, and $C_{\mathrm{DI,IN}}$. The parameter values obtained in the initial calibration, referred to as default values, were used as the means of the prior parameter distributions in the recalibrations. In contrast to the initial calibration, only one final parameter chain with 1500 parameter sets was produced in each recalibration of the model application using one of the incorporated models for the gas exchange velocity.

6.3 Model forcing for climate impact analysis

In this work, the effect of climate change-induced atmospheric warming and the additional effect of predicted increases in terrestrial carbon loading on the water column CO_2 concentration and CO_2 efflux in Lake Kuivajärvi between the control period 1980–2009 and the scenario period 2070–2099 were studied. The meteorological forcing data for the control period as well as for the scenario period under two alternative representative concentration pathway (RCP) forcing scenarios were obtained from three global climate models (GCMs). The predictions of changes in stream discharge were obtained from the literature, and the examined range of increase in the concentrations of carbon species in stream inflow was based on literature estimates. All the parameter values were kept unchanged in all simulations. Also, the proportions of the lability pools of inflow DOC were the same as in the calibration simulations. In the model runs for both the control period and the scenario period, the simulation period was 4 years, of which the first 3 years were classified as a spin-up period because the applied in-lake initial conditions were approximations. The simulation results for the fourth year were selected for the climate impact analysis.

6.3.1 Climate scenarios

The RCPs illustrate paths for the development of the concentrations of GHGs and air pollutants that affect the radiative forcing of the climate system over time (van Vuuren et al., 2011). They are named according to the radiative forcing target levels in units W/m^2 for the year 2100. The present radiative forcing is approaching the level of $3\,W/m^2$ (Myhre et al., 2013). The developed RCPs vary from a very low mitigation scenario RCP2.5 to a high-emission scenario RCP8.5 (Meinshausen et al., 2011). Atmospheric temperature projections produced using RCP4.5 and RCP8.5 forcing were utilized in the climate impact analysis in this work. RCP4.5 is an intermediate mitigation scenario in which radiative forcing increases moderately until 2050 and then stabilizes toward 2100, and it has a moderate impact on climate. By contrast, RCP8.5 is a high-emission scenario with a continuous increase in the radiative forcing at a steady rate comparable with or even higher than the present rate. GCMs use the time series of the concentrations and emissions of the atmospheric constituents and land-use change predicted by RCPs to produce scenarios for climate change. A set of climate models produce a wide range of future projections, and the uncertainty of the results of a single GCM is notable (Jylhä et al., 2009). It is recommended to use several climate scenarios from different GCMs in climate-related studies because GCMs are often reported to be the largest or one of the largest uncertainty sources in climate impact analysis (Prudhomme and Davies, 2009).

The possible impacts of other meteorological factors than increasing air temperature were not assessed in this work. Changes in wind speed may have an effect on stratification and atmospheric gas exchange in lakes, but recent-generation cli-

Table 6.1: Projected changes in annual and seasonal mean air temperatures (°C) in the Hyytiälä region for the scenario period 2070–2099 relative to the control period 1980–2009. Spring comprises March, April, and May; summer comprises June, July, and August; autumn comprises September, October, and November; and winter comprises December, January, and February. [Kiuru et al. (2018)]

Global circulation model	Annual	Winter	Spring	Summer	Autumn
RCP4.5					
CanESM2	3.2	3.5	3.1	2.6	3.6
HadGEM2-ES	3.6	3.5	5.1	3.6	2.1
MIROC5	2.8	2.6	3.9	1.9	2.6
RCP8.5					
CanESM2	5.3	5.5	4.5	5.2	6.1
HadGEM2-ES	5.8	5.7	6.6	6.5	4.3
MIROC5	5.5	5.9	6.7	4.6	4.9

mate projections show neither a clear increase nor a clear decrease in wind speed in Finland (Ruosteenoja et al., 2016). The projections of future temperature were obtained from three downscaled and bias-corrected CMIP5 GCMs: CanESM2 (von Salzen et al., 2013), HadGEM2-ES (Collins et al., 2011), and MIROC5 (Watanabe et al., 2010). These three models have been shown to reproduce the current local climate well, and their predictions of air temperature show a sufficiently wide range of variability for model uncertainty assessment. The details of the downscaling of the daily GCM data are described in Kiuru et al. (2018). The projected annual and seasonal mean temperature changes in the Hyytiälä region are presented in Table 6.1. The division into seasons is based on the meteorological definition of seasons.

6.3.2 Loading scenarios

The impacts of the ongoing climate change can be seen in the magnitude of annual streamflow and its seasonal distribution in northern regions (Korhonen and Kuusisto, 2010; Wilson et al., 2010). Increased streamflow during winter and spring seasons has been observed widely, and the spring flood peak caused by snowmelt has shifted to an earlier date in many observation sites. Trends toward higher winter streamflow and an earlier occurrence of the spring peak with a lower peak flow are predicted to continue in regions across the boreal zone (Teutschbein et al., 2015; Veijalainen, 2012; Woo et al., 2008). Precipitation is predicted to increase under climate change, which may enhance the transport of both terrestrial organic carbon (Pumpanen et al., 2014; Tranvik and Jansson, 2002) and terrestrial inorganic carbon (Dinsmore et al., 2013b; Roehm et al., 2009) to boreal lakes. In addition, the seasonal dynamics of TOC export from catchments are predicted to be altered because of the changing discharge patterns and shorter soil frost periods (Blenckner et al., 2010; Mattsson et al., 2015). In regard to inorganic carbon, in-

creased terrestrial productivity (Maberly et al., 2013) or the predicted increase in soil CO_2 concentration, due to accelerated heterotrophic soil respiration in warmer temperature (Karhu et al., 2010), may belong to the factors that increase the CO_2 concentration in streams and hence enhance the hydrologic CO_2 import to lakes (Dinsmore et al., 2013a).

There are many, considerably differing estimates of the extent of climate change-induced changes in stream water DOC concentration and terrestrial DOC loading to lakes in the boreal zone. Catchment runoff and DOC export are generally found to be linearly dependent (Mulholland, 2003). That implies that temporal differences in DOC export from a catchment are likely caused by variation in runoff and that the terrestrial DOC pool available for mobilization is large and not easily depleted. Thus, increasing precipitation generally results in higher DOC export within catchments with the exception of catchments with a large proportion of water-saturated wetlands. In water-saturated conditions, DOC concentrations may be diluted in peat pore water (Schiff et al., 1998). Sarkkola et al. (2009) found an historical increase of 6 to 24% in the average yearly stream water TOC concentrations due to environmental conditions in boreal, forested headwater catchments in eastern Finland during ten years but no clear trend in TOC export loads. However, precipitation was the main hydrometeorological driver for TOC export also in Sarkkola et al. (2009). The increasing trend in TOC concentration was supposed to be resultant from increased organic carbon production due to increased soil and stream water temperatures. On the basis of an extensive literature analysis, Laudon et al. (2012) suggested that stream water DOC concentration may increase with warmer temperatures only in regions that have the present mean annual atmospheric temperature below 0 °C. In regions under warmer present-day conditions, stream water DOC concentration may decrease likely because of higher soil degradation rates in warmer temperature.

Several modeling studies exist on the impact of climate change on DOC concentration in boreal streams. A mechanistic modeling study by Holmberg et al. (2014) indicated a change in the discharge DOC concentration in Lake Valkea-Kotinen ranging from a 3% decrease to a 9% increase by the period 2080–2099, depending on the projected changes in air temperature and precipitation. Köhler et al. (2009) predicted increases of around 15% in TOC concentration in a boreal stream by the period 2091–2100 with only small variation under four different climate scenarios. However, the predicted changes were concluded to be notably smaller than the present-day intra-annual variation. Oni et al. (2015) estimated an increase of the order of 10% in the DOC concentration of a boreal stream by the period 2061–2090 using a sophisticated hydrological and biogeochemical model chain forced with climate change projections based on a medium-to-high emission scenario. By contrast, Larsen et al. (2011) predicted TOC loading in boreal lakes to increase by 30% over a span of 100 years despite the fact that the climate change projections in their statistical modeling study were based on a moderate climate scenario.

So far, the impact of climate change on CO_2 concentration in boreal streams has been studied less than the impact on stream DOC concentration. In their

statistical study, Campeau and Giorgio (2014) predicted stream CO_2 concentration to increase by 15% under the scenario with the most severe climate effects on stream water temperature, velocity, and DOC concentration for the time horizon 2041–2070. Under more moderate scenarios, the increases were 2 and 9%.

6.3.3 Scenario forcing data

Meteorological forcing
The date-specific 30-year averages of air temperature calculated from the GCM outputs for the control and scenario periods, shown in Fig. 6.1, were used as the model forcing in the scenario simulations. The measurements at the Jokioinen weather station (FMI) during the control period were applied to obtain the time series of the other required meteorological variables with the exception of precipitation, which was obtained from the Hyytiälä weather station (FMI). The date-specific 30-year averages of these variables were used as forcing data for both the calibration period and the scenario period. The atmospheric mixing ratio of CO_2 was set to be 362 ppm in the control period and 533 ppm for RCP4.5 and 807 ppm for RCP8.5 in the scenario period (Meinshausen et al., 2011).

Terrestrial loading
The date-specific averages of the respective two-year calibration time series were used for inflow volume and the inflow concentrations of DOC and CO_2 for the control period. Because the calibration time series for inflow volume consisted of only two years of data, the individual high-discharge events caused sharp peaks in the averaged inflow volume time series, which was inconsistent with the highly smooth meteorological forcing time series. For this reason, the discharge peaks were smoothed out by using 14-day running average. The time series for inflow temperatures for both periods were calculated from respective air temperatures by using a regression formula (see Kiuru et al., 2018). The inflow total phosphorus concentration during the control period was set to be the same as in the calibration period.

The time series for inflow volume for the scenario period was constructed using discharge predictions obtained from Veijalainen (2012). In the study, percentage changes in the seasonal mean discharges from 1971–2000 to 2070–2099 were simulated for four catchments located in different parts of Finland. The direct bias-corrected data from four regional climate models (RCMs) were used as scenario forcing data for atmospheric temperature and precipitation in the simulations, which were performed with the WSFS. The emission scenario used in the RCM simulations was an older-generation Special Report on Emissions Scenarios (SRES) emission scenario A1B, located approximately between the recent-generation scenarios RCP4.5 and RCP8.5 (Meinshausen et al., 2011). The averages of the percentage changes obtained with these four scenarios were selected as the final estimates.

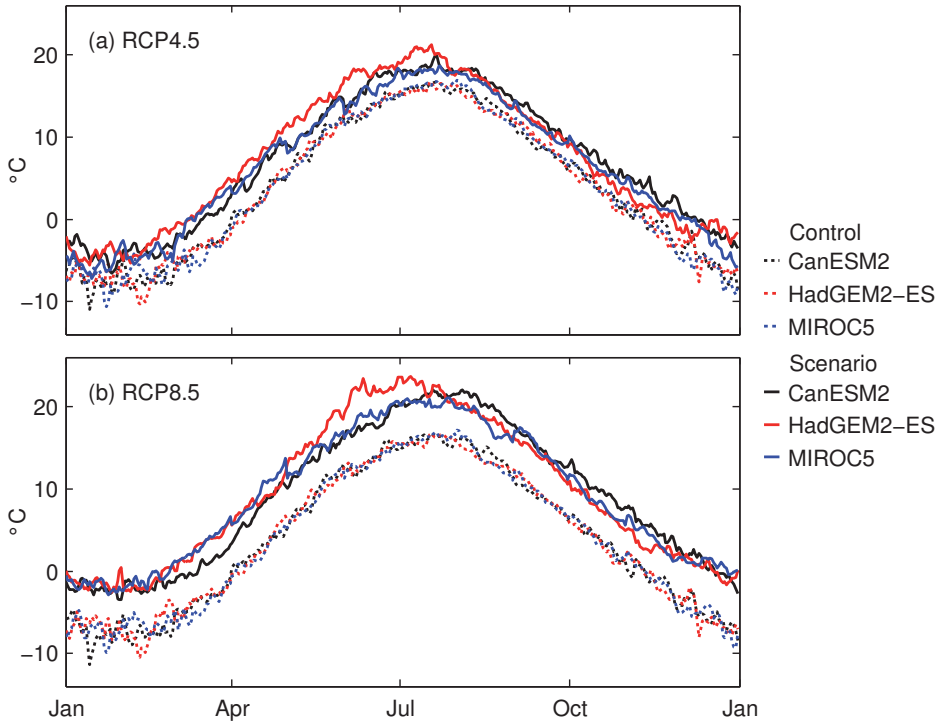

Figure 6.1: Date-specific 30-year averages of atmospheric temperature for the control and scenario periods used as model forcing. The averages were calculated from the downscaled and bias-corrected outputs of three global climate models using (a) RCP4.5 and (b) RCP8.5 forcing.

The seasonal percentage changes in discharge at a site in the river Aurajoki in Veijalainen (2012) were applied in this work. The site is located closest of the study catchments to Lake Kuivajärvi, at the distance of approximately 150 km. It was assumed to best represent the discharge regime of the Lake Kuivajärvi catchment even though the upslope catchment area of the river Aurajoki at the study site, 350 km^2, is much larger than that of Lake Kuivajärvi. The catchments of the river Aurajoki and Lake Kuivajärvi belong to different climate zones at present (Jylhä et al., 2010; Solantie, 2005), but the situation is predicted to change by the year 2100 as the warmer climate zone extends farther to the north (Jylhä et al., 2010). The predicted seasonal changes in Veijalainen (2012) were −42.9% for spring (March to May), +10.0% for summer (June to August), +14.2% for autumn (September to November), and +84.6% for winter (December to February). Monthly discharge changes were obtained from these values by spline interpolation, and they were applied to the inflow time series for the control period. The inflow phosphorus concentration was not altered for the scenario period either; nutrient loading was thus only affected by the changes in stream discharge volume. The overall climate change-induced trends in annual discharge patterns in the boreal zone (Schneider et al., 2013) are largely included in the utilized discharge scenario obtained from Veijalainen (2012). Still, utilizing only one discharge scenario and combining it with meteorological forcing data from three different, more recent-generation climate models generated some hidden uncertainty in this work.

The model runs performed using forcing data with only increased atmospheric temperatures and changing seasonal discharge volumes during the scenario period under RCP4.5 and RCP8.5 are hereafter referred to as the baseline scenarios. In addition to those, simulations with separate, additional constant increases of the inflow concentrations of DOC and CO_2 during the scenario period under RCP4.5 were performed. The levels of increase were chosen to be 10%, 20%, and 40% for both substances. Inflow pH was not altered; thus, the percentage increases in the inflow CO_2 and DIC concentrations were the same. The selected range of increase in the inflow concentration can be thought to be based on quite realistic assumptions in the case of DOC, whereas the increases of more than 10% in the inflow CO_2 concentration may have been unrealistically high. However, studying the effect of substantial increases in the inorganic and organic carbon loading gave better insight into the resultant trends in in-lake inorganic carbon dynamics.

7 Simulation of CO_2 in a boreal lake

In this chapter, the results of the calibration of the MyLake DO-DIC application to Lake Valkea-Kotinen are presented and the model performance with respect to water column CO_2 and DO concentrations and air-water CO_2 flux is discussed.

7.1 Results

Thermal submodel
The time series of the simulated and measured water column temperatures at the calibration depths in 2001–2005 are shown in Fig. 7.1, and the thermal submodel performance statistics are included in Table 7.1. The model slightly underestimated the temperatures at 1 m, the biases being -0.14 and $-0.27\,^{\circ}\mathrm{C}$ in the calibration period 2002–2003 and in the validation period 2004–2005, respectively. Overall, the model biases were rather small with the exception of a notable systematic overestimation of hypolimnetic temperatures during the validation period, which was caused by the simulated complete spring turnover in 2004 that mixed the slightly warmer surface water with bottom waters. The observed temperature stratification was reproduced rather correctly during the open water seasons, which can be seen in the simulated temporal evolution of the temperature profile in Fig. 7.2, even though the meteorological forcing data were obtained from a rather distant location. The thermocline depth depicted in the figure was calculated as the temperature gradient-weighted average of the depths at which the water column temperature gradient was greater than $1\,^{\circ}\mathrm{C/m}$.

The thermal submodel parameter values resulting from the calibration along with the calibrated parameter values of the other submodels are presented in Table 7.2. The calibrated values for the open water season turbulent diffusion parameter and the wind sheltering coefficient were rather close to those calculated with the default parameterization formulas, 1.18×10^{-3} and 0.0123, respectively. The small value for the wind sheltering coefficient implies that only a very small proportion of wind kinetic energy calculated from wind conditions at 10 m height is available for water

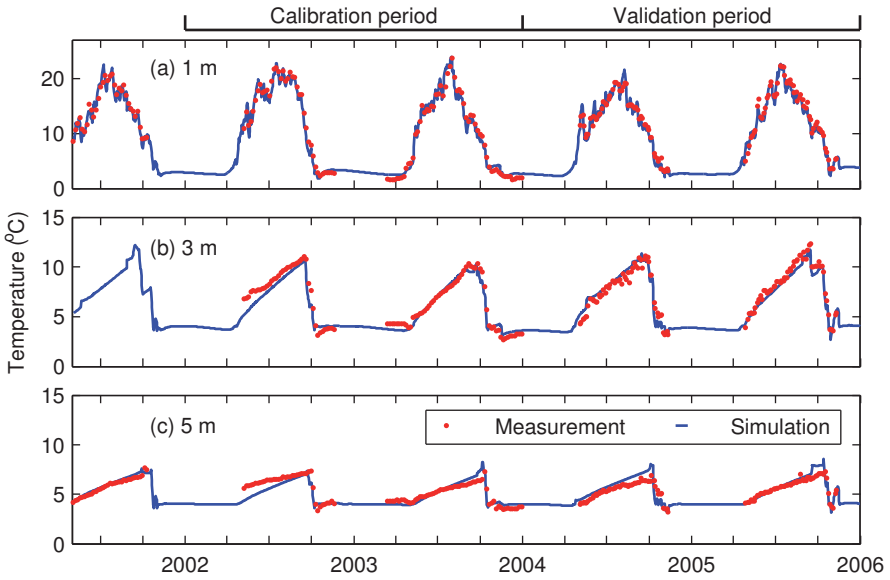

Figure 7.1: Simulation results (May 2001 to December 2005) for temperature (°C) versus measurements at depths of (a) 1 m, (b) 3 m, and (c) 5 m in Lake Valkea-Kotinen. In 2001–2002 the measurements were conducted at 4.5 m instead of 5 m. The measured temperatures shown in 2001–2003 are at 5-day intervals, and in 2004–2005 the measurements were taken on average twice a week.

column mixing, which is in accordance with the fact that the location of the lake is highly sheltered.

The observed open water seasons were 8 May to 21 November with a short intervening ice-covered period during 24 October to 1 November in 2003 (Vesala et al., 2006) and 26 April to 27 November in 2005 (Huotari et al., 2009). The respective simulated open water seasons lasted from 9 May until 21 October and then again from 11 November until 22 November in 2003 and from 25 April until 19 November in 2005. The simulated ice-off dates matched the observed dates very well, which was crucial considering the correct timing of the CO_2 exchange events after ice-off. However, the water column temperature profile tended to be overly homogeneous at the beginning of the ice-covered period in 2002 possibly because of excessive heat flux from the bottom sediment to the upper part of the water column, and the temperature stayed slightly too high in the upper water column during the following winter. Also, insufficient cooling of the water column due to the insulating effect of the simulated temporary ice cover in early November 2003 resulted in an overly high water column temperature after the onset of the final seasonal ice cover in late November.

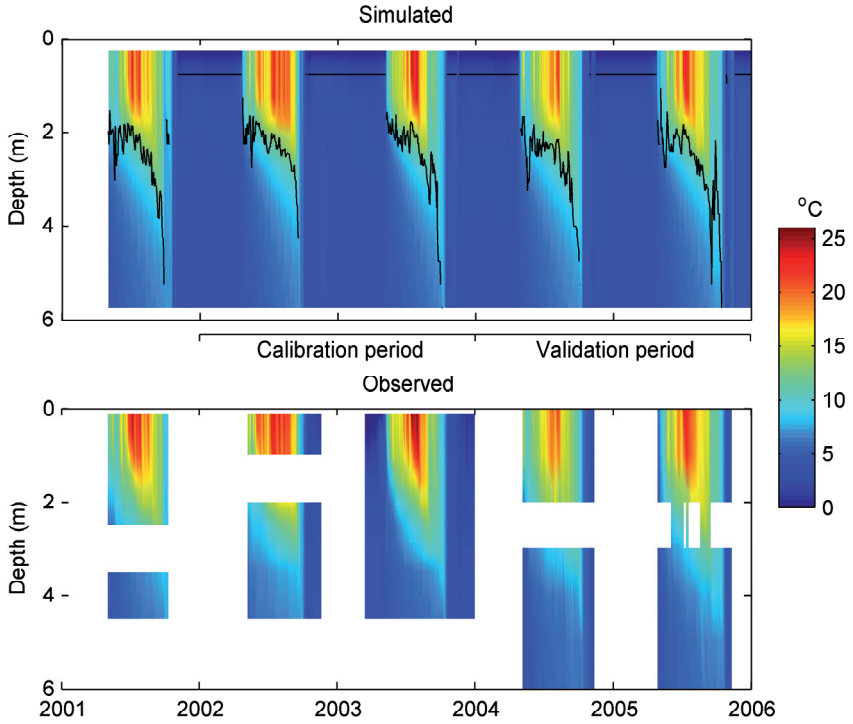

Figure 7.2: Simulated (top) and observed (bottom) isotherms (°C) in Lake Valkea-Kotinen in 2001–2005. The simulated location of the thermocline is depicted by a black line. The measurements were performed at depths of 0.1, 0.5, 1, 1.5, 2, 2.5, 3, 3.5, and 4.5 m in 2001–2003 and at depths of 0, 1, 2, 2.5, 3, 4, 5, and 6 m in 2004–2005.

Table 7.1: Statistical results for the performance of the thermal, biochemical, and DO-DIC submodels in the calibration and validation periods[a].

Variable[b]	R^2	p	RMSE	NS	RMSD′*	B^*	n
Calibration (2002–2003)							
Temp. 1 m	0.98	< 0.001	1.07	0.98	−0.15	−0.019	100
Temp. 3 m	0.94	< 0.001	0.72	0.92	−0.25	−0.012	100
Temp. 4.5 m	0.76	< 0.001	0.64	0.71	0.54	−0.011	100
Total P 1 m	0.06	0.441	2.67	−0.06	−0.99	0.27	13
Chl *a* 0–1 m	0.003	0.888	5.70	−0.17	−1.06	−0.19	10
DO 1 m	0.43	0.014	29.7	−0.13	1.06	0.12	13
DO 3 m	0.88	< 0.001	38.5	0.86	0.36	−0.063	13
DO 5 m	0.99	< 0.001	21.1	0.96	0.16	0.13	13
CO_2 0 m	0.78	< 0.001	27.2	0.77	−0.47	0.11	12
CO_2 3 m	0.83	< 0.001	73.1	0.79	−0.46	−0.002	12
CO_2 5 m	0.64	0.010	99.4	0.46	−0.62	−0.40	9
Validation (2004–2005)							
Temp. 1 m	0.96	< 0.001	1.00	0.96	0.19	−0.056	112
Temp. 3 m	0.92	< 0.001	0.68	0.92	−0.28	−0.049	112
Temp. 5 m	0.80	< 0.001	0.62	0.57	0.59	0.27	112
Total P 1 m	0.24	0.088	2.95	−0.64	−0.88	−0.93	13
Chl *a* 0–1 m	0.25	0.114	7.03	−0.57	−0.96	−0.81	11
DO 1 m	0.60	< 0.001	28.5	0.26	0.72	0.46	14
DO 3 m	0.83	< 0.001	62.2	0.63	−0.42	0.45	13
DO 5 m	0.65	< 0.001	71.1	0.05	0.76	0.61	14
CO_2 0.5 m	0.46	< 0.001	34.7	0.22	0.81	0.35	169
CO_2 1.5 m	0.55	< 0.001	35.5	0.54	−0.68	−0.028	146

[a] Coefficient of determination (R^2), p value (p), root-mean-square error (RMSE), Nash–Sutcliffe efficiency (NS), normalized unbiased root-mean-square difference (RMSD′*), normalized bias (B^*).
[b] Units: temperature, °C; phosphorus, mg/m^3; Chl *a*, mg/m^3; DO, mmol/m^3; CO_2, mmol/m^3.

Table 7.2: Values of the parameters of the thermal, biochemical, and DO-DIC submodels obtained through model calibration for Lake Valkea-Kotinen. OWS: open water season; ICP: ice-covered period; PP: phytoplankton.

Parameter	Symbol	Value	Unit
Thermal submodel			
Turbulent diffusion parameter (OWS)	a_k	1.38×10^{-3}	-
Turbulent diffusion parameter (ICP)	$a_\mathrm{k,ice}$	5.0×10^{-4}	-
Minimum buoyancy frequency	N^2_min	3.94×10^{-5}	$1/\mathrm{s}^2$
Wind sheltering coefficient	W_str	0.0162	-
Albedo of melting ice	α_i	0.355	-
Albedo of melting snow	α_s	0.505	-
Non-chlorophyll-related PAR attenuation coefficient of water	$K_\mathrm{0,P}$	1.5	1/m
Non-chlorophyll-related non-PAR attenuation coefficient of water	$K_\mathrm{0,nP}$	1.5	1/m
Biochemical submodel			
Epilimnetic resuspension rate	$U_\mathrm{res,epi}$	1.0×10^{-8}	m/d
Hypolimnetic resuspension rate	$U_\mathrm{res,hyp}$	6.0×10^{-9}	m/d
Sinking speed of particulate inorganic matter	w_S	0.2	m/d
Sinking speed of PP	w_Chl	0.01	m/d
PP yield coefficient	y_c	1.05	mg Chl *a*/ mg P
PP remineralization rate at 20 °C	m_{20}	0.1	1/d
Maximal PP growth rate at 20 °C	μ'_{20}	2.0	1/d
DO-DIC submodel			
Biochemical oxygen demand	D_BO	1950	$\mathrm{mg/m}^3$
Sediment oxygen demand	S_b	900	$\mathrm{mg/(m}^2\,\mathrm{d)}$
Temperature adjustment factor for oxygen demand at $T < 4\,°\mathrm{C}$	a_OD	1.25	-
Respiratory quotient (OWS / ICP)	Q_r	1 / 0.65	mol CO_2/ mol O_2
Air-water CO_2 flux adjustment factor	α	0.85	-
DIC inflow concentration scaling factor	$C_\mathrm{DI,IN}$	2.5	-

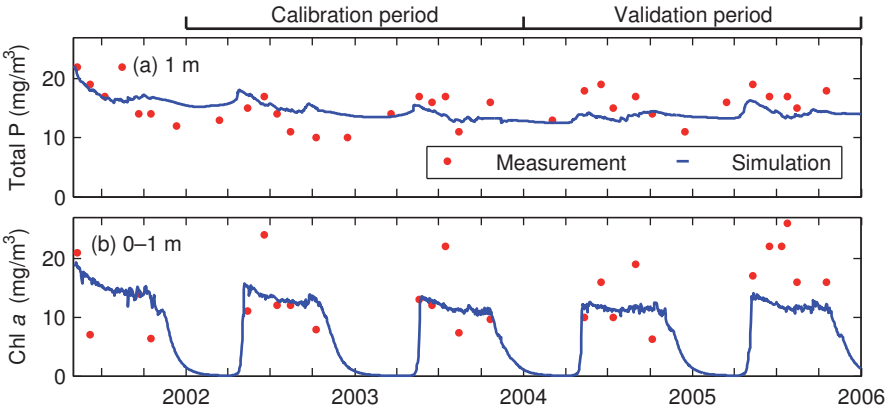

Figure 7.3: Simulation results (May 2001 to December 2005) for (a) total phosphorus concentration (mg/m^3) at 1 m and (b) Chl *a* concentration (mg/m^3) at 0–1 m in Lake Valkea-Kotinen and the respective measurements performed monthly during the open water seasons.

Biochemical submodel

The time series of the simulated and measured water column total phosphorus concentrations at 1 m and Chl *a* concentrations at 0–1 m in 2001–2005 are shown in Fig. 7.3, and the biochemical submodel performance statistics are included in Table 7.1. The simulated total phosphorus concentration was in accordance with the measurements only occasionally as the model was not able to reproduce the monthly variation in the phosphorus concentration. However, the annual levels of total phosphorus were captured slightly better: only in 2002 did the simulation notably overpredict the total phosphorus concentration. The simulated seasonal variation stayed too low partly because of the homogeneity of the wintertime concentration profile.

The accumulation of algal biomass took place in early summer in the simulation, after which the surface concentration remained quite stable. The simulation did not catch the phytoplankton growth peaks in midsummer, which resulted in rather large root-mean-square errors, 5.70 and 7.03 mg/m^2, in the calibration and validation periods, respectively. The measured Chl *a* concentration was occasionally higher than the concentration of total phosphorus (see Fig. 7.3). The model presumes that the ratio of the mass fraction of phosphorus to the mass fraction of Chl *a* is fixed in phytoplankton, which was clearly an oversimplification in this case and which may have resulted in discrepancies especially in midsummer.

DO-DIC submodel

The time series of the simulated and measured water column DO concentrations at the three calibration depths are shown in Fig. 7.4, and the DO-DIC submodel performance statistics are included in Table 7.1. The wintertime oxygen consump-

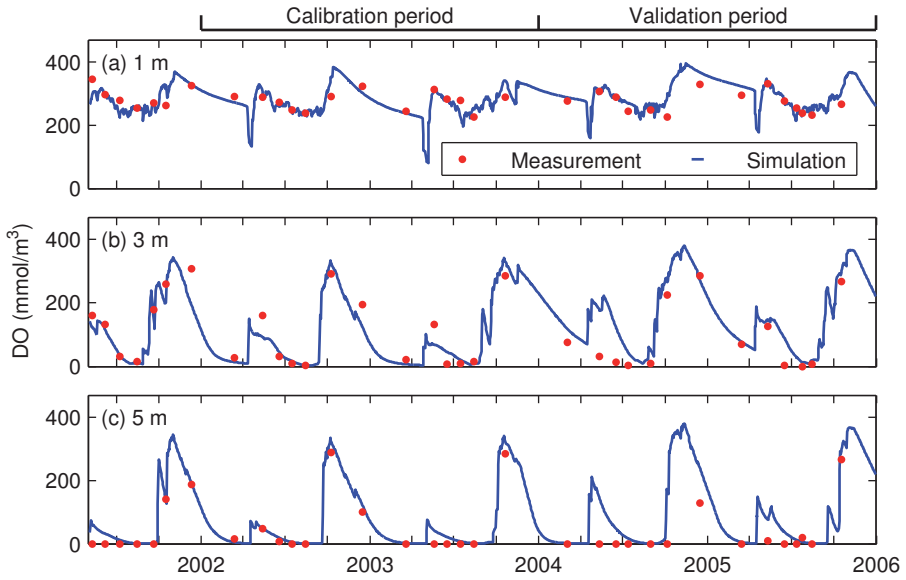

Figure 7.4: Simulation results for DO concentration (mmol/m^3) and the corresponding measurements at depths of (a) 1 m, (b) 3 m, and (c) 5 m in Lake Valkea-Kotinen in the calibration and validation periods. The calibration period was 1 January 2002 to 31 December 2003, and the validation period was 1 January 2004 to 31 December 2005).

tion was very sensitive to water temperature, which partly explains the differences in the simulated under-ice DO concentrations between the calibration and validation periods. The overly high water temperature increased oxygen consumption during the early winters in the calibration years, whereas the lower water column temperature during the corresponding periods in the validation years diminished the oxygen consumption rate. In addition, the simulated vertical temperature distribution was homogeneous from 3 m to 6 m during the entire winter 2002–2003, which resulted in the simulated oxygen consumption rate at 3 m being equal to that near the bottom of the lake. By contrast, there was a clear temperature difference between 3 m and 6 m during the winters in the validation period. However, the overall wintertime results were rather good especially near the bottom (1 m: $R^2 = 0.70$, $p = 0.037$, $n = 6$; 3 m: $R^2 = 0.87$, $p = 0.006$, $n = 6$; 5 m: $R^2 = 0.94$, $p = 0.002$, $n = 6$).

The simulated DO level decreased near the surface and rose in deeper layers every spring because of an under-ice turnover. As a result, the simulated hypolimnetic DO concentrations, in particular near the bottom, remained too high during summer except for in the year 2002 because of partial ventilation of bottom waters in the spring of that year seen in the observations. There was a spring turnover after ice-off in the simulation only in 2004, whereas it was the only year when the DO concentration measurements at 3 m indicated no mixing after ice melt.

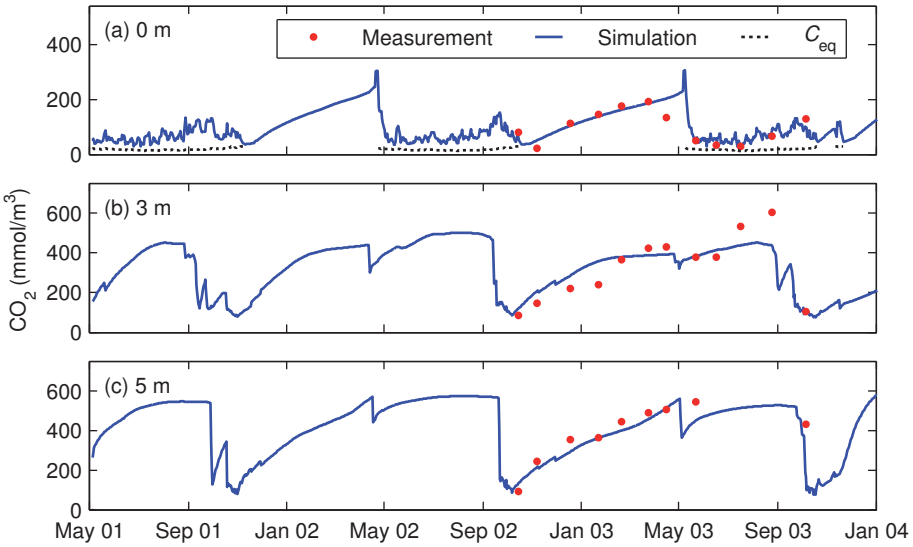

Figure 7.5: Simulation results for CO_2 concentration (mmol/m^3) in Lake Valkea-Kotinen during the calibration period January 2002 to December 2003 and the monthly CO_2 concentration measurements (a) at the surface and at the depths of (b) 3 m and (c) 5 m in October 2002 to October 2003. The simulated atmospheric equilibrium concentration of CO_2 (C_{eq}) over the simulated open water seasons is also presented in (a).

The spring-meromictic nature of Lake Valkea-Kotinen makes it challenging for biochemical modeling.

The time series of the simulated and measured water column CO_2 concentrations at the three calibration depths during the first three simulation years are shown in Fig. 7.5, and the respective variables at the two validation depths in 2004–2005 are presented in Fig. 7.6. In early winter 2002–2003, too much CO_2 was produced at the depth of 3 m, which may be explained by an overly high water temperature. The steady CO_2 increase near the bottom under ice was quite well captured in the simulation ($R^2 = 0.95$, $p = 0.001$, $n = 6$). The simulated under-ice accumulation continued until ice-out, whereas the observation showed a drop near the surface in April. The near-surface CO_2 concentration in the open water season of 2003 was overestimated, but the overall course in the sporadic measurements was caught in the simulation. The simulated CO_2 concentration increased slowly in the hypolimnion in the open water season, being constrained by the nearly anoxic conditions. Because the model includes only oxygen consumption and external loading as sources of CO_2, the concentration increase in the hypolimnion is maintained mainly by groundwater discharge when there is no oxygen in the hypolimnion. The constant discharge DIC concentration and the simple treatment of groundwater DIC load in the model may not have fully captured the seasonal and

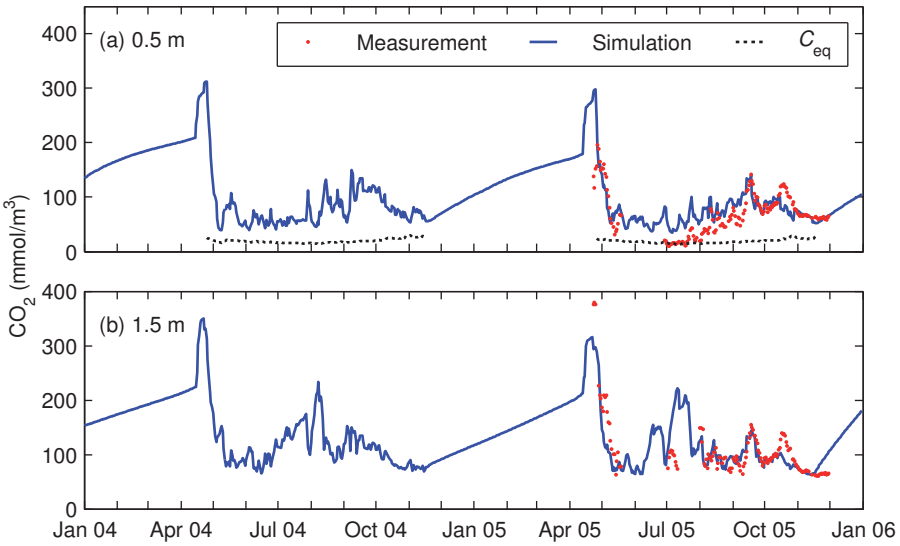

Figure 7.6: Simulation results for CO_2 concentration (mmol/m^3) in Lake Valkea-Kotinen during the validation period January 2004 to December 2005 and the daily averages of CO_2 concentration measurements at the depths of (a) 0.1 m and (b) 1.5 m in April to November 2005. The simulated atmospheric equilibrium concentration of CO_2 (C_{eq}) over the simulated open water season of 2005 is also presented in (a).

interannual variability in DIC input, which was emphasized in the hypolimnion in the open water season.

The simulated epilimnetic CO_2 concentrations at the depths of 0.5 and 1.5 m during the open water season of 2005 followed the seasonal pattern of the measured daily average concentrations rather well with the clear exceptions of July and August at 0.5 m and July at 1.5 m (see Fig. 7.6). The simulated under-ice turnover in April homogenized the CO_2 concentration near the surface, whereas the measurements showed a distinctive concentration gradient between 0.5 and 1.5 m before ice-out. The simulated surface concentration was smaller than the measured concentration after ice melt in early May because of a rapid net increase of phytoplankton biomass and the resulting substantial CO_2 consumption in the simulation. The production rate of phytoplankton did not notably exceed the remineralization rate in the topmost grid layer at any other period during the open water season in the model, which diminished the uptake of CO_2.

The CO_2 flux from the water column to the atmosphere during the open water season of 2005 and the corresponding daily average CO_2 fluxes calculated using the high-frequency CO_2 concentration measurements at 0.1 m with Eqs. (3.25) and (3.27) are shown in Fig. 7.7. The simulated CO_2 flux was closely related to the

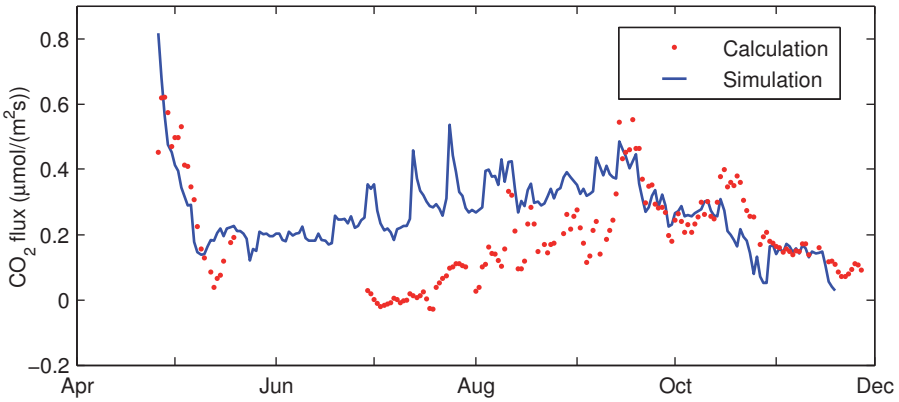

Figure 7.7: Simulated air-water CO_2 flux (µmol/(m^2 s)) in Lake Valkea-Kotinen over the open water season of the year 2005 and the daily averages of CO_2 fluxes calculated using the high-frequency measurements of CO_2 concentration at the depth of 0.1 m. Positive fluxes are directed from the lake to the atmosphere.

surface water CO_2 concentration, thus not being very well in accordance with the measurement-based fluxes apart from relatively short periods in spring and autumn ($R^2 = 0.15$, $p < 0.001$, RMSE = 0.17 µmol/(m^2 s), $n = 155$). The simulation overestimated the annual flux by 41%. The algal community was occasionally even a CO_2 source in June–July in the simulation as CO_2 production in the epilimnion through remineralization of phytoplankton exceeded CO_2 consumption via net phytoplankton primary production, which enhanced the simulated air-water flux. According to the measurements, the lake was supersaturated with CO_2 during most of the open water season in 2005. In July, the measured CO_2 flux was occasionally directed into the lake. In the simulation, the CO_2 flux was directed from the lake to the atmosphere throughout the open water season. However, the simulation performance was rather adequate during two weeks after ice-off (percent bias −10%, $R^2 = 0.56$, $p = 0.002$, RMSE = 0.13 µmol/(m^2 s), $n = 14$) and two weeks before ice-on (percent bias −18%, $R^2 = 0.83$, $p < 0.001$, RMSE = 0.041 µmol/(m^2 s), $n = 10$).

7.2 Discussion

The results of the MyLake DO-DIC application to Lake Valkea-Kotinen with respect to surface temperature, hypolimnetic temperature, the onset and the progress of stratification, and ice-off dates were in good agreement with the measured data and observations. The physical in-lake conditions related to dissolved gas dynamics were hence reproduced well, but the performance of the rather simple phosphorus-phytoplankton submodel included in MyLake was inadequate. The model described the temporal pattern of DO depletion and CO_2 accumulation in the hy-

polimnion during the ice-covered period rather properly, whereas the open water season epilimnetic CO_2 dynamics, which are largely governed by phytoplankton-related processes, were not caught by the simulation. Hence, the overall model performance considering the simulation of CO_2 dynamics was not very good.

Huotari et al. (2009) employed the daily averages of measured surface water CO_2 concentration, CO_2 equilibrium concentration, surface water temperature, and wind speed to calculate air-water CO_2 fluxes over Lake Valkea-Kotinen during the open water season of 2005 using the concentration gradient method with the same equations as in MyLake DO-DIC but without an additional flux adjustment factor. Vesala et al. (2006) obtained air-water CO_2 flux estimates for Lake Valkea-Kotinen for the open water season of 2003 both by the concentration gradient method similar to Huotari et al. (2009) and the EC method. Diel dynamics were visible both in CO_2 flux (Vesala et al., 2006) and in surface water CO_2 concentration (Huotari et al., 2009) nearly throughout the open water seasons. The simulated concentrations represented the daily average, thus taking the diel CO_2 dynamics into account by temporal integration. Short-term biochemical cycles are often difficult to reproduce with vertical models (Kara et al., 2012), and the time step of 24 h further rules out the simulation of diurnal cycles in MyLake DO-DIC.

In Vesala et al. (2006), the general intra-annual variation obtained by the concentration gradient method matched the EC observations even though the temporal resolution of the gradient flux calculations was much lower, and thus the direct comparison of daily and monthly averages was somewhat misleading. Both methods gave similar average air-water CO_2 fluxes, $0.22\,\mu mol/(m^2\,s)$, over the whole open water season of 2003. The corresponding simulation result was $0.27\,\mu mol/(m^2\,s)$, yielding a yearly flux of $4.1\,mol/m^2$. In 2005, the measured (Huotari et al., 2009) and simulated yearly CO_2 fluxes to the atmosphere were 3.7 and $4.8\,mol/m^2$, respectively, the simulated flux being equivalent to $0.27\,\mu mol/(m^2\,s)$. The simulation thus overestimated the total annual CO_2 flux from the lake to the atmosphere both in 2003 and 2005, most pronouncedly during midsummer.

The highest CO_2 efflux from lakes with a seasonal ice cover often occurs immediately after ice breakup as the CO_2 accumulated under ice degasses to the atmosphere in a short time (Anderson et al., 1999; Striegl et al., 2001). This was the case both in the simulation and in the measurements in 2005. Short periods of influx were observed when the surface water CO_2 concentration was below the atmospheric equilibrium in July 2005, but the simulated flux was never directed into the lake, the daily efflux staying above the level of $15\,mmol/m^2$. This was probably due to the fact that the simple biochemical submodel was not fully capable of giving the correct net CO_2 consumption by phytoplankton in midsummer. The simulated epilimnetic Chl *a* concentration was too low and unvarying, which reduced inorganic carbon fixation by phytoplankton. The simulated Chl *a* concentration stayed in 11–14 mg/m^3 in 2005 and there were no growth peaks, whereas the measurements showed concentrations up to $26\,mg/m^3$ in June and July.

The simulated CO_2 flux matched the observed flux better during late summer and the autumn turnover period than in spring and early summer, but the highest flux

peaks were lower in the simulation. The late summer of 2005 was especially rainy, which resulted in increases of surface water CO_2 concentration and thus CO_2 efflux (Huotari et al., 2009) because of rain-induced lateral transport of CO_2-rich water from the riparian zone to the epilimnion of the lake (Rasilo et al., 2012). The heavy precipitation events did not cause significant responses in the discharge time series used as input data in the simulation, and the resultant effect of precipitation on water column CO_2 concentration was minor. In addition, precipitation events often co-occurred with strong winds that deepened the thermocline. That resulted in an epilimnetic CO_2 concentration increase due to the release of hypolimnetic CO_2 to the epilimnion, which hinders the detection of the individual effect of increased terrestrial CO_2 loading.

Technical uncertainties caused by the use of approximations and catchment model outputs as hydrological input because of the lack of measurement data on terrestrial nutrient and inorganic carbon loading may have resulted in discrepancies in the simulation results. Keeping the water column pH constant might have been a source of significant methodological uncertainty in MyLake DO-DIC. Inorganic carbon speciation and pH have been shown to vary considerably on episodic and seasonal bases due to physical and biological processes (Heini et al., 2014; Maberly, 1985). For example, high net primary production under calm conditions in a lake undersaturated with CO_2 results in a decrease in the relative abundance of CO_2 in the epilimnion because of carbon fixation in phytoplankton and slow CO_2 influx. Formation of a new carbonate equilibrium, however, increases the proportion of CO_2 of DIC, reducing the final loss of CO_2 from the epilimnion. Also, the method of calculating CO_2 concentration from pH and DIC is not generally valid in humic lakes (Herczeg and Hesslein, 1984). Huotari et al. (2009) conducted also weekly measurements of DIC concentration, pH, and water temperature in Lake Valkea-Kotinen during the open water season of 2005. Although there was a rather good overall agreement between the CO_2 concentration estimates calculated from DIC concentration and pH and the direct CO_2 concentration measurements at the corresponding times in the study, the calculated concentrations were somewhat higher than the results of the direct measurements, which further points out the potential for simulation discrepancy resulting from the calculation method applied also in MyLake DO-DIC.

The effect of wind on the air-water exchange of CO_2 in Lake Valkea-Kotinen is rather small because of the sheltered location of the lake in the middle of a mature forest. The simple parameterization of the scaling of the wind speed described in Section 4.1 was therefore adequate. However, a straightforward, general parameterization is needed in order to apply MyLake DO-DIC to lakes of different types.

7.2.1 Impact of physical processes

The role of physical processes in dissolved gas dynamics is pronounced in boreal lakes, which are usually monomictic or dimictic (Kankaala et al., 2013). Lake

Valkea-Kotinen is steeply stratified with respect to temperature and DO concentration. The lake is characterized by weak winds because of its sheltered location, and wind-induced mixing events are remarkably rare (Nordbo et al., 2011). Furthermore, the dark water color and low water transparency hinder the penetration of solar radiation to deeper layers. Thus, the success of lake water temperature simulation is especially significant considering the simulation results on the vertical distributions of CO_2 and DO in Lake Valkea-Kotinen. The calibration of the thermal submodel was very successful and produced consistent results when comparing the evolution of seasonal water column temperature and thermocline deepening to measurements. This was reflected in the performance of the simulation of DO and CO_2 concentrations in deeper levels during late summer and autumn. In addition, the simulation of ice-off dates was successful, and the performance of the simulation of near-surface CO_2 concentration during short periods after ice-off and before ice-on was rather good. Hence, the model could be a valuable tool in the estimation of air-water CO_2 fluxes near ice-off and ice-on when manual measurements are difficult to perform.

The thermal submodel performance was also well comparable to those of the five one-dimensional physical lake models of different complexity that were run for Lake Valkea-Kotinen for the comparison of surface temperature and surface heat flux simulation performance in Stepanenko et al. (2014). The models contain different parameterizations of turbulent lake-atmosphere heat fluxes and turbulent mixing within the water column. All the models have a higher temporal resolution than MyLake. In contrary to all those models, the thermal submodel bias for surface temperature was slightly negative. The radiative heating used as the forcing of the models in Stepanenko et al. (2014) was obtained from on-lake measurements. By contrast, in this work, shortwave radiation was obtained from a rather distant location (95 km), and the net longwave radiative heat flux was calculated on the basis of the simulated air-water temperature difference. Thus, the resultant radiative heat exchange applied in the simulation was more vulnerable to inaccuracies.

Although the overall level of surface CO_2 concentration was overestimated in the late summer of the validation year 2005, the model followed the observed daily CO_2 concentration variation at 0.5 and 1.5 m relatively well. This was due to the successful simulated variation of the thickness of the mixed layer, which was around 1.5 m in the late summer. However, the model produced an overly deep mixed layer in midsummer 2005, which prevented CO_2 from being released from the hypolimnion. A minor deviation in the stratification dynamics may hence have resulted in major discrepancies in the simulated CO_2 concentration in June–July 2005. During the stratified period, the temperature and thickness of the epilimnion are indeed shown to be important contributors to the longer-term epilimnetic CO_2 concentration variation (Åberg et al., 2010; Huotari et al., 2009). Penetrative convection during cooling periods occurring especially in late summer and autumn, along with wind-induced mixing, may also notably impact the dynamics of epilimnetic CO_2 concentration and the magnitude of air-water CO_2 flux (Heiskanen et al., 2014).

The conditions of DO and CO_2 in the hypolimnion during summer stratification are greatly affected by the thermal dynamics and turnover dynamics before and after the ice-off period. The vertical extent of the partial mixing after ice-out in the simulations was very crucial to the conditions of oxygen and CO_2 under the thermocline during summer stratification. Also, efficient convective mixing or even a complete under-ice turnover a few days before ice-out evened out the DO concentration gradient and broke down the anoxia at the bottom part of the lake in the simulation. Stefan and Fang (1994) simulated the DO conditions only during summertime with the lake model that MyLake DO-DIC is based on, starting with isothermal conditions for temperature and uniform saturated conditions for DO. All the modeled lakes were dimictic or polymictic. The model produced better results in deep or medium-depth, dimictic lakes with strong stratification than in shallow, more weakly stratified lakes. By contrast, the simulation was performed all year round in the MyLake DO-DIC application in this work. The depletion of hypolimnetic oxygen takes place in Lake Valkea-Kotinen during winter, and spring mixing does not usually reach the bottom as the humic surface water of the sheltered lake is heated rapidly by solar radiation (Salonen et al., 1984). Hence, the absence of a complete spring turnover results in the lake being anoxic near the bottom during the whole stratification season.

7.2.2 Challenges in biochemical modeling

Lake Valkea-Kotinen can be classified as oligotrophic or mesotrophic in terms of surface water nutrient concentrations, but it appears meso-eutrophic because of the occasionally high Chl *a* concentrations (Wetzel, 2001). Thus, despite its shallow productive layer, Lake Valkea-Kotinen is very productive for a humic lake. The sediment oxygen demand at 20 °C had a calibrated value of $900\,\mathrm{mg/(m^2\,d)}$, which corresponds to a sandy bottom and a mesotrophic lake according to the parametrization based on lake trophic state by Stefan and Fang (1994). By contrast, the value for the biochemical oxygen demand at 20 °C, $1950\,\mathrm{mg/m^3}$, corresponds to a eutrophic lake. This reflects the difficulties in defining the proper oxygen consumption rates in the water column and in the sediment. However, the amount of humic matter was not included in the lake classification in Stefan and Fang (1994). In addition, the ice-covered period is the paramount period in hypolimnetic oxygen dynamics, which makes it difficult to compare the oxygen demands applied in MyLake DO-DIC with the parameterizations in Stefan and Fang (1994).

The possible variations in the effect of allochthonous carbon loading on the biochemical consumption of DO were not seen in the simulation because in-lake BOD was kept constant, which corresponded to a steady resupply of degradable organic matter to the lake water column so that its in-lake degradation was exactly compensated for. In addition, the discharge concentration of DIC was set constant. However, the terrestrial DIC loading varied with the discharge volume. A considerable amount of CO_2 of terrestrial origin is estimated to enter Lake Valkea-Kotinen annually, and high-discharge events due to heavy rains may directly increase the

water column CO_2 concentration during the open water season (Rasilo et al., 2012). By contrast, the seasonal dynamics of oxygen consumption by autochthonous organic matter were included because the degradation of phytoplankton carbon is described as the direct remineralization of phytoplankton in the model. MyLake DO-DIC does not explicitly include the additional photochemical production of CO_2 in the surface water during the open water season, but it is contained in the temperature-dependent biochemical oxygen consumption calculated through vertically invariant BOD. However, the effect of photochemical mineralization on the production of CO_2 is estimated to be rather small in Lake Valkea-Kotinen, being responsible for about 8% of total carbon mineralization in the 0–1 m layer and being negligible at deeper levels (Vähätalo et al., 2003).

The simulation of phytoplankton dynamics is especially challenging in Lake Valkea-Kotinen because of the dominating, vertically migrating algal species (e.g., Peltomaa et al., 2013). The high primary production in Lake Valkea-Kotinen consumes most of the nutrients in the epilimnion in early summer, but the production rate stays high also later in the growing season, even when nutrient concentrations near the surface are low (Keskitalo et al., 1998). During summer, the phytoplankton community is probably limited by phosphorus in the epilimnion (Salonen and Rosenberg, 2000). This was also seen in the model results as the epilimnetic phosphate concentration remained very low (less than $0.5\,mg/m^3$) for most of the phytoplankton growing season. The notably low settling speed of phytoplankton, 0.01 m/d, can be explained by the abundance of vertically migrating flagellate species. Stefan and Fang (1994) did not simulate the growth of phytoplankton; instead, they used measured Chl *a* concentrations as model input parameters. This improved the model performance regarding phytoplankton-related DO dynamics in comparison with MyLake DO-DIC.

The high primary production rates in the lake are largely sustained by the diel migration of flagellated algae from the epilimnion into the nutrient-rich metalimnion and hypolimnion. Two vertically migrating flagellate taxa, *Cryptomonas* spp. and *Gonyostomum semen* (Ehrenberg) Diesing, dominate the phytoplankton biomass in the lake after midsummer (Peltomaa et al., 2013). The large *G. semen* migrates into the anaerobic hypolimnion at night in order to acquire nutrients and returns to the epilimnion in the morning (Salonen and Rosenberg, 2000). Part of the population generally stays in the hypolimnion at noon. Some algae evidently migrate to the bottom of the lake even during the strongest anoxia. The vertical migration thus enhances the respiratory production of CO_2 below the thermocline and CO_2 consumption in the epilimnion.

8 Climate change-induced effects on lake CO_2 dynamics

In this chapter, the results of the calibration of the MyLake C application to Lake Kuivajärvi are presented. In addition, the simulated effects of higher atmospheric temperature and possible climate-induced changes in terrestrial carbon loading on lake water CO_2 concentration and air-water CO_2 flux are presented and discussed.

8.1 Results

8.1.1 Model calibration

The model performance statistics for the concentrations of CO_2 and DO and water temperature are presented in Table 8.1, and the model parameter values obtained via calibration are presented in Table 8.2. The calibration was overall quite successful, and the simulation results were not considerably biased in the calibration period apart from CO_2 concentration at 1 m, which was mostly lower than the measured concentration. The temperature simulation performance was well comparable to or even better than those of the two one-dimensional physical lake models run for Lake Kuivajärvi over the open water season of 2013 in Heiskanen et al. (2015). Unlike the simulation with MyLake C, one of the models in Heiskanen et al. (2015) did not catch the evolution of the thermocline and the other model yielded too low hypolimnetic temperatures. Thus, both the extent of wind-induced epilimnetic mixing and the extent of turbulent heat flux through the thermocline were caught properly by MyLake C. However, in contrast to the simulations with the two models in Heiskanen et al. (2015), the simulated open water season average surface temperature was slightly lower than the observed average during both the calibration period and the validation period. There are no major differences in the performance statistics for temperature and DO between the calibration year and the validation year, but the CO_2 simulation results were clearly less satisfactory in the validation year.

Table 8.1: Statistical results for the performance of MyLake C in the calibration and validation periods[a]. [Kiuru et al. (2018)]

Variable[b]	R^2	p	RMSE	NS	RMSD′*	B^*	n
Calibration (2013)							
Temp. 1 m	0.99	< 0.001	0.71	0.99	0.09	−0.011	356
Temp. 5 m	0.99	< 0.001	0.63	0.98	0.12	−0.049	356
Temp. 10 m	0.86	< 0.001	0.86	0.78	0.46	0.067	356
DO 1 m	0.91	< 0.001	16.9	0.83	0.41	−0.028	34
DO 5 m	0.95	< 0.001	14.9	0.95	−0.22	0.029	34
DO 9 m	0.96	< 0.001	24.1	0.95	0.22	0.029	34
CO_2 1 m	0.89	< 0.001	28.7	0.63	−0.36	−0.49	36
CO_2 5 m	0.81	< 0.001	26.2	0.66	0.57	−0.11	34
CO_2 9 m	0.87	< 0.001	34.6	0.84	0.38	−0.11	34
Validation (2014)							
Temp. 1 m	0.99	< 0.001	0.82	0.99	0.11	−0.044	348
Temp. 5 m	0.97	< 0.001	1.00	0.96	0.20	0.048	348
Temp. 9 m	0.93	< 0.001	1.00	0.87	0.32	0.16	348
DO 1 m	0.82	< 0.001	19.8	0.67	0.57	0.039	36
DO 5 m	0.85	< 0.001	31.0	0.78	−0.42	0.21	36
DO 9 m	0.95	< 0.001	24.8	0.94	0.23	0.053	36
CO_2 1 m	0.95	< 0.001	18.0	0.87	0.22	−0.29	25
CO_2 5 m	0.64	< 0.001	48.0	0.11	−0.60	−0.73	27
CO_2 9 m	0.85	< 0.001	43.6	0.56	−0.45	−0.49	28

[a] Coefficient of determination (R^2), p value (p), root-mean-square error (RMSE), Nash–Sutcliffe efficiency (NS), normalized unbiased root-mean-square difference (RMSD′*), normalized bias (B^*).
[b] Units: temperature, °C; DO, mmol/m^3; CO_2, mmol/m^3.

Table 8.2: Values of the model parameters obtained through model calibration for Lake Kuivajärvi. New parameters introduced to MyLake C and the parameters already included in MyLake v.1.2 are presented separately. PP: phytoplankton. [Modified from Kiuru et al. (2018).]

Parameter	Symbol	Value	Unit
MyLake v.1.2			
Open water season turbulent diffusion parameter	a_{k}	3.92×10^{-3}	-
Albedo of melting ice	α_{i}	0.3	-
Albedo of melting snow	α_{s}	0.8	-
Wind sheltering coefficient	W_{str}	0.285	-
Labile DOC degradation rate at 20 °C	$k_{\mathrm{DOC},1}$	8.01×10^{-2}	1/d
Semilabile DOC degradation rate at 20 °C	$k_{\mathrm{DOC},2}$	1.01×10^{-2}	1/d
PP death rate at 20 °C	m_{20}	0.206	1/d
Maximal PP growth rate at 20 °C	μ'_{20}	2.37	1/d
PP yield coefficient	y_{c}	1.27	mg Chl *a*/ mg P
MyLake C			
DOC-related specific PAR attenuation coefficient of water	β_{DOC}	2.85×10^{-5}	m^2/mg
Autochthonous POC fragmentation rate at 20 °C	$k_{\mathrm{POC},1}$	9.42×10^{-2}	1/d
Allochthonous POC fragmentation rate at 20 °C	$k_{\mathrm{POC},2}$	9.01×10^{-3}	1/d
Sedimentary POM degradation rate at 20 °C	$k_{\mathrm{POC,sed}}$	2.53×10^{-4}	1/d
Photosynthetic quotient	Q_{p}	1.27	mmol O_2/ mmol CO_2
Respiratory quotient	Q_{r}	0.762	mmol CO_2/ mmol O_2
Temperature adjustment coefficient for organic carbon degradation ($T < 4$ °C)	θ_{c}	2.16	-

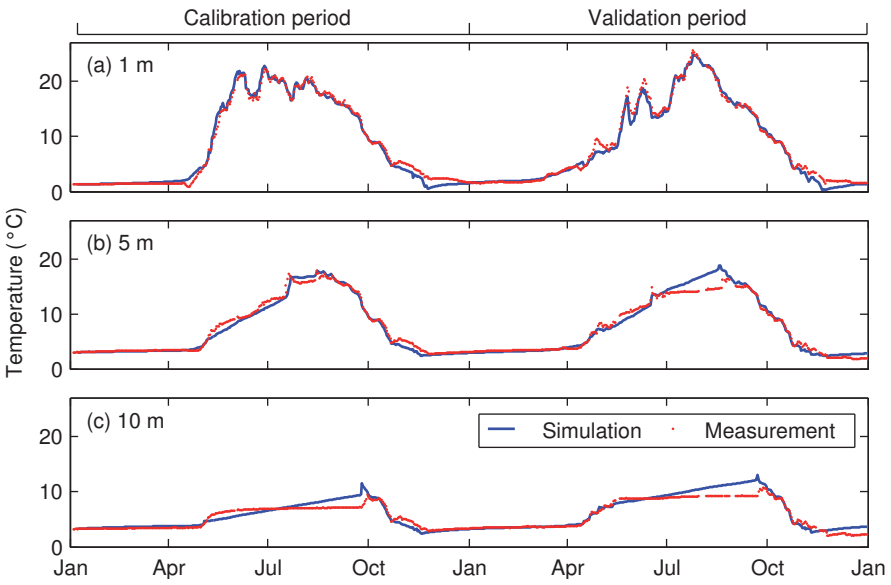

Figure 8.1: Simulation results (January 2013 to December 2014) for water temperature (°C) and the daily averages of automatic temperature measurements at depths of (a) 1 m, (b) 5 m, and (c) 10 m in Lake Kuivajärvi.

Water temperature

The time series of the simulated and measured water column temperatures at the depths of 1, 5, and 10 m in 2013–2014 are shown in Fig. 8.1. Even though the model was not explicitly calibrated against temperature measurements, the mixing patterns and the position and the deepening of the thermocline were taken into account also by the calibration conducted against CO_2 and DO concentrations. Thus, the observed stratification was caught rather correctly, as seen in Fig. 8.2 showing the temporal evolution of simulated and measured temperatures. The average water column temperatures at 1 m during the open water seasons were underestimated by 0.5 °C in the calibration year 2013 and by 0.6 °C in the validation year 2014. The observed open water season extended from 1 May to 27 November in 2013. In 2014, the observed ice-off date was 12 April. On the basis of water temperatures and atmospheric temperatures in November–December 2014, the seasonal ice cover may not have developed until late December. The respective simulated open water seasons lasted from 2 May until 25 November in 2013 and from 15 April until 23 November in 2014.

An under-ice spring turnover occurred in the simulation in 2013, resulting in sudden jumps in dissolved gas concentrations before ice-off. In addition, a short mixing event occurred on 9 May 2013 according to the temperature measurements. The preceding day was sunny, and solar radiation heated the near-surface water. Heat was transported to deeper layers because of simultaneous wind-induced turbulent mixing, and the water column was eventually only weakly stratified. Hence, strong

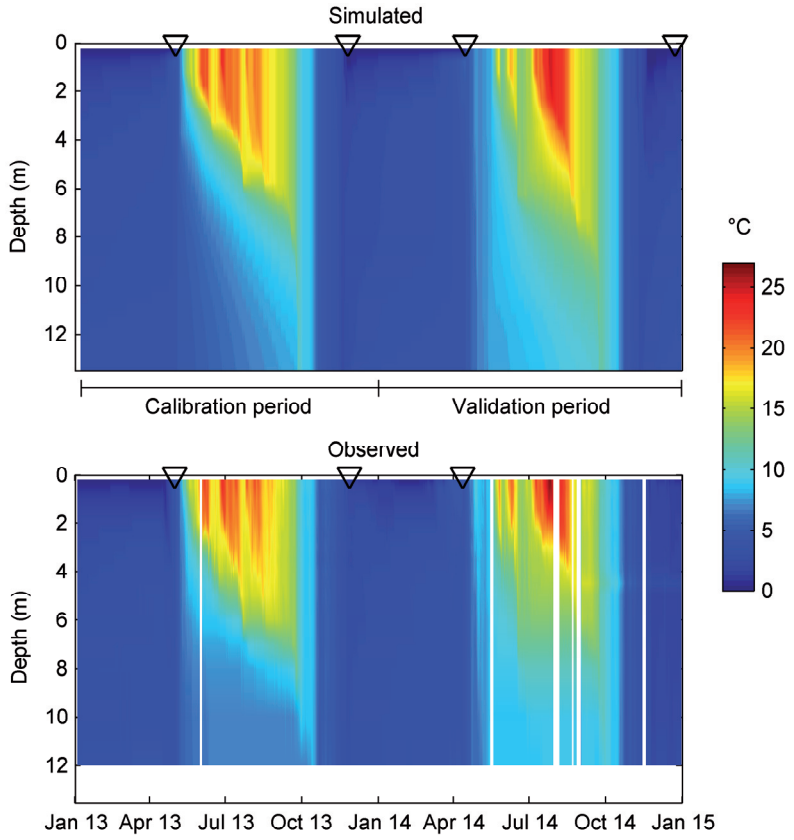

Figure 8.2: Simulated (top) and observed (bottom) isotherms (°C) in Lake Kuivajärvi in 2013–2014. Simulated and observed ice-off and ice-on dates are denoted by white triangles. Information on the ice-on date in autumn 2014 is missing. [Kiuru et al. (2018)]

winds under cloudy conditions on 9 May 2013 were able to break the stratification. The model with a daily time step was not able to simulate the outcome of the simultaneous heating and mixing processes. Because the ice-off had occurred rather late, solar radiation intensity was already high at the onset of the stratified period. Thus, the density difference between the warmed topmost water layers and the deeper layers was so high after the calculation of atmospheric heat exchange that the subsequent wind-induced mixing did not extend deep enough. The incomplete mixing had to be compensated for by applying higher turbulent diffusion, which increased heat transport to deeper layers during the stratified period. This was reflected by less steep stratification and faster deepening of the thermocline resulting in more efficient transport of heat to the hypolimnion in the late summer of 2014. Thus, the simulation of the temperature evolution in the hypolimnion was less successful compared to the other depth levels as seen in Table 8.1. The calibrated turbulent diffusion parameter was, however, smaller than the default value 5.5×10^{-3}. Nevertheless, the calibrated wind sheltering coefficient was notably larger than the surface area-based default value 0.17, which may indicate that winds oriented along the longest fetch of the oblong-shaped lake are able to efficiently mix upper layers of the water column.

The calibrated value of the DOC-related specific PAR attenuation coefficient β_{DOC} was $0.029\,\mathrm{m^2/g}$, which corresponds to a value of 0.3–$0.45\,\mathrm{m^{-1}}$ for the DOC-related PAR attenuation coefficient $K_{\mathrm{DOC,P}}$ in the DOC concentration range of Lake Kuivajärvi, 10–15 $\mathrm{g/m^3}$. Heiskanen et al. (2015) monitored PAR irradiance in the surface water in Lake Kuivajärvi, obtaining a range of 0.4–$0.7\,\mathrm{m^{-1}}$ for K_{P}. The measured light attenuation is generally a combined effect of DOC and other substances, such as phytoplankton and particulate inorganic matter, whereas β_{DOC} is related to DOC alone. The shading effect of phytoplankton is handled separately in MyLake C.

Dissolved oxygen and CO_2

The time series of the simulated and measured DO concentrations at the calibration depths 1, 5, and 9 m in 2013–2014 are shown in Fig. 8.3. The weaker performance of the DO simulation during the validation year was partly caused by overly cold conditions that slowed down bacterial degradation in the wintertime. The epilimnetic open water season DO concentration was slightly underestimated in the simulation in both years. The measured DO saturation at the surface water was between 90% and 110% from mid-May to mid-September 2013, whereas the corresponding simulated range was 80% to 103%. The simulated saturation was above 100% only during five days in early June. However, the manually measured DO concentrations may not have represented the daily average. DO measurements were made in daytime when the epilimnetic DO concentration is beginning to approach the daily maximum because of the diurnal cycle of primary production. The difference may also have been resulted from too low gas exchange velocities or too low oxygen production by primary producers. The durations of the simulated summertime anoxic periods (DO concentration $< 0.5\,\mathrm{mg/m^3} = 15.625\,\mathrm{mmol/m^3}$) at 9 m were 59 and 54 d in 2013 and 2014, respectively, and the duration of the

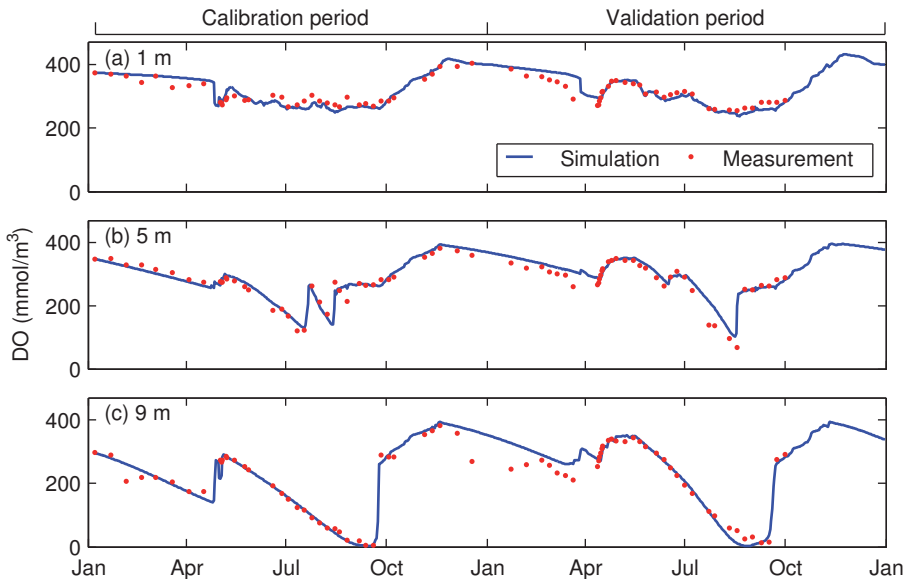

Figure 8.3: Calibrated and validated model results (January 2013 to December 2014) for DO concentration (mmol/m^3) versus measurements at the depths of (a) 1 m, (b) 5 m, and (c) 9 m in Lake Kuivajärvi. [Kiuru et al. (2018)]

respective hypoxic period (DO concentration $< 3\,\mathrm{mg/m^3} = 93.75\,\mathrm{mmol/m^3}$) was 24 d in both years. However, because of the excessive hypolimnetic warming in 2014 in the simulation, hypolimnetic anoxic conditions developed too early in August–September.

The time series of the simulated and measured CO_2 concentrations at the calibration depths in 2013–2014 are shown in Fig. 8.4. The simulated CO_2 concentration at 1 m was too low in the winter and in the autumn of the calibration year, and the concentration decreased too fast after ice-off in May. The wintertime discrepancy can be explained by the functioning of the model. The inflow was more CO_2-rich than the lake water near the surface in the winter, but the resulted CO_2 concentration increase occurred only in the topmost 0.5 m layer. The surface layers are steeply stratified under ice in the model because the temperature of the topmost layer in contact with ice is always close to 0 °C when the net surface heat flux is directed out of the lake. Thus, the cold wintertime inflow is mixed only with the topmost layer, and only little heat diffuses from the warmer adjacent layers to the topmost layer because of the steep stratification.

Both the simulations and the daily averages of the automatic near-surface CO_2 concentration measurements indicated that the lake was supersaturated with CO_2 and was thus a source of CO_2 to the atmosphere. The manual measurements showed even higher CO_2 concentrations at 1 m than the daily averages of the automatic measurements nearly throughout the open water seasons. The corresponding simu-

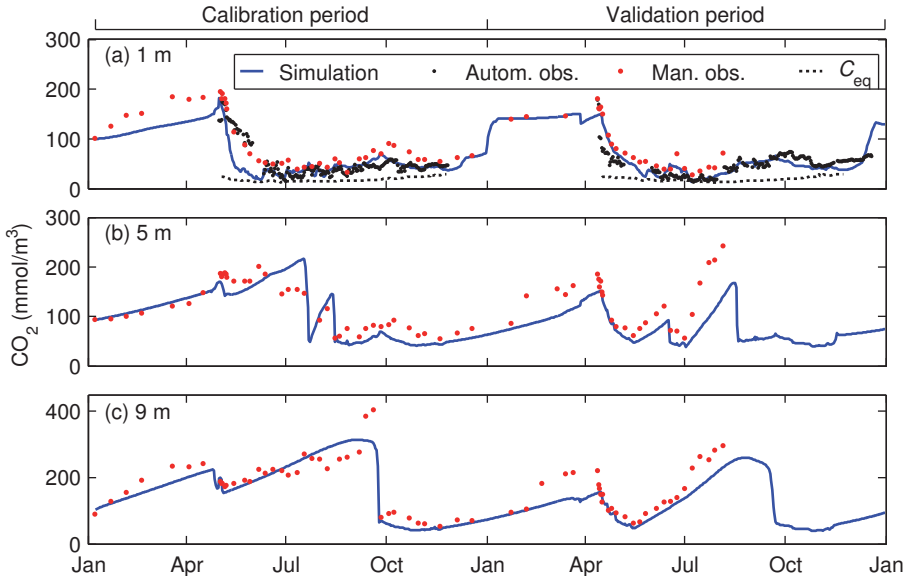

Figure 8.4: Calibrated and validated model results (January 2013 to December 2014) for CO_2 concentration (mmol/m^3) versus manual measurements and the daily averages of automatic measurements at depths of (a) 1 m, (b) 5 m, and (c) 9 m in Lake Kuivajärvi and the atmospheric equilibrium concentration of CO_2 (C_{eq}) over the simulated open water seasons. [Kiuru et al. (2018)]

lated CO_2 concentrations followed more closely the automatic measurements than the manual ones during the open water seasons both in the calibration year and in the validation year. This result agrees with the fact that the manual measurements were made in the morning when CO_2 concentrations were close to their daily maximum (Heiskanen et al., 2014; Huotari et al., 2009).There were also large discrepancies between the CO_2 concentration measurements and the simulated values in the vicinity of the thermocline in the metalimnion at 5 m during the summers. The internal wave-induced diel fluctuations of the thermocline (Heiskanen et al., 2014) may partly give a reason for the difference between the simulated concentrations that represent the daily average and the manual measurements, which were performed at a random instant.

The time series of the simulated and measured near-surface (0.5 m) and near-bottom (12 m) pH values in 2013 are shown in Fig. 8.5. The model performance for surface water pH was very good (RMSE = 0.12, NS = 0.84, $B^* = 0.25$, $n = 13$). Nevertheless, similarly to CO_2 concentration, surface water pH varies within the course of a day, especially during periods of vigorous photosynthesis. The measurements were performed at daytime, when pH usually reaches its maximum during the open water season; thus, the measured pH values may have been above the daily average. However, neither the overall hypolimnetic pH nor its short-term variation was captured. The relative proportion of CO_2 of DIC was smaller under

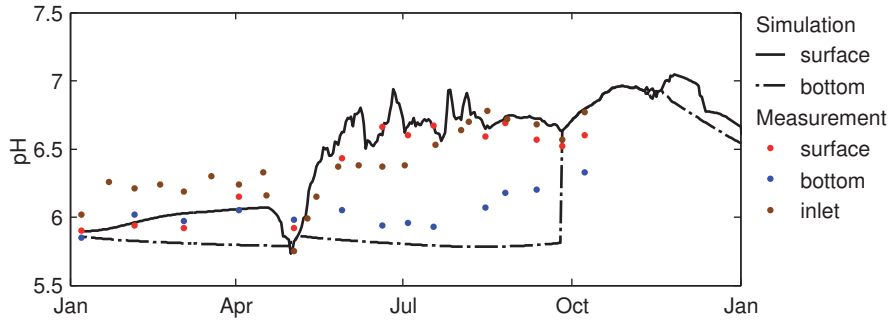

Figure 8.5: Simulated and measured water column pH values near the surface (0.5 m) and near the bottom (12 m) in Lake Kuivajärvi and measured pH values at the main inlet of the lake in 2013. [Kiuru et al. (2018)]

the conditions with a lower in-lake pH in wintertime, and the decrease of CO_2 concentration due to efflux and carbon fixation to phytoplankton increased the near-surface pH under open water conditions. The observed seasonal variation in the epilimnetic CO_2 concentration due to changes in pH was thus captured rather well by MyLake C.

8.1.2 Future scenarios

Changes in atmospheric temperature
The simulated water column temperatures near the surface (1 m) and in the hypolimnion (9 m) in the control period 1980–2009 and in the scenario period 2070–2099 under the baseline conditions are shown in Fig. 8.6. The differences between the water column temperatures during the control period obtained with different GCMs were very small due to the consistent results for atmospheric temperature between GCMs (see Fig. 6.1). In the baseline scenarios, only the changes in atmospheric temperature and seasonal discharge volumes were applied in the model forcing data. Both epilimnetic and hypolimnetic temperatures were notably higher over the entire open water season in the scenario period compared with the control period under the temperature forcing obtained from the three GCMs. The highest water temperature at 1 m was 1.6–3.7 °C higher under the more moderate RCP4.5 scenario and 3.7–6.0 °C higher under the high-emission scenario RCP8.5. Projected increases in springtime and summertime mean atmospheric temperatures were highest in HadGEM2-ES, which also was the GCM that resulted in the highest changes in epilimnetic water temperature at 1 m during summer. The ice-covered period was 44–49 d shorter under RCP4.5 and 69–88 d shorter under RCP8.5. The duration was shortest under MIROC5 forcing because of the mildest winter and the resulting lowest ice thickness.

The ice-off occurred earlier in the scenario period, which resulted in a longer spring mixing period. The radiative heat flux from the atmosphere was rather low in early

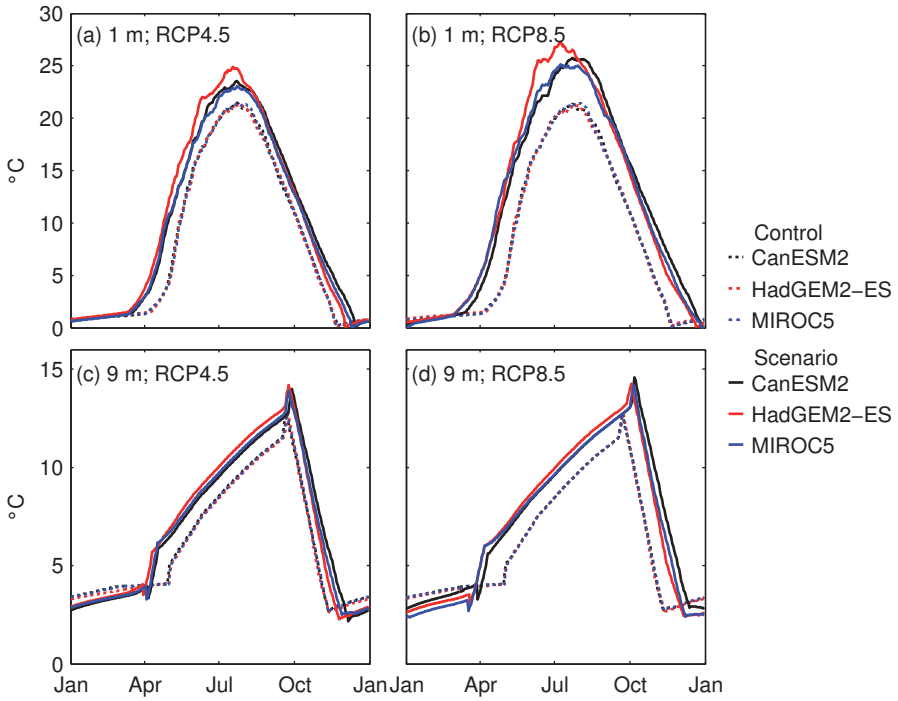

Figure 8.6: Simulated water column temperatures (°C) in Lake Kuivajärvi in the control period (dashed lines) and the scenario period (solid lines) at the depths of (a, b) 1 m and (c, d) 9 m under RCP4.5 (a, c) and RCP8.5 (b, d) forcing. [Kiuru et al. (2018)]

spring, and the surface water was not heated efficiently enough for the development of stratification right after ice-off. The strength of summer stratification, described by the difference between the epilimnetic and hypolimnetic temperatures, was increased especially under RCP8.5. The thermocline was located 0.5–1.0 m and 0.3–0.7 m deeper in early summer in the scenario period under RCP4.5 and RCP8.5, respectively. However, because the stratification period was longer and the epilimnion remained warm in late summer in the scenario period, thermocline deepening occurred more slowly, and the thermocline was eventually 1–2 m shallower than in the control period before the autumn turnover.

The simulated DO concentrations at 1 m and at 9 m during the control period and during the scenario period under the baseline conditions are shown in Fig. 8.7. The DO saturation of the water column at the onset of stratification was higher in the scenario period because the water column was more thoroughly ventilated during the longer spring mixing period. However, accelerated bacterial degradation in a higher temperature and the longer duration of the stratified period resulted in longer hypolimnetic anoxia in the scenario period. The anoxic period at 9 m

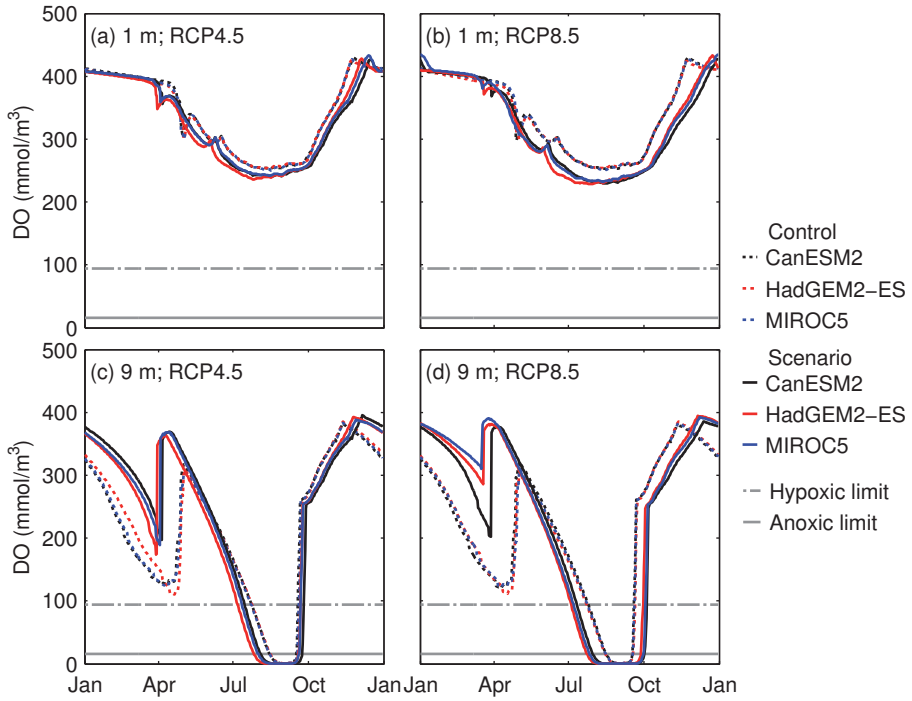

Figure 8.7: Simulated DO concentrations (mmol/m^3) in Lake Kuivajärvi in the control period (dashed lines) and the scenario period (solid lines) at the depths of (a, b) 1 m and (c, d) 9 m under RCP4.5 (a, c) and RCP8.5 (b, d) forcing. [Kiuru et al. (2018)]

lengthened from 33–34 d to 51–55 d under RCP4.5 and from 31–34 d to 63–66 d under RCP 8.5. The duration of the hypoxic period was increased by 14–19 d under RCP4.5 and by 29–31 d under RCP8.5. The hypoxic period lasted 56–58 d in the control period, which is roughly in the range of the simulated duration in the model calibration and validation years; however, the anoxic period was considerably longer in the control period. Under-ice DO concentration remained significantly higher in the scenario period because the ice-covered period preventing oxygen flux from the atmosphere was of shorter duration and because organic matter degradation rates were lower because of colder conditions in deeper layers.

The simulated CO_2 concentrations at 1 m and at 9 m during the control period and during the scenario period under the baseline conditions are shown in Fig. 8.8, and the respective air-water CO_2 fluxes are presented in Fig. 8.9a. Because the winter-time inflow volume was substantially higher in the scenario period and the inflow was estimated to be rich in CO_2, the near-surface CO_2 concentration in early winter was higher in the scenario period than in the control period. In total, however, less CO_2 was accumulated in the water column during winter because of the shorter

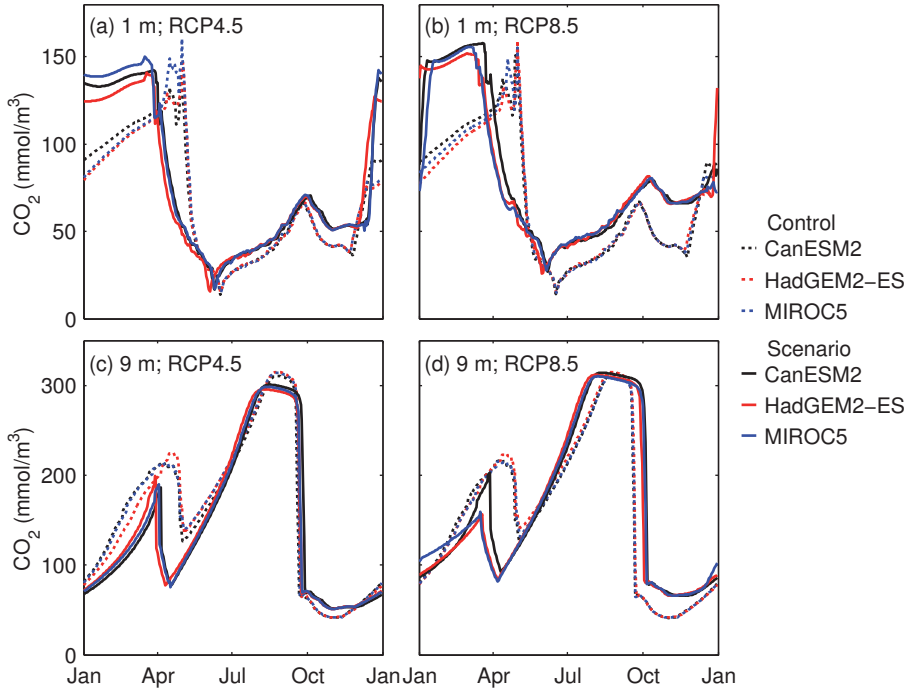

Figure 8.8: Simulated CO_2 concentrations (mmol/m^3) in Lake Kuivajärvi in the control period (dashed lines) and the scenario period (solid lines) at the depths of (a, b) 1 m and (c, d) 9 m under RCP4.5 (a, c) and RCP8.5 (b, d) forcing. [Kiuru et al. (2018)]

duration of the ice-covered period. Therefore, the CO_2 flux peak after ice-off was smaller in the scenario period. However, the longer spring mixing period increased the total CO_2 efflux during spring. CO_2 efflux was high in late autumn because of the longer stratification period and the later ice-on. The inflow phosphorus concentration was not altered for the scenario period, but the higher wintertime inflow volume increased the phosphorus loading, which resulted in a higher summertime in-lake phosphorus concentration. Increased nutrient availability, along with warmer conditions, increased primary production in the scenario period. As a result, the phytoplankton growth peak in early summer was stronger, and the duration of the period with undersaturated surface water CO_2 conditions and a reversed air-water CO_2 flux was longer.

The open water season average CO_2 concentrations at 1 m were increased by 13–15% under RCP4.5 and by 40–44% under RCP8.5 in the scenario period compared to the control period. Along with the surface water CO_2 concentration, the CO_2 flux to the atmosphere was higher in the scenario period. However, a relatively smaller concentration gradient due to a higher atmospheric CO_2 mixing ratio in

the scenario period moderated the increase somewhat. The total annual CO_2 flux increase was 17–20% under RCP4.5 and 33–38% under RCP8.5. The annual flux period was longer because of the longer ice-free season, and the in-lake production of CO_2 through bacterial degradation was higher in warmer summertime conditions. The total annual fluxes were about 2% and 5% higher under RCP4.5 and RCP8.5, respectively, when the atmospheric CO_2 concentration for the control period, 362 ppm, was applied in the simulations for the scenario period.

Changes in terrestrial carbon loading

The annual and seasonal changes in the air-water CO_2 flux and in the volume-weighted average water column CO_2 concentration resulting from the increases of 10%, 20%, and 40% in the inflow concentration of either CO_2 or DOC during the scenario period under RCP4.5 forcing are presented in Table 8.3. Also, the daily time series of the respective CO_2 fluxes with the 40% increases are shown in Fig. 8.9b and Fig. 8.9c. An increase in the inflow CO_2 concentration resulted in a significantly higher increase in both the annual water column CO_2 concentration and the annual CO_2 flux than a corresponding increase in the inflow DOC concentration. A doubling of the inflow CO_2 or DOC concentration percentage increase was reflected as doubling of both the annual and seasonal in-lake responses for both CO_2 concentration and CO_2 flux.

The stream inflow was most CO_2-rich in winter and early spring, and the inflow volumes were largest in late autumn and early winter. Hence, the terrestrial CO_2 loading was highest in early winter, and a further inflow CO_2 concentration increase resulted in an instant, notable increase in the in-lake CO_2 concentration. However, an increased CO_2 loading had a greater increasing effect on CO_2 flux than on the average water column CO_2 concentration during the short (6–18 d) ice-free period in early winter. The stream inflow, which was estimated to be colder than the inversely stratified lake water column, remained in the already supersaturated topmost layer instead of mixing with deeper layers, and the inflowing CO_2 was hence largely released to the atmosphere or removed through outflow. In late winter and early spring, a higher CO_2 inflow concentration resulted in greater under-ice CO_2 accumulation, which increased the CO_2 efflux after ice-off. Inflow volumes were lowest in late summer, and the difference between the inflow CO_2 concentration and the epilimnetic CO_2 concentration was smallest in late summer and early autumn in baseline conditions. Thus, the overall effect of an increased CO_2 loading on CO_2 flux was lowest during summer and autumn, and its effect on in-lake CO_2 concentration was even smaller than that of an increased DOC loading during those seasons.

An increased inflow DOC concentration did not affect the in-lake CO_2 concentration during the high inflow period in early winter because degradation was slow in the cool conditions prevailing in winter. As a result, the springtime CO_2 flux pattern was largely unaffected by an increase in inflow DOC concentration. A higher inflow DOC concentration increased the in-lake CO_2 concentration most in warmer conditions during the stratified period as the relatively slowly degradable

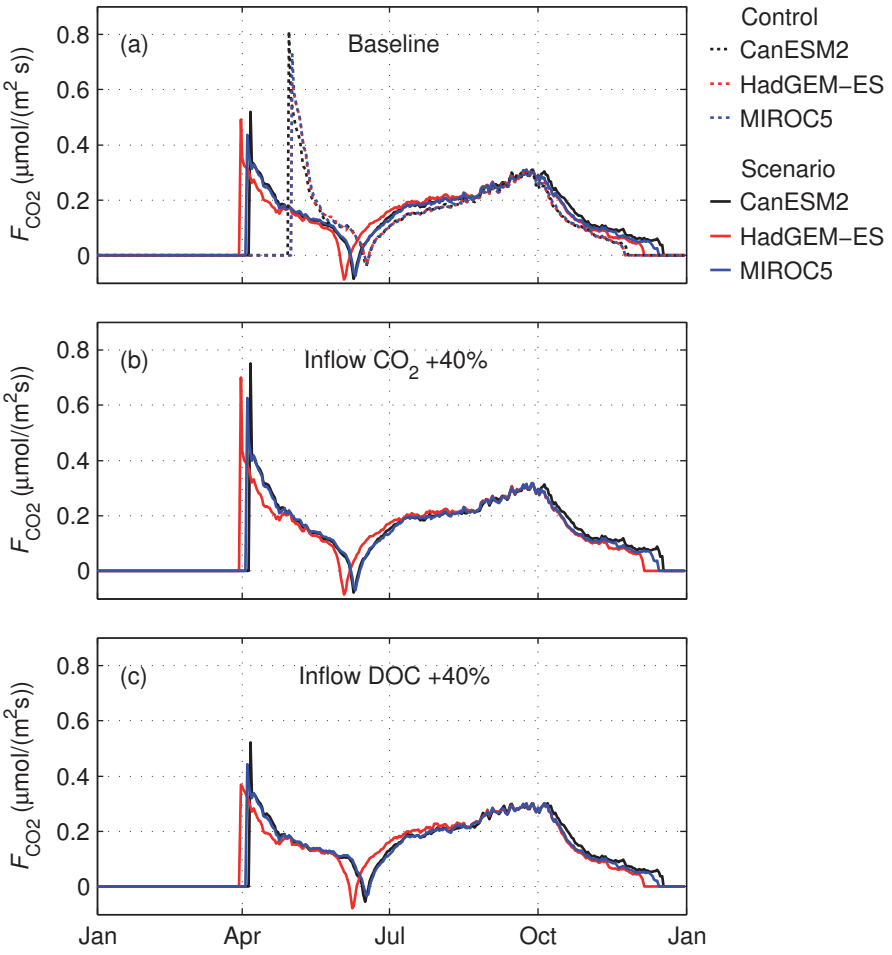

Figure 8.9: Simulated air-water CO_2 fluxes (µmol/(m^2 s)) in Lake Kuivajärvi (a) in the control period and without changes (baseline) in the inflow carbon concentrations in the scenario period under RCP4.5, (b) with a 40% increase in the inflow CO_2 concentration under RCP4.5, and (c) with a 40% increase in the inflow DOC concentration under RCP4.5. [Modified from Kiuru et al. (2018).]

allochthonous organic carbon was gradually mineralized by bacteria and solar radiation. The changes in surface water CO_2 concentration also largely governed the seasonal CO_2 flux trends caused by changes in inorganic or organic carbon loading. The interseasonal variation in the impact of a higher inflow DOC concentration on CO_2 flux was rather small, but a higher inflow CO_2 concentration yielded a considerably higher efflux only under the coolest conditions near the beginning and near the end of the ice-free period.

Increases in terrestrial CO_2 loading did not affect in-lake temperatures, and the changes in lake thermal conditions due to a higher water column DOC concentration were rather small even in the case of the highest inflow DOC concentration increase. The 40% increase in the inflow DOC concentration resulted in a 2.5–3.0% smaller percentage increase in the open water season average in-lake DOC concentration at 1 m because some of the additional semilabile allochthonous DOC was degraded in the water column and the amount of autochthonous DOC remained virtually the same. Because of stronger attenuation of radiative heat flux in the case of the 40% higher inflow DOC concentration, lake water temperature increased faster in spring, and the surface water was on average 0.2 °C warmer during the open water season. However, the mean temperature of the water column was approximately 0.2–0.3 °C lower in late summer and early autumn. The summer stratification was stronger because the temperature difference between the epilimnion and the hypolimnion was up to 1.5 °C higher, but the location of the thermocline was almost unaltered until late summer. Thereafter, thermocline deepening occurred slower, and the stratification finally broke down 3–5 d later. The slight increase of the average summertime water column CO_2 concentration was not only caused by a greater amount of terrestrially derived degradable organic matter but also by more intense CO_2 production because of the slightly warmer epilimnetic conditions. The stronger extinction of PAR under the higher epilimnetic DOC concentration also delayed primary production in spring and early summer, which is seen in the later onset of the CO_2 influx period.

A higher water column DOC concentration due to an increase in terrestrial DOC loading also affected phytoplankton dynamics in the lake. The average in-lake phytoplankton biomass decreased by 15–17% during the open water season because of the 40% increase in inflow DOC concentration. Photosynthesis was lower in darker conditions, and the duration of active growing season was slightly shorter. Also, nutrient supply from the hypolimnion was lower because of stronger stratification and the shallower thermocline. These factors reduced the excretion of easily degradable organic matter and CO_2 production through autotrophic respiration as well as CO_2 consumption by gross primary production. The delay in primary production due to stronger extinction of PAR in spring and early summer was also seen in the later onset of the CO_2 influx period.

Table 8.3: Annual and seasonal changes (%) in air-water CO_2 flux and water column CO_2 concentration in Lake Kuivajärvi resulting from increases of 10%, 20%, and 40% in the inflow concentration of CO_2 or DOC during the scenario period under RCP4.5[a]. [Kiuru et al. (2018)]

	Annual	OWS	Spring	Summer	Autumn	Winter
CO_2 air-water flux						
Inflow DOC +10%	1.1–1.2	1.1–1.2	1.3–2.2	0.7–1.4	0.9–1.0	0.2–0.4
Inflow DOC +20%	2.2–2.3	2.2–2.3	2.3–3.6	1.6–2.9	1.7–1.9	0.6–0.7
Inflow DOC +40%	4.0–4.3	4.0–4.3	4.1–6.1	3.8–5.7	2.9–3.5	0.1–1.6
Inflow CO_2 +10%	2.1–2.5	2.1–2.5	4.5–5.0	1.0–1.3	1.3–1.5	9.3–13.5
Inflow CO_2 +20%	4.3–4.9	4.3–4.9	9.2–10.0	2.1–2.6	2.5–2.8	18.6–24.6
Inflow CO_2 +40%	8.5–9.6	8.5–9.6	18.9–20.3	4.6–5.2	5.0–5.2	37.2–43.4
Volume-weighted average water column CO_2 concentration						
Inflow DOC +10%	0.6–0.7	1.0–1.1	0.2–0.5	1.1–1.3	1.3–1.5	−0.05–0.01
Inflow DOC +20%	1.3–1.5	2.0–2.3	0.5–0.7	2.2–2.5	2.6–2.9	−0.3–0.03
Inflow DOC +40%	2.7–2.9	4.1–4.5	1.1–1.9	4.5–5.1	5.2–5.5	−0.3–0.1
Inflow CO_2 +10%	2.6–3.1	1.2–1.5	3.4–4.1	0.9–1.2	0.9–1.0	5.3–5.8
Inflow CO_2 +20%	5.2–6.1	2.5–3.1	6.7–8.2	1.8–2.4	1.7–1.8	10.4–11.4
Inflow CO_2 +40%	10.2–12.1	5.0–6.1	13.4–16.4	3.8–4.8	3.3–3.5	20.0–22.5

[a]OWS, open water season; spring, March–April–May; summer, June–July–August; autumn, September–October–November; winter, December–January–February.

8.2 Discussion

8.2.1 Impact of higher atmospheric temperature

The simulation results for the effect of increasing atmospheric temperature on water column temperature and the strength of thermal stratification in boreal lakes were in line with earlier studies. The simulated changes in water temperature between the control period and the scenario period resembled the predictions by Saloranta et al. (2009), who studied the impacts of climate change on the thermal regime of two lakes in Finland. The older-generation SRES emission scenario A2 applied in the study corresponded approximately to the RCP8.5 forcing scenario. However, the annual difference in the average water column temperature between the control and scenario periods under RCP8.5 was 2.6–2.7 °C, whereas the corresponding differences were less than 2 °C in Saloranta et al. (2009). The reason for the difference may be that the climate projections applied in this work predicted the greatest temperature increase to occur during the open water season, whereas the largest warming took place in wintertime in the climate projection used in Saloranta et al. (2009) as described in Jylhä et al. (2004). By contrast, in a climate change study on four lakes in Finland by Elo et al. (1998) the maximum increase of surface water temperature under a climate scenario with an annual air temperature increase close to RCP4.5 was slightly higher than in this work.

A daily 30-year averaged time series was used as meteorological forcing in the control and scenario simulations instead of a daily 30-year time series, which may have resulted in too low ice thickness because the averaging smoothed out the low temperature periods essential for substantial ice thickening. However, a long-term discharge time series for Lake Kuivajärvi was not available, and using an averaged discharge time series together with a daily meteorological time series would have induced temporal asynchrony between high-flow periods and ice-off dates. In a climate change study on four Finnish lakes by Huttula et al. (1992), the delays in freezing dates and hence the shortening of ice-covered periods were somewhat smaller than in this work. The atmospheric CO_2 concentration increase in the climate scenario used in the study corresponded roughly to RCP8.5, but the predicted autumnal air temperature increase was a little lower than in this work, which may explain the lesser delays in the freezing dates. By contrast, the shortening of the ice-covered period in Saloranta et al. (2009) was of similar magnitude to this work.

The scenario simulations showed that humic boreal lakes that are at present supersaturated with CO_2 will be even larger CO_2 sources to the atmosphere on an annual basis under warmer climate conditions. Production of CO_2 through degradation of autochthonous and allochthonous organic matter was faster in the warmer water column and bottom sediment in the scenario period 2070–2099 compared to the control period 1980–2009 close to present conditions. As a result, water column CO_2 concentration was increased almost throughout the year. Only the maximum CO_2 concentration right before ice-off was lower because of lesser CO_2

accumulation under ice during a shorter ice season. The largest release of CO_2 occurred during the mixing periods before and after the summer stratification, which are often hot moments for CO_2 flux in dimictic boreal lakes also in present climate (Ducharme-Riel et al., 2015; Karlsson et al., 2013; López Bellido et al., 2009). The maximum springtime CO_2 efflux was lower in the scenario period, but the efflux was spread over a longer period because of an earlier ice-off and a slower development of stratification after ice-off. The efflux was higher in the scenario period than in the control period also in late autumn, and CO_2 evasion lasted longer because of a later ice-on.

Only the impact of higher atmospheric temperature was assessed in this work, and the projections indicating increasing carbon emissions from boreal lakes due to higher organic matter degradation rates were based on the effect of warmer in-lake conditions. Climate change is predicted to inflict diverse changes in physical, hydrological, and biogeochemical processes both in catchments and in lakes. Those will, in turn, promote an intricate response in lake carbon pool, which is suggested to bring about an increase in lacustrine CO_2 emissions (Tranvik et al., 2009). However, several empirical cross-system studies have found a linkage between lake water column temperature and CO_2 emission. Based on the results of a comparative study, Kosten et al. (2010) suggested that climate warming may increase carbon emission from cool lakes as a consequence of higher organic carbon mineralization rates in warmer water. Also, Gudasz et al. (2010) found in a cross-system survey that the organic carbon mineralization in lake sediments correlated strongly with water temperature and suggested that GHG emissions from lake sediments may thus increase in a warmer climate. On the other hand, results of a mesocosm experiment by Davidson et al. (2015) indicated that GHG fluxes from shallow lakes may largely be regulated by factors that are only indirectly related to temperature, such as nutrients and primary producer biomass. For example, phosphorus losses from catchments to surface waters and the net accumulation of phosphorus in lakes may increase (Jeppesen et al., 2009), which may lead to increased productivity and changes in rates of photosynthetic CO_2 losses and phytoplankton respiration.

The simulation results for the effects of climate change on water column DO conditions showed that the hypolimnetic DO concentration remained higher during winter, whereas the onset of summertime hypolimnetic anoxia occurred earlier in a warmer hypolimnion. Anoxic conditions also prevailed longer in autumn because of a longer stratified period. These findings are in line with studies on climate effects on DO by Fang and Stefan (2009) and Couture et al. (2015). Pulkkanen and Salonen (2013) observed that the wintertime hypolimnetic water temperature in a large, deep Finnish lake was lowest when freezing occurred exceptionally late. The phenomenon was also seen in the climate change simulations in Saloranta et al. (2009) as well as in the scenario simulations in this work. When freezing is delayed under the conditions of low shortwave radiative heating, the autumnal mixing period is longer and the entire water column and sediment may cool more efficiently (Arvola et al., 2010), which may result in lower water temperature at the onset of the ice-covered period and potentially also in reduced organic matter

degradation rates during winter. Better oxygenation of the hypolimnion because of a longer autumnal mixing period and higher oxygen solubility in colder water may also increase the water column DO concentration right after ice-on.

The hypolimnion of Lake Kuivajärvi is anoxic in late summer in present climate, and the duration of summertime anoxia may be considerably longer in the future. In accordance with the results of this work, Couture et al. (2015) suggested that even though an earlier ice-off and a longer spring mixing period may enhance water column ventilation resulting in a higher hypolimnetic oxygen saturation at the onset of summer stratification in boreal lakes in the future, the effect of greater allochthonous organic matter loading and its faster degradation consuming DO may be stronger and thus lead to anoxia. As a result, the consequences of summertime anaerobic methane production and consequent CO_2 production via methanotrophy in the water column may be considerably higher in some boreal lakes in the future. The highest CO_2 concentrations in the hypolimnion during the anoxic conditions in summertime in the calibration period may have partially been caused by methane-related processes. They may have not been captured by the simulation because CO_2 is not produced in anoxic conditions in the model. The summertime hypolimnetic CO_2 levels may thus have been even more underestimated in the scenario simulations because of the longer anoxic period. Therefore, the estimates of the CO_2 efflux after the breakdown of stratification may be classified conservative.

Even though the reliability of the simulation results for the scenario period can be considered adequate regarding the model performance, which was satisfactory on a seasonal scale also in the calibration and validation period, the applied climate scenarios caused uncertainties in the predictions of future CO_2 evasion from boreal lakes. Also, along with atmospheric temperature, precipitation is a meteorological variable that mainly governs the hydrological regime of catchments. Future projections for precipitation were not taken into account directly but through estimates of climate-induced changes in seasonal stream discharge. The inclusion of a single, hypothetical scenario for discharge and few hypothetical scenarios for carbon loading brought about uncertainty in the scenario results in that regard. However, there is not considerable variation in the future estimates of seasonal streamflow trends in the boreal region (Veijalainen, 2012). By contrast, predictions on changes in stream DOC concentration, which is also affected by the amount and the seasonality of precipitation, are more diverse (Jennings et al., 2010).

8.2.2 Impact of changes in terrestrial loading

An increase in terrestrial CO_2 loading had a notably greater impact on in-lake CO_2 dynamics in the scenario simulations than a corresponding increase in terrestrial DOC loading. On a yearly scale, a fourfold inflow DOC concentration increase compared to an inflow CO_2 concentration increase, that is, 40% versus 10%, was needed to attain similar increases in the average in-lake CO_2 concentration; however, only a twofold inflow DOC concentration increase was needed for similar increases in annual CO_2 efflux. Nevertheless, the additional increases in terrestrial

organic carbon loading resulted only in a moderate additional increase in in-lake CO_2 concentration and CO_2 efflux compared to only the effects of warmer climate conditions and changes in seasonal inflow volumes under RCP4.5 forcing. In total, the annual CO_2 flux increased by 23–25% and the average open water season CO_2 concentration at the depth of 1 m increased by 14–16%, of which about 4 and 1 percentage points, respectively, were caused by the 40% increase in inflow DOC concentration. In their statistical study on CO_2 evasion from boreal lakes, Hastie et al. (2018) projected the average surface water CO_2 partial pressure to increase by 27% and the total CO_2 efflux over the boreal region to increase by 38% by the end of the 21st century under a low-emission scenario RCP2.6. Atmospheric temperature was not used as a predictor in the study, but the increase in CO_2 evasion was mainly due to a predicted substantial increase in terrestrial net primary production, to which carbon loading to lakes is related. However, the figures cannot be fully contrasted with the predictions of this work because of a large number of lakes with a wide size distribution were included in the study. Still, the predictions of this work are moderate compared to Hastie et al. (2018) considering that a higher-emission scenario and a presumably high increase in DOC loading were applied in this work.

DOC may mitigate the impacts of warming climate on lakes by reducing heat flux from the atmosphere to the deeper water layers (Read and Rose, 2013). Higher DOC concentration results in a stronger attenuation of radiative heat flux; thus, the epilimnion gets thinner and warmer and the hypolimnion remains cooler, which may also decrease hypolimnetic CO_2 production in spite of warmer climate conditions in the future (Heiskanen et al., 2015). This was seen also in the scenario simulations in this work. Because of the linearity of the dependence of light attenuation on water column DOC concentration, the percentage increase of the DOC-related PAR attenuation coefficient $K_{\mathrm{DOC,P}}$ resulting from the 40% increase in inflow DOC concentration in the scenario period equaled that of DOC concentration. The value of $K_{\mathrm{DOC,P}}$ increased from 0.25–0.26 1/m to 0.34–0.35 1/m. As a result, the surface water temperature increased on average by 0.2 °C during the open water season. Even though the accumulation of CO_2 at the depth of 9 m started 1–3 d earlier because of the faster development of stratification, organic matter degradation rates were lower in the cooler hypolimnetic conditions during the stratified period. The DO concentration at 9 m decreased below the anoxic limit 6–7 d later, and also the hypolimnetic CO_2 concentration reached its maximum level later. However, the anoxic period was not considerably shortened as the deepening of the mixed layer to 9 m occurred 4–5 d later.

Nevertheless, considerably varying estimates have been made of the effect of increasing water column DOC concentration on lake thermal conditions. Heiskanen et al. (2015) presented the effect of variations of ±25% of the light extinction coefficient on thermal conditions in Lake Kuivajärvi using the results from two one-dimensional thermodynamic lake models. They showed that darker water would decrease the surface temperature by approximately 0.3 °C. On the contrary, an increase in lake surface temperatures under the conditions with greater light attenuation was seen in one-dimensional model simulations in Perroud and

Goyette (2010) and Read and Rose (2013). The seasonal thermocline elevation was about 0.1–0.2 m under a 37% larger β_{DOC} in this work, which is in accordance with Heiskanen et al. (2015). However, they concluded that darker water color would result in an earlier breakdown of stratification, whereas our simulations showed that the autumn turnover will occur later because of a warmer epilimnion and stronger stratification in summer.

9 Applicability and implications of alternative models for gas exchange velocity

In this chapter, the performance of different parameterizations for the gas exchange velocity k, or shortly gas exchange models (hereafter abbreviated as GEMs), incorporated into MyLake C regarding the simulation of near-surface CO_2 concentration and air-water CO_2 flux and implications thereof are presented and discussed. The magnitude of CO_2 transfer between lake water column and the atmosphere also affects the whole-lake carbon budget. If a GEM yields a relatively high gas exchange velocity and thus an increased CO_2 flux out of the water column, the in-lake net production of CO_2 or the terrestrial supply of CO_2 must be enhanced to balance the output. Thus, the model must somehow adjust to changes in carbon efflux.

Some of the GEMs include the flux-increasing effect of turbulence generated by water-side penetrative convection. Thermal convection is driven by heat flux between the epilimnetic mixed layer and the atmosphere. To yield proper estimates of gas exchange, the lake model has to simulate also the air-water heat flux correctly. Thus, also the model performance considering air-water heat flux is assessed in this chapter. The simulated components of the heat flux were compared with the daily averages of corresponding in-lake measurements. The simulated k_{CO2}'s and CO_2 fluxes were compared with k_{CO2}'s and CO_2 fluxes that were calculated with the respective formulas using the daily averages of measured heat fluxes and other required meteorological and in-lake variables, referred to as calculated k's and calculated CO_2 fluxes.

The phrase "with/for the MyLake C application using each of the incorporated models for the gas exchange velocity in the calculation of air-water CO_2 flux" is hereinafter in this chapter denoted shortly as "with/for each GEM". Correspondingly, the MyLake C simulations using the models for the gas exchange velocity by Cole and Caraco (1998) (corresponding to the gas exchange velocity k_{CC}), Heiskanen et al. (2014) (k_{HE}), MacIntyre et al. (2010) (k_{MI}), and Tedford et al. (2014) (k_{TE}), presented in Section 3.3, are denoted as CC, HE, MI, and TE, respectively.

9.1 Results

9.1.1 Model recalibrations

Fig. 9.1 presents the calibrated results for CO_2 concentration with each GEM and the daily averages of the automatic high-frequency measurements at the depths of 0.2, 2.5, and 7 m. Despite the functional differences between the GEMs, the simulated CO_2 concentrations did not differ substantially between GEMs. The performance metrics for CO_2 presented in Table 9.1 show that all of the models underestimated the CO_2 concentrations ($B^* < 0$) at all depths with few exceptions. The averages of the measured CO_2 concentrations at 0.2 m, or the near-surface CO_2 concentrations, over the open water seasons were 45.2 mmol/m^3 in the calibration year 2013 and 37.2 mmol/m^3 in the validation year 2014. Automatic near-surface CO_2 concentration measurements during the ice-covered periods were largely inapplicable because of system malfunction. CC yielded a considerably higher open water season near-surface CO_2 concentration than the other GEMs (average concentrations 44.3 and 40.3 mmol/m^3 for the calibration period and for the validation period, respectively, for CC; 34.2 and 31.6 mmol/m^3 for HE; 31.5 and 29.4 mmol/m^3 for MI; and 36.9 and 34.1 mmol/m^3 for TE.) Only the days with applicable measurement data were included in the calculation of these simulated average CO_2 concentrations. The open water seasons were determined according to the simulated ice-off and ice-on dates, which were the same as in the initial calibration. However, the air-water flux is nonzero starting from the day after the ice-off date in MyLake C; thus, the open water seasons applied in the analysis of the results in this chapter extended from 3 May to 25 November in 2013 and from 16 April to 22 November in 2014.

The recalibrated parameter values with each GEM are presented in Table 9.2. The optimal gain and loss of in-lake CO_2 can be attained through many possible combinations of processes in MyLake C. Therefore, the resultant optimal parameter sets were notably different between GEMs and emphasized different processes. However, regarding the primary objective of this work, the simulation of the near-surface concentration and efflux of CO_2, the different outcomes of the calibration processes can be considered equally applicable, giving insight on the diversity of processes impacting lacustrine CO_2 dynamics.

The recalibration procedure differed from the initial calibration presented in Chapter 8 in a way that the greatest depth used was only 7 m. The simulated epilimnetic CO_2 concentration was too low after the onset of summer stratification in May of the calibration year. However, insufficient water column mixing during the first days of the stratified period in the simulations prevented a corresponding decline of CO_2 concentration at 7 m. Thus, the model performance was most successful at the depth of 7 m. The timing of thermocline deepening matched the observations during the calibration period, and the extent of turbulent diffusion through the metalimnion before the thermocline reached the 7 m depth was minor because of the small values of a_k. The mixed layer thickness did not differ substantially be-

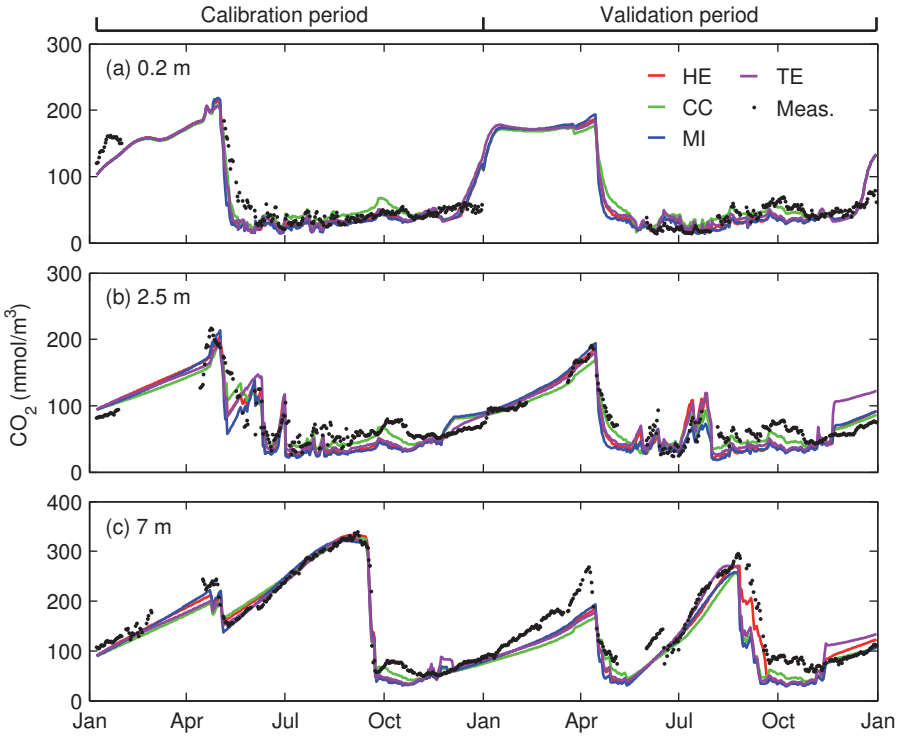

Figure 9.1: Simulation results for CO_2 concentration (mmol/m^3) with each GEM versus the daily averages of automatic measurements at the depths of (a) 0.2 m, (b) 2.5 m, and (c) 7.0 m in Lake Kuivajärvi during the calibration year 2013 and the validation year 2014.

Table 9.1: Statistical results for the performance of the CO_2 simulations with the MyLake C application to Lake Kuivajärvi during the calibration and validation periods using different incorporated models for the gas exchange velocity in the calculation of air-water CO_2 flux[a].

	R^2	p	RMSE[b]	NS	RMSD′*	B^*	n
Calibration (2013)							
Heiskanen							
0.5 m	0.70	< 0.001	23.03	0.63	−0.55	−0.26	246
2.5 m	0.74	< 0.001	24.08	0.62	0.57	−0.23	258
7 m	0.97	< 0.001	18.46	0.96	0.19	−0.06	276
Cole & Caraco							
0.5 m	0.69	< 0.001	21.22	0.68	−0.56	−0.054	246
2.5 m	0.79	< 0.001	18.31	0.78	−0.46	−0.088	258
7 m	0.97	< 0.001	19.50	0.96	0.19	−0.069	276
MacIntyre							
0.5 m	0.62	< 0.001	26.17	0.52	−0.62	−0.31	246
2.5 m	0.69	< 0.001	27.55	0.51	0.63	−0.30	258
7 m	0.97	< 0.001	18.49	0.96	0.18	−0.08	276
Tedford							
0.5 m	0.64	< 0.001	23.65	0.61	−0.60	−0.18	246
2.5 m	0.72	< 0.001	23.84	0.63	0.57	−0.20	258
7 m	0.97	< 0.001	19.47	0.96	0.19	−0.08	276
Validation (2014)							
Heiskanen							
0.5 m	0.41	< 0.001	17.41	−0.09	1.03	−0.14	191
2.5 m	0.77	< 0.001	20.20	0.67	0.55	−0.17	264
7 m	0.84	< 0.001	34.44	0.69	−0.40	−0.39	307
Cole & Caraco							
0.5 m	0.49	< 0.001	15.58	0.13	0.89	0.28	191
2.5 m	0.87	< 0.001	13.33	0.85	−0.36	−0.11	264
7 m	0.77	< 0.001	44.71	0.48	−0.49	−0.53	307
MacIntyre							
0.5 m	0.42	< 0.001	18.01	−0.16	1.05	−0.23	191
2.5 m	0.78	< 0.001	21.83	0.61	0.58	−0.24	264
7 m	0.76	< 0.001	43.74	0.50	−0.49	−0.50	307
Tedford							
0.5 m	0.40	< 0.001	17.11	−0.05	1.02	−0.03	191
2.5 m	0.59	< 0.001	25.99	0.45	0.74	0.02	264
7 m	0.68	< 0.001	42.75	0.52	−0.59	−0.36	307

[a]Coefficient of determination (R^2), root-mean-square error (RMSE), Nash–Sutcliffe efficiency (NS), normalized unbiased root-mean-square difference (RMSD′*), normalized bias (B^*).
[b]Units: CO_2, mmol/m^3.

Table 9.2: Calibrated model parameters for the MyLake C application to Lake Kuivajärvi with different incorporated models for the gas exchange velocity and the default values used as the means of the prior parameter distributions in the calibrations.

	Default	HE	CC	MI	TE	Unit
a_{k}	3.92	0.27	0.45	0.39	1.18	$\times 10^{-3}$
β_{DOC}	2.85	2.94	3.47	3.22	2.75	$\times 10^{-5}\,\mathrm{m^2/mg}$
$C_{\mathrm{DI,IN}}$	1.00	1.86	1.55	1.91	3.05	-
$k_{\mathrm{DOC},1}$	0.801	5.71	1.11	0.46	9.01	$\times 10^{-1}/\mathrm{d}$
$k_{\mathrm{DOC},2}$	1.01	1.40	2.41	3.35	1.07	$\times 10^{-2}/\mathrm{d}$
$k_{\mathrm{POC},1}$	0.942	4.54	0.91	1.78	0.60	$\times 10^{-1}/\mathrm{d}$
$k_{\mathrm{POC},2}$	0.901	2.91	5.01	15.9	4.49	$\times 10^{-2}/\mathrm{d}$
$k_{\mathrm{POC,sed}}$	2.53	4.11	2.43	2.84	3.72	$\times 10^{-4}/\mathrm{d}$
m_{20}	0.206	0.11	0.24	0.090	0.31	$1/\mathrm{d}$
μ'_{20}	2.37	2.96	5.95	1.62	3.84	$1/\mathrm{d}$
W_{str}	0.285	0.33	0.35	0.35	0.24	-

tween GEMs during the calibration period, but more variation occurred during the summer of the validation year. Thermocline deepening occurred too early in the summer of the validation year as was the case also in the initial calibration. The deepening occurred slower and more gradually in HE than in other GEMs because of a slightly shallower and steeper thermocline during summer, which was caused by the smallest value for a_{k}. A stronger temperature gradient in the metalimnion resisted thermocline erosion caused by wind mixing.

The simulated CO_2 exchange velocities and air-water CO_2 fluxes during the open water seasons of the calibration year and the validation year are shown in Fig. 9.2. CC yielded clearly the lowest simulated k (average values 2.81 and 2.76 cm/s for the calibration period and the validation period, respectively), whereas the other GEMs gave k's rather similar to each other (HE: 5.44 and 5.33 cm/s; MI: 5.87 and 5.82 cm/s; TE: 4.73 and 4.66 cm/s). However, the simulated fluxes showed a differing behavior between GEMs because of the differences in the simulated near-surface concentrations of CO_2, and the flux differences between GEMs were smaller than the differences in the values of k (open water season average effluxes 0.22 and 0.20 µmol/(m^2 s) for the calibration period and the validation period, respectively, for CC; 0.28 and 0.26 µmol/(m^2 s) for HE; 0.25 and 0.24 µmol/(m^2 s) for MI; and 0.28 and 0.27 µmol/(m^2 s) for TE). The simulated effluxes obtained with CC were 77–86% of the fluxes obtained with the other GEMs, whereas the simulated average k_{CC}'s were only 47–59% of the other k's. The high efflux in MI due to a high k_{MI} reduced the near-surface CO_2 concentration compared to the other GEMs during the whole simulation period. The high springtime CO_2 efflux in MI and the low efflux in CC are most distinctly seen in the CO_2 concentrations at 2.5 m (Fig. 9.1b).

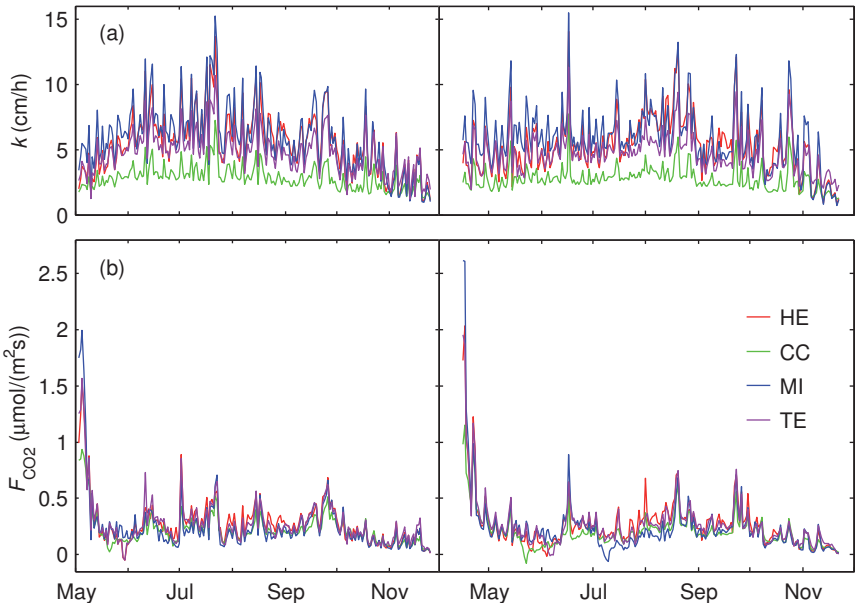

Figure 9.2: Simulated (a) gas exchange velocities for CO_2 (cm/h) and (b) air-water CO_2 fluxes (µmol/(m^2 s)) with each GEM in Lake Kuivajärvi during the open water seasons of 2013 (left) and 2014 (right).

9.1.2 Air-water heat and CO_2 exchange

The measurements of sensible and latent heat fluxes in 2014 were largely unavailable. Therefore, the comparisons between the simulated and calculated air-water heat fluxes and CO_2 fluxes were performed over the period 3 May to 31 October 2013.

Surface heat fluxes

The measured values of daily sensible heat flux (Q_H), latent heat flux (Q_L), and net longwave radiative heat flux (Q_{LW}) and the calculated portion of measured shortwave radiative heat flux trapped in the actively mixing layer (AML) ($Q_{SW,AML}$) together with the corresponding fluxes simulated with each GEM are presented in Fig. 9.3. The simulations overestimated Q_H slightly (RMSE = 6.87–7.54 W/m^2, NS = 0.79–0.82, $B^* = -0.095 \ldots -0.16$, $n = 166$) and Q_L somewhat more notably (RMSE = 16.5–18.7 W/m^2, NS = 0.56–0.66, $B^* = -0.25 \ldots -0.35$, n = 166) during the study period. Also the daily Q_{LW}, which was mostly directed from the lake water column to the atmosphere, was overestimated (RMSE = 18.4–18.9 W/m^2, NS = 0.49–0.51, $B^* = -0.51 \ldots -0.53$, $n = 180$). High daily values of Q_{LW} were rather well caught by the bulk model used in MyLake, but small-magnitude fluxes directed out of the lake were invariably overestimated as seen in Fig. 9.3b. Con-

trary to the measurements, the simulated daily time series contained no events of Q_{LW} directed into the lake. $Q_{\mathrm{SW,AML}}$ was simulated more correctly on average, but the variation was rather large (RMSE = 31.6–32.2 $\mathrm{W/m^2}$, NS = 0.16–0.19, $B^* = -0.07 \ldots 0.05$, $n = 180$).

In the simulations, the calculation of Q_{H} was based on the air-water temperature gradient, and Q_{LW} was also influenced by water surface temperature. Hence, the differences in simulated Q_{H} and Q_{LW} between GEMs were partly caused by differences in surface temperatures applied in the heat flux calculation, presented in Fig. 9.4a. The average surface temperature in May–October was lowest in TE (0.2 °C lower than the corresponding measured average) and highest in MI (0.1 °C higher than the measured average). The simulated surface temperatures were 0.4–0.7 °C too high during early summer and midsummer (May–July) and 0.5–0.7 °C too low in late summer and autumn (August–October). This is seen most clearly in the simulated Q_{H} in Fig. 9.3a: the simulated flux from the lake to the atmosphere was too high in May and early June because of the high surface temperature. The primary reason for the surface temperature differences was different attenuation of shortwave radiation between GEMs. The low phytoplankton death rate resulted in a higher Chl *a* concentration and the high allochthonous POC fragmentation rate resulted in a higher DOC concentration in MI than in the other GEMs, which resulted in a stronger attenuation of shortwave radiation and a higher surface temperature because of a thinner and warmer epilimnion.

The fraction of the net shortwave radiation that heats the AML depends on the depth of the AML, z_{AML}. The time series of the simulated and the measured depths of the AML are presented in Fig. 9.4b. The measured daily z_{AML} was estimated from the daily average temperature profile, whereas the corresponding depth applied in MyLake C was determined through the simulated temperature profile during the calculation of CO_2 flux. If the simulated z_{AML} was higher than the measurement estimate, the model yielded a higher amount of heat trapped in the AML compared to the measurement-based calculation, and vice versa.

The thermal submodel of MyLake did not generate notable temperature variation in the epilimnetic layer with the exception of days with a high amount of surface heating in early summer and midsummer, and thus the AML tended to be overly deep. By contrast, the measured AML was often rather shallow despite the comparatively high value of the threshold temperature difference, 0.25 °C, used in the calculation. However, the topmost layer was effectively heated in the simulation right after ice-off in early May because solar radiation was high and because also sensible heat flux was directed into the water, which resulted in an overly shallow AML. Also, a weak temperature gradient was formed below the topmost grid layer on some days in late October when the surface heat flux was positive, which resulted in a shallow AML in the simulation. On 31 October the topmost layer cooled below 4 °C, and a weak inverse stratification was formed near the surface. The simulation with a daily time step and a sequential description of in-lake processes did not catch simultaneous wind mixing and surface warming or cooling that were seen in temperature profile measurements and that resulted in a deeper

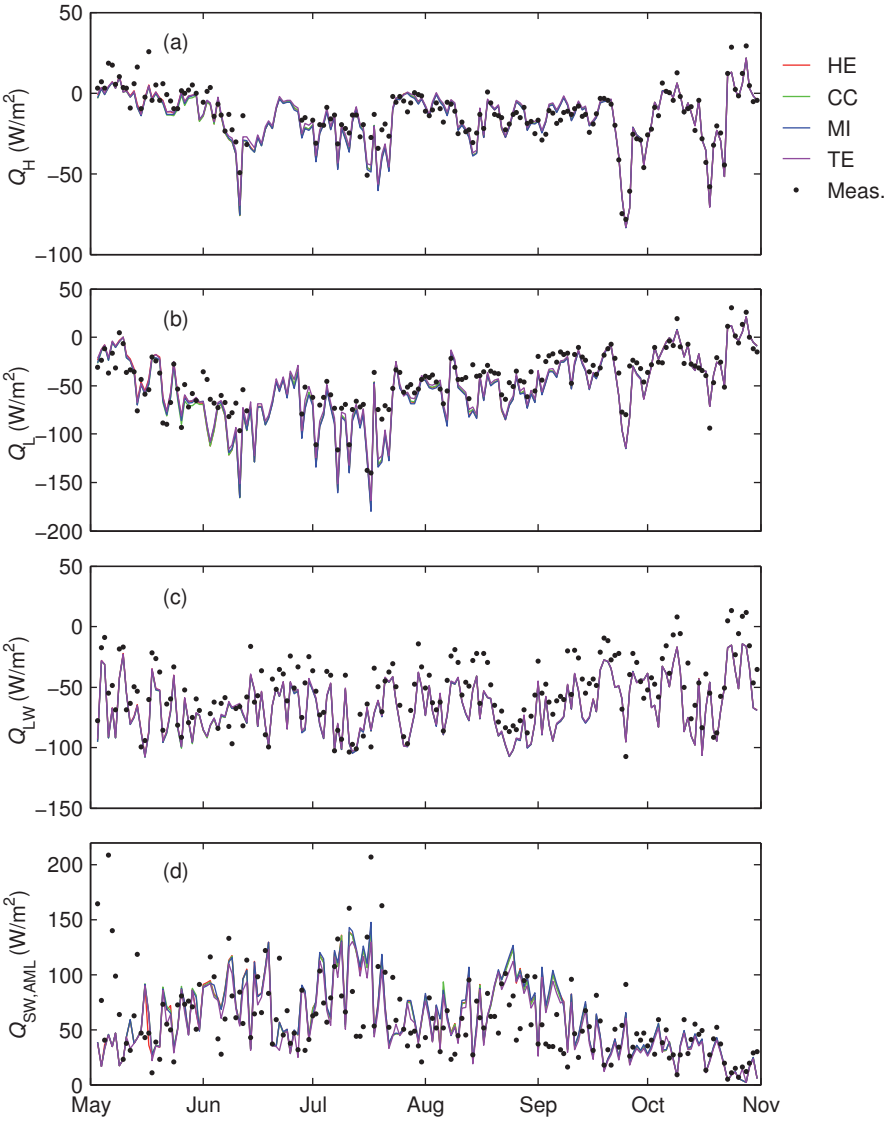

Figure 9.3: Simulated and measured daily (a) sensible heat fluxes (W/m^2), (b) latent heat fluxes (W/m^2), and (c) net longwave radiative heat fluxes (W/m^2) at the surface of Lake Kuivajärvi and (d) simulated and calculated daily portions of shortwave radiative heat flux trapped in the active mixing layer of the lake (W/m^2) in May–October 2013. The simulations were performed using each of the models for the gas exchange velocity incorporated into MyLake C. Positive fluxes are directed into the water column.

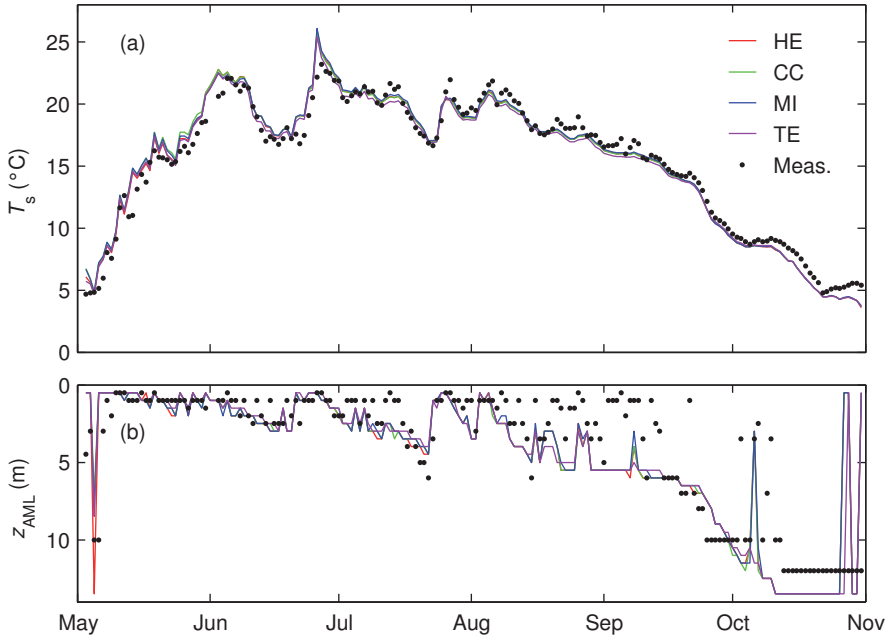

Figure 9.4: (a) Simulated surface (0–0.5 m) temperatures (°C) during CO_2 flux calculation and the daily averages of measured surface (0.2 m) temperatures and (b) simulated and empirically determined depths of the daily actively mixing layer (m) in Lake Kuivajärvi in May–October 2013. The simulations were performed using each of the models for the gas exchange velocity incorporated into MyLake C.

observed AML.

The effective heat fluxes (Q_{eff}) between the AML and the atmosphere simulated with each GEM and calculated on the basis of heat flux measurements are presented in Fig. 9.5a. The simulated Q_{eff} was directed from lake to the atmosphere throughout the study period except for one day in early May and five days in October. The negative Q_{eff} from the lake was largely overestimated in the simulation, and the occasions of positive measured Q_{eff} were either not captured or significantly underestimated. The overall performance of Q_{eff} simulation was thus rather poor (RMSE = 48.2–49.2 W/m^2, NS = 0.11–0.14, $B^* = -0.47 \ldots -0.46$, $n = 164$). The overestimation of the negative values of Q_{H}, Q_{L}, and Q_{LW} resulted in the overestimation of the negative Q_{eff}, and the large variation in the discrepancy in the shortwave heating of the AML decreased the efficiency of the simulation. The largest difference between the simulated and measured effective heat fluxes occurred in early May. Only a minor fraction of shortwave radiation was trapped in the AML in the simulations because of the shallowness of the AML, and the resulting Q_{eff} was negative. On the contrary, the measured AML was deeper, and

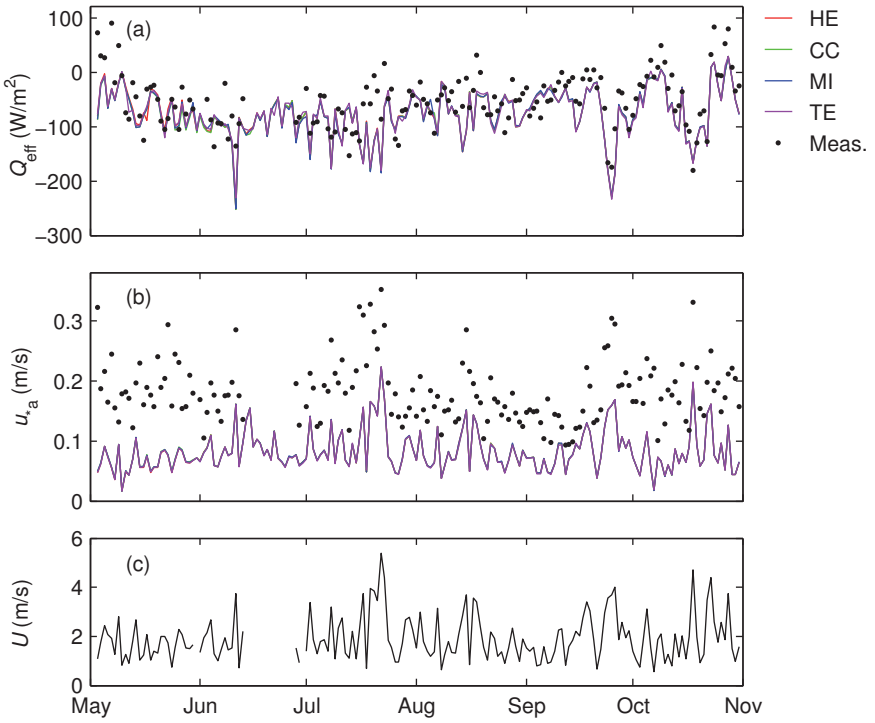

Figure 9.5: (a) Daily effective heat fluxes (W/m^2) between the actively mixing layer and the atmosphere simulated with each GEM and calculated from heat flux measurements, (b) atmospheric friction velocities (m/s) simulated with each GEM and obtained from measurements, and (c) measured daily wind speed (m/s) at 1.7 m height over Lake Kuivajärvi.

the heating of the AML by shortwave radiation overrode the cooling of the surface of the AML by negative Q_{LW} and Q_{L}, which resulted in a highly positive Q_{eff}.

The simulated and measured atmospheric friction velocities $u_{*\mathrm{a}}$ are presented in Fig. 9.5b, and Fig. 9.5c shows the daily wind speed over the lake during the study period. The differences in the simulated values of $u_{*\mathrm{a}}$ between GEMs, which were due only to different water surface temperatures, were very small. The atmospheric friction velocity was greatly underestimated by the model (RMSE = 0.11 m/s, NS = −3.2, $B^* = -1.89$, $n = 166$). The simulated $u_{*\mathrm{a}}$ was on average 46% of the measured daily average value.

CO_2 exchange

The gas exchange velocities simulated with each GEM and the corresponding calculated gas exchange velocities on 3 May to 31 October 2013 are shown in Fig. 9.6, and the corresponding performance statistics are presented in Table 9.3. The re-

spective simulated and calculated values were rather similar in the simpler, wind-based GEMs, CC and MI, whereas the discrepancies were higher in the other two GEMs, which include also the effect of buoyancy flux. The reason for the slight overestimation of k in the simulations with CC and MI is that the simulated surface temperature during the CO_2 flux calculation was higher than the measured daily average surface temperature especially in early summer (see Fig. 9.4a) and the temperature correction of k was thus different. In addition, the opposite directions of Q_{eff} affected the difference in MI in early May: the occurrences of a negative buoyancy flux in the simulations yielded a higher k_{MI} compared to the corresponding calculated value obtained from the observed positive buoyancy flux. The effect of different surface temperatures is seen also in k_{HE}. In addition, a high Q_{eff} (Fig. 9.5) and a deep AML, especially during the deepening of the epilimnion in August–September (Fig. 9.4b), often resulted in a high simulated k_{HE}. The difference between the simulated and calculated k_{HE} was conspicuous during the occasions of a very shallow observed AML. The impacts of wind shear and buoyancy flux are parameterized to be roughly of the same order of magnitude in HE, whereas CO_2 flux is principally driven by wind shear in TE. Because the simulated atmospheric friction velocities were significantly lower than the daily averages of measured atmospheric friction velocities, the simulated k_{TE} was on average 40% lower than the calculated value.

The simulated CO_2 concentrations in the model surface layer (0–0.5 m) obtained with each GEM and the daily averages of the automatic CO_2 concentration measurements at 0.2 m on 3 May to 31 October 2013 are presented in Fig. 9.7, and the performance metrics for the simulation are presented in Table 9.3. As also the normalized biases show, the near-surface CO_2 concentration was mostly notably underestimated during the whole period in all GEMs apart from CC, which yielded too high concentrations in autumn. The near-surface CO_2 concentration declined overly fast in all GEMs in May. The decline was most rapid in MI, which yielded the highest k. The near-surface CO_2 concentration decreased close to the atmospheric equilibrium concentration in late July and early August in the simulations. Warm and calm weather conditions decreased the thickness of the epilimnion, and the gain of CO_2 in the shallow epilimnion was insufficient to compensate for the loss via efflux in the simulations.

The air-water CO_2 fluxes simulated and calculated with each GEM on 3 May to 31 October 2013 are presented in Fig. 9.8, and the corresponding statistics for the performance of the CO_2 flux simulation are presented in Table 9.3. The total and monthly averages of both the simulated and the calculated CO_2 fluxes are shown in Table 9.4. All GEMs yielded a low efflux in May in the simulations because of the low simulated air-water CO_2 concentration gradient. TE gave a low efflux during the whole period in the simulation because of the low k_{TE}, and CC overestimated the efflux in August–September because of the high near-surface CO_2 concentration. The performance of HE was rather good in July–October (RMSE = 0.13 µmol/(m^2 s), NS = 0.49, $B^* = -0.043$, $n = 123$).

The CO_2 flux calculations were based on the same air-water CO_2 concentration

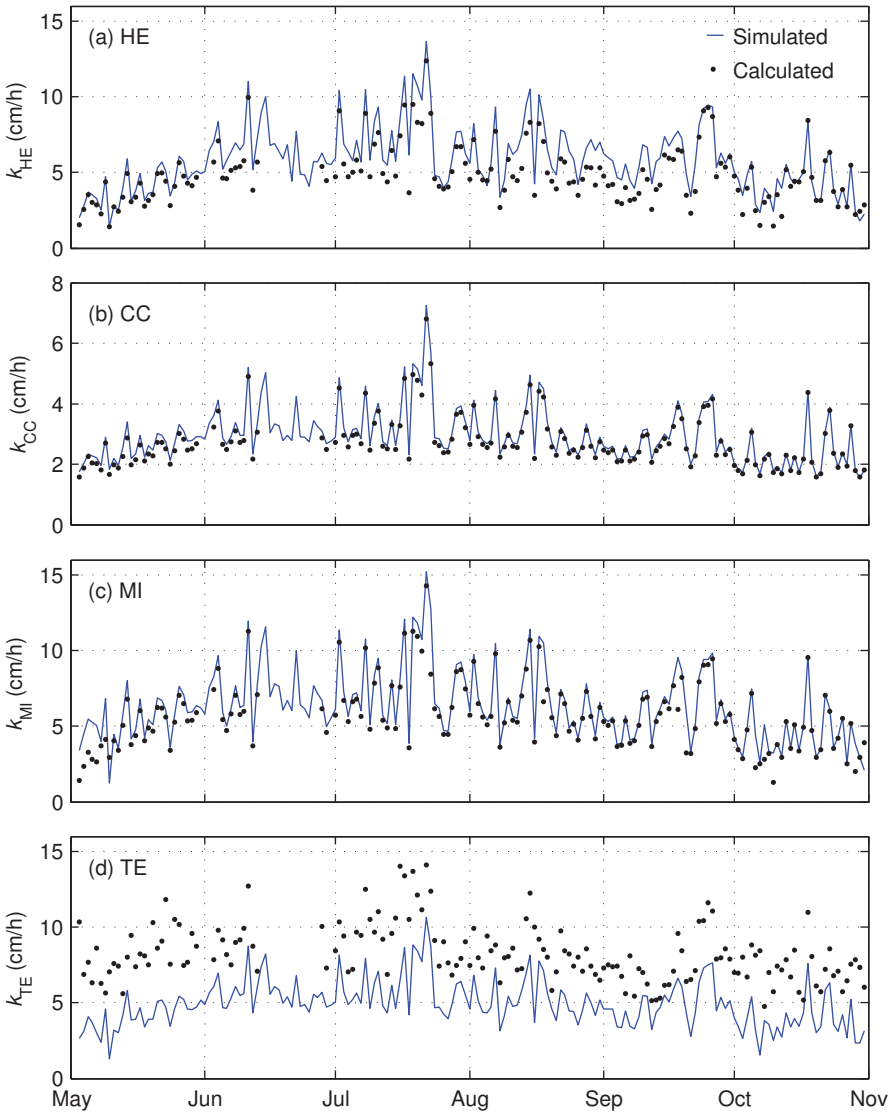

Figure 9.6: Simulated and calculated gas exchange velocities for CO_2 (cm/h) in Lake Kuivajärvi on 3 May to 31 October 2013 obtained with the gas exchange models by (a) Heiskanen et al. (2014), (b) Cole and Caraco (1998), (c) MacIntyre et al. (2010), and (d) Tedford et al. (2014).

Table 9.3: Statistical results for the performance of the simulation of water column CO_2 concentration at 0.2 m, gas exchange velocity for CO_2, and air-water CO_2 flux using different models for the gas exchange velocity incorporated into MyLake C against the respective measured or calculated counterparts in Lake Kuivajärvi in 3 May to 31 October 2013[a].

	R^2	RMSE	NS	RMSD′*	B^*	n
CO_2 concentration at 0.2 m[b]						
Heiskanen	0.63	21.70	0.35	−0.66	−0.47	161
Cole & Caraco	0.54	18.51	0.53	−0.69	−0.05	161
MacIntyre	0.45	26.49	0.027	−0.79	−0.59	161
Tedford	0.58	20.96	0.39	−0.69	−0.36	161
Gas exchange velocity for CO_2[b]						
Heiskanen	0.91	1.13	0.64	0.35	0.48	164
Cole & Caraco	0.99	0.19	0.95	0.11	0.19	164
MacIntyre	0.90	0.91	0.83	0.33	0.24	164
Tedford	0.45	3.65	−2.82	−0.76	−1.80	164
Air-water CO_2 flux[b]						
Heiskanen	0.46	0.23	0.38	−0.74	−0.26	158
Cole & Caraco	0.55	0.13	0.54	−0.67	0.082	158
MacIntyre	0.29	0.35	−0.035	−0.89	−0.49	158
Tedford	0.45	0.70	−0.026	−0.82	−0.60	158

[a] Coefficient of determination (R^2), root-mean-square error (RMSE), Nash–Sutcliffe efficiency (NS), normalized unbiased root-mean-square difference (RMSD′*), normalized bias (B^*).
[b] Units: CO_2 concentration, mmol/m^3; gas exchange velocity, cm/h; CO_2 flux, µmol/(m^2 s).

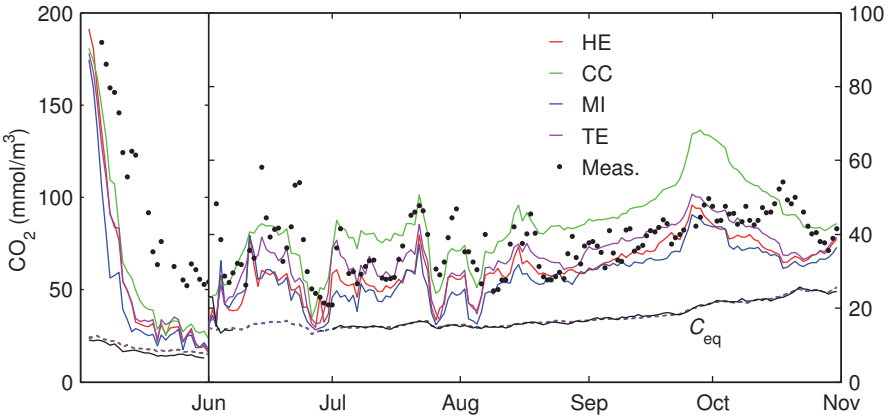

Figure 9.7: Simulated CO_2 concentrations (mmol/m^3) in the surface layer (0–0.5 m) obtained with each GEM and the daily averages of the automatic measurements at 0.2 m in Lake Kuivajärvi in May–October 2013. The atmospheric equilibrium concentrations of CO_2 (C_{eq}) obtained from the simulations (dotted lines) and calculated from the measured atmospheric CO_2 concentration and surface temperature (solid black line) are also shown. Note the different vertical scales in May and June–October.

gradients in all GEMs, and the differences between the calculated fluxes in Table 9.4 were due only to different values of k. When comparing the two wind-based models MI and CC, the monthly averages of the fluxes calculated with MI were mainly more than double of those calculated with CC. Most of the days with a positive buoyancy flux and a resulting lower k_{MI} occurred in May and October; thus, the ratio between the CO_2 fluxes calculated with MI and CC was lower during those months. The CO_2 fluxes calculated with HE were slightly lower than those calculated with MI, and the average flux over the whole period calculated with TE was by far the highest. The days when the ratio of the measured atmospheric friction velocity to wind speed was high co-occurred with a large air-water concentration gradient in early May; therefore, the CO_2 flux calculated with TE, which uses atmospheric friction velocity, was exceptionally high during those days.

The differences between the monthly CO_2 fluxes calculated with different GEMs were notably high (Table 9.4). The differences between GEMs were much smaller in the case of simulated CO_2 fluxes, and the simulated CO_2 fluxes were clearly lower than the calculated CO_2 fluxes with the exception of CC. The calculated CO_2 fluxes were based on the measured CO_2 concentration, which was not affected by the amount of CO_2 flux; on the contrary, the higher the CO_2 flux in the simulation, the greater the decrease in near-surface CO_2 concentration. MyLake C with other GEMs than CC was not capable of producing enough CO_2 to compensate for the efflux, and the simulated near-surface CO_2 concentrations were too low. In addition, a small value of k decreased the simulated CO_2 flux significantly in

Table 9.4: Total and monthly averages of simulated and calculated CO_2 fluxes (µmol/(m^2 s)) in May–October 2013 obtained by different gas exchange models. Only the days with available data for CO_2 flux calculation are included in the averaging of the simulated fluxes. Monthly values for June are excluded from the table because measurement data was available only for 7 days.

	May–Oct	May	Jul	Aug	Sep	Oct
Calculated						
Heiskanen	0.38	0.79	0.37	0.27	0.31	0.24
Cole & Caraco	0.23	0.53	0.20	0.15	0.16	0.13
MacIntyre	0.45	0.97	0.44	0.33	0.35	0.25
Tedford	0.71	1.90	0.56	0.41	0.45	0.43
Simulated						
Heiskanen	0.31	0.41	0.34	0.30	0.35	0.16
Cole & Caraco	0.24	0.33	0.26	0.22	0.27	0.17
MacIntyre	0.29	0.52	0.26	0.22	0.32	0.16
Tedford	0.30	0.43	0.33	0.26	0.34	0.17

TE. Net epilimnetic CO_2 production was highest in HE, which resulted in the simulated flux being even slightly higher than the calculated CO_2 flux in August and September. In CC, the simulated CO_2 flux was higher than the calculated CO_2 flux especially in August and September when the simulated near-surface CO_2 concentration was high. The simulated CO_2 flux was lowest in CC because of the smallest values of k, and the simulated gain of CO_2 was sufficient to sustain a high enough CO_2 concentration gradient in July–October.

Also the choice of the calculation interval had an effect of the calculated values of k and CO_2 flux. The calculations of the daily k and CO_2 flux presented here were performed using the daily averages of the input variables; hence, the conditions were compatible with the daily time step in the simulations. However, if the daily k was instead calculated as the daily average of calculated half-hour values of k, the results were different. The daily averages of half-hour k_{HE} (RMSE = 0.48 cm/h, NS = 0.94, $B^* = 0.20$) and k_{CC} (RMSE = 0.16 cm/h, NS = 0.96, $B^* = 0.15$) were higher than the respective values calculated using daily averages of input variables, whereas the opposite was the case for k_{MI} (RMSE = 0.70 cm/h, NS = 0.90, $B^* = -0.16$) and k_{TE} (RMSE = 0.22 cm/h, NS = 0.99, $B^* = -0.04$). In addition to the effect of nonlinearities in temperature corrections in the gas exchange models, the differences in the values of k between GEMs can partly be explained by the behavior of the driving variables of the flux in each model.

The effect of diel variation in the magnitude of water-side convection caused by buoyancy may be notable, which was seen in the performance of HE and MI. Using the daily averages of the input variables in the calculation may have smoothed out the effects of the spells of stronger negative buoyancy flux or a deeper AML

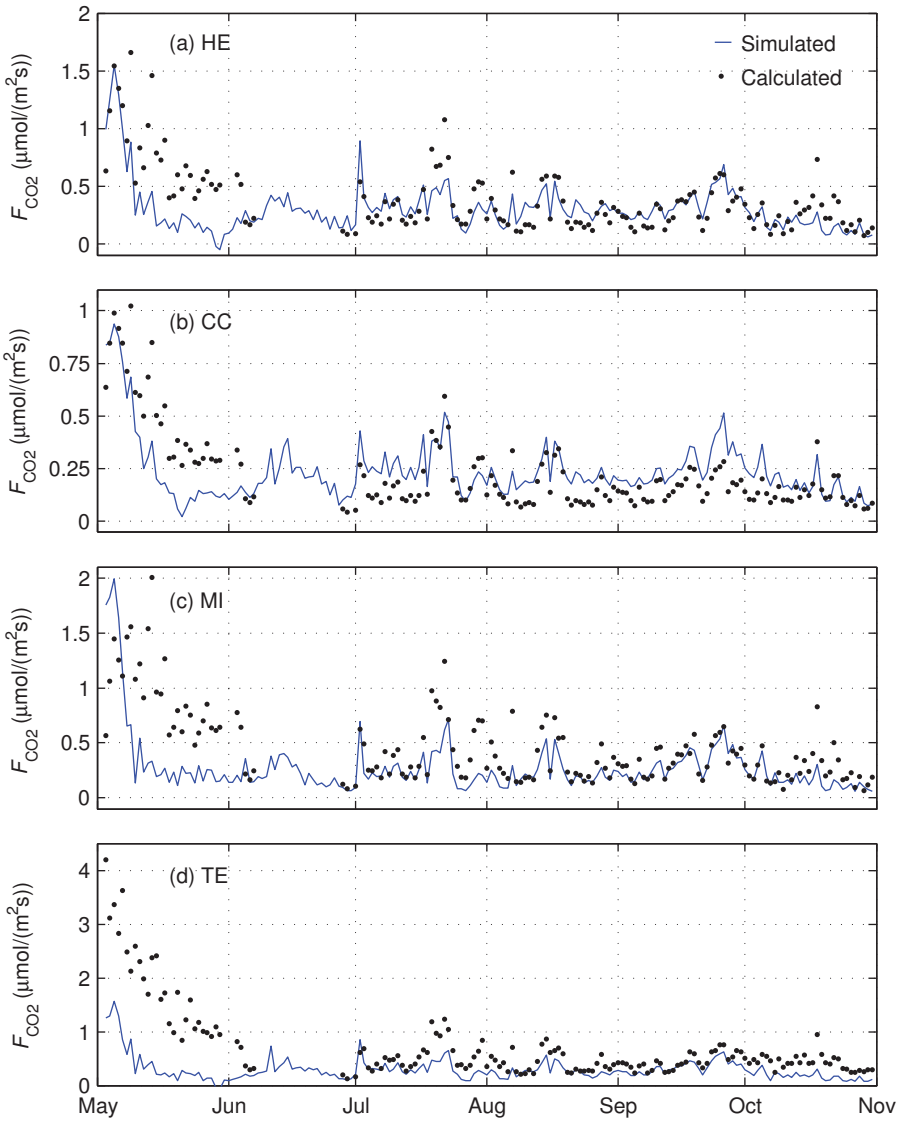

Figure 9.8: Simulated and calculated air-water CO_2 fluxes (µmol/(m^2 s)) in Lake Kuivajärvi on 3 May to 31 October 2013 obtained with the gas exchange models by (a) Heiskanen et al. (2014), (b) Cole and Caraco (1998), (c) MacIntyre et al. (2010), and (d) Tedford et al. (2014).

that increased the half-hour k, resulting in a lower daily k_{HE}. In MI, the sign of the effective heat flux determines the choice of the wind-based parameterization formula. The daily average Q_{eff} was chiefly negative during the study period; thus, the occasions of positive buoyancy flux that decreased the half-hour k were excluded in the calculation of k_{MI} with the daily averages of the input variables. However, the effect of buoyancy flux on k_{TE} is weak and the magnitude of k_{TE} is governed by $u_{*\mathrm{a}}$. Because k_{TE} is dependent on $u_{*\mathrm{a}}^{0.75}$, the effect of the diel variation of $u_{*\mathrm{a}}$was not very large when comparing the daily averages of half-hour k_{TE} with the values of k_{TE} obtained via the daily averages of $u_{*\mathrm{a}}$. The dependence of k on U is stronger than linear in CC, and the averaging of wind speed cut out the increase of k under the conditions of stronger wind during the day; hence, the k_{CC} obtained via the daily average of U was lower than the daily average of half-hour k_{CC}.

As a consequence of both different values of k and a different calculation method, also the daily CO_2 flux was different depending on if it was calculated as the average of half-hour CO_2 fluxes or as the product of the k calculated using daily averages of input variables and the daily average of the air-water CO_2 concentration gradient. The former method yielded a higher CO_2 flux in all GEMs (HE: RMSE = 0.066 µmol/(m^2 s), NS = 0.95, B^* = 0.13; CC: RMSE = 0.034 µmol/(m^2 s), NS = 0.97, B^* = 0.11; MI: RMSE = 0.10 µmol/(m^2 s), NS = 0.92, B^* = 3.4×10^{-4}; TE: RMSE = 0.11 µmol/(m^2 s), NS = 0.97, B^* = 0.05).

9.1.3 Lake CO_2 budgets

During the stratified period, CO_2 efflux from the epilimnion to the atmosphere is compensated in the model by the terrestrial loading of CO_2, the net in-lake production of CO_2 in the epilimnion, and the release of CO_2 from deeper layers due to the deepening of the epilimnion. The epilimnion is defined here as the layer in which water temperature is within 1 °C of the surface temperature. The simulated CO_2 budgets for the epilimnion during the periods of continuous summer stratification are presented in Table 9.5. The budget calculations were restricted to the periods when the thickness of the epilimnion z_{epi} was less than 7 m, that is, before the rapid deepening of the thermocline and the autumn turnover. The simulated and observed z_{epi}'s during those periods are presented in Fig. 9.9. The summer epilimnion formed 11 d later and reached the 7 m depth 16–22 d earlier in 2014 than in 2013. The observed epilimnion was shallow on some days in late August and early September 2013 as the water temperature in the topmost 1–2.5 m layer increased notably in daytime under conditions with high radiative heating and low winds. The lake was less effectively ventilated and the in-lake CO_2 concentrations were thus higher at the onset of the summer stratification in 2013 than in 2014, which resulted in a decrease in the amount of CO_2 in the epilimnion during the summer stratification period; by contrast, the amount of CO_2 in the epilimnion increased slightly during the corresponding period in 2014.

Phytoplankton concentration, which is governed in the model by the maximal

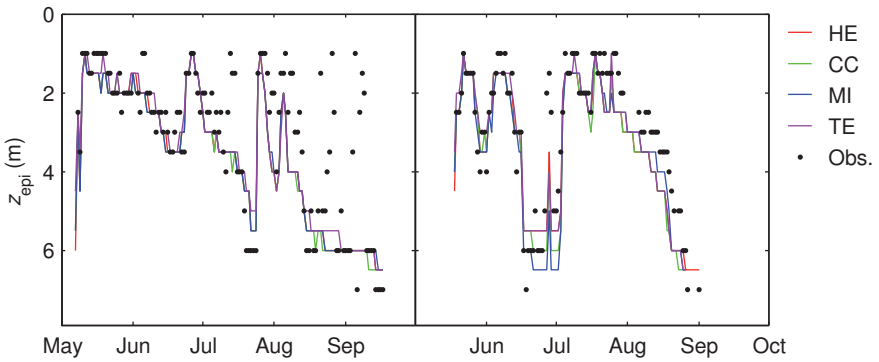

Figure 9.9: Simulated and observed depths of the epilimnion (m) in Lake Kuivajärvi during the periods of continuous summer stratification in 2013 (left panel) and 2014 (right panel). The simulations were performed using each of the models for the gas exchange velocity incorporated into MyLake C.

Table 9.5: Simulated CO_2 budgets (kg CO_2) for the epilimnion of Lake Kuivajärvi during summer stratification in 2013 and 2014 using different models for the gas exchange velocity in the calculation of air-water CO_2 flux incorporated into MyLake C. The change in water column CO_2 content due to efflux was of the order of 1% smaller than the total simulated amount of CO_2 evaded because of the equilibrium reactions in the carbonate system.

	Heiskanen	Cole & Caraco	MacIntyre	Tedford
2013				
Net production	52 300	38 700	40 400	44 800
Change due to efflux	−89 900	−72 300	−74 500	−89 200
Net external loading	10 800	8600	11 000	18 500
Change due to epilimnion deepening	16 100	15 100	15 800	18 800
Change in epilimnetic storage	−10 700	−9900	−7200	−7100
Duration (d)	134	134	134	134
2014				
Net production	38 300	24900	25 400	28 700
Change due to efflux	−63 600	−42 700	−46 600	−57 100
Net external loading	8300	6300	8100	12 200
Change due to epilimnion deepening	17 500	13 100	14 100	17 400
Change in epilimnetic storage	500	1600	1000	1200
Duration (d)	107	101	101	101

phytoplankton growth rate μ' and the phytoplankton death rate m, impacts CO_2 dynamics both directly by regulating the intensity of carbon fixation and indirectly via changes in epilimnetic thermal conditions due to attenuation of shortwave radiation. However, the phytoplankton growth is limited by the amount of available dissolved inorganic phosphorus (phosphate): if Chl *a* concentration is high, there is no available phosphate to sustain photosynthesis and to consume CO_2. Hence, a doubling of Chl *a* concentration did not imply a doubling of CO_2 consumption by phytoplankton in the simulations. Instead, if m was high, Chl *a* concentration was low, and CO_2 was fixed by phytoplankton at a steady rate over the whole growing season; thus, the total CO_2 consumption was relatively higher under the conditions of low Chl *a* concentration.

Phytoplankton growth started earlier and the growth peak occurred earlier in GEMs whose calibration yielded a high μ', whereas a small m resulted in a higher phytoplankton biomass during midsummer and late summer. These factors resulted in seasonal differences in simulated net CO_2 production and thus in the surface CO_2 concentration gradient between GEMs. For example, high simulated phytoplankton concentration in the late summer of the validation year resulted in a decline in CO_2 in MI because carbon was fixed in phytoplankton. The maximum near-surface Chl *a* concentrations were largest in HE and MI, around $15\,mg/m^3$ in 2013 and close to $20\,mg/m^3$ in 2014. In CC and TE, Chl *a* concentrations exceeded $10\,mg/m^3$ during the spring peaks but were less than $5\,mg/m^3$ at other times. The open water season average near-surface Chl *a* concentration was higher in HE (9.6 and $9.3\,mg/m^3$ in 2013 and 2014, respectively) than in MI (7.5 and $6.1\,mg/m^3$) because of longer growing seasons. The corresponding values for CC (3.9 and $4.0\,mg/m^3$) and TE (2.3 and $2.1\,mg/m^3$) were clearly lower because of the high values of m.

GEMs that yielded higher values for the gas exchange velocity required a higher net in-lake production or a higher external load of CO_2 to balance the higher efflux (Table 9.5). The fixation of CO_2 in phytoplankton was highest in HE because of the highest average phytoplankton biomass, but the degradation coefficients were also high in HE, which resulted in the highest net CO_2 production. CO_2 fixation was low and sedimentary degradation was high in TE, but slow fragmentation of autochthonous POC and slow degradation of allochthonous DOC resulted in a relatively low net CO_2 production. Small or moderate fragmentation and degradation coefficients and a rather high amount of CO_2 fixed by phytoplankton because of a long growing season resulted in the lowest net CO_2 production in CC.

The net terrestrial CO_2 loads to the epilimnion presented in Table 9.5 were lower than the total net loads to the lake over the summer stratification periods because the stream inflow was occasionally directed in metalimnetic layers under the epilimnion in the simulations. This occurred when the temperature of the inflow was lower than the epilimnetic temperature. The epilimnetic net CO_2 loads were 90–92% and 98–99% of the total net CO_2 loads during summer stratification in 2013 and 2014, respectively. The proportion was highest in CC and lowest in MI. The highest near-surface CO_2 concentration among the GEMs in CC during the

stratification period also increased the amount of CO_2 outflow. As a result, the net load was relatively lower in CC than in other GEMs compared to the differences in $C_{DI,IN}$ between CC and the other GEMs.

The inflow CO_2 concentration was around 200–250 mmol/m^3 during the ice covered period, declined to less than 80 mmol/m^3 during May, and remained mainly between 50 and 100 mmol/m^3 during the remaining open water season. Even though the nonscaled inflow CO_2 concentration was approximately double the simulated near-surface concentration after May, the simulated net external CO_2 loading would have been rather small especially during the low-discharge season in late summer and autumn. Scaling of the inflow DIC concentration was therefore needed to notably increase the gain of in-lake CO_2 through terrestrial loading. The DIC inflow concentration scaling factors $C_{DI,IN}$ were rather proportional to the simulated CO_2 effluxes in the GEMs. The GEM with the highest $C_{DI,IN}$, TE, yielded the highest net CO_2 load (87 000 kg CO_2) over the whole two-year simulation period, and the net loads in other GEMs were ordered by the respective values of $C_{DI,IN}$ (58 900, 57 100, and 48 000 kg CO_2 for MI, HE, and CC, respectively).

However, the magnitude of $C_{DI,IN}$ did not solely govern the extent of the effect of terrestrial CO_2 loading on the in-lake CO_2 concentration. The inflow pH was kept constant in the scaling of inflow DIC concentration. A portion of the higher inflowing CO_2 load due to scaling was eventually evaded to the atmosphere in the simulations, but the bicarbonate fraction accumulated in the water column, increasing the in-lake pH slightly. The impact of external bicarbonate loading on the in-lake pH was, however, minor compared to the effect of spring efflux. Models with a high k ventilated more CO_2 out of the water column during the first days after the ice-off in spring, leaving the lake less acidic. The open water season average surface water pH was 0.20–0.26 and 0.18–0.25 units lower in CC than in the other GEMs in 2013 and 2014, respectively. The differences were generated largely during the first week after the ice-off and remained mainly rather constant during the open water seasons, excepting a short-lasting peak in pH in CC during a strong phytoplankton growth peak under the conditions of relatively low wind speed and k_{CC} in late May 2014. As a result, a higher fraction of the inflow DIC was eventually in the form of CO_2 in the lake during the open water seasons in CC.

The lower pH may also have affected the near-surface CO_2 concentration in CC. Because of the lower CO_2 evasion after ice off and also the lower bicarbonate accumulation during the open water season, the average fraction of CO_2 of DIC in the near-surface layer was 6–8 and 5–6 percentage units higher in CC than in other GEMs during the open water seasons of 2013 and 2014, respectively. In addition to a lower CO_2 efflux, the higher pH may have contributed to the higher open water season CO_2 concentration in near-surface water in CC than in other GEMs seen in Fig. 9.1. When compared to measurements, all GEMs overestimated the open water season pH in 2013, the difference being around 0.2–0.3 units in CC. However, pH may have differed from the daily average at the time of the measurement in daytime because of its diurnal variation, whereas the simulated values represented

the daily average. In addition, the open water season average surface water pH was 0.22 units higher in all GEMs in 2014 than 2013. There are no measurements available for pH in 2014; however, it is possible that the simulated pH was too high in 2014 because of excessive bicarbonate accumulation in the water column in the course of the simulation.

9.2 Discussion

9.2.1 Comparison of simulated fluxes with EC measurements

CO_2 flux

The simulated air-water CO_2 fluxes obtained with the gas exchange models incorporated into MyLake C covered a smaller range than the CO_2 fluxes obtained by the models via calculation on the basis of direct in-lake measurements of surface heat fluxes and the air-water CO_2 concentration gradient (Table 9.4). This was caused both by differences between the simulated and calculated gas exchange velocities and by insufficient CO_2 production in the MyLake C simulations. The calculated fluxes were lowest in the wind-based CC and highest in the surface renewal model TE, which is in accordance with Mammarella et al. (2015) and Erkkilä et al. (2018) who compared the performance of different GEMs in Lake Kuivajärvi. However, the differences between the results of CC and the other GEMs were much smaller in the simulations than in the two experimental studies because of the interplay between the simulated surface water CO_2 concentrations and the corresponding air-water CO_2 fluxes: a higher k was compensated for by a higher gain of water column CO_2 in the calibrations. The results are also in line with Dugan et al. (2016) who compared the performance of different gas exchange models in DO exchange in temperate lakes of various sizes. Wind-based models produced the lowest values of k in lakes that were of the order of Lake Kuivajärvi in size in Dugan et al. (2016), but in larger lakes, where wind speed was usually higher and wind-induced mixing was the dominant process in the epilimnion, the differences between wind-based models and more sophisticated models were smaller.

The air-water CO_2 fluxes measured with the EC method cannot be directly compared to the results of the simulations with a time step of 24 h because data coverage for the EC measurements of CO_2 flux is often rather low. In Erkkilä et al. (2018) the coverage was 27% of the original EC CO_2 flux data over a 16-day period. Mammarella et al. (2015) analyzed EC data from the open water seasons in 2010 and 2011; the data coverage for CO_2 flux was 37% because of data omission due to quality screening or system malfunction. A large portion of EC measurement data during light winds and cooling is often inapplicable because of flux nonstationarity (Heiskanen et al., 2014), which often results in nighttime data being excluded. Also, advection of CO_2 from the surrounding forest during nighttime may cause scatter in the flux measurements over the lake (Erkkilä

et al., 2018). Podgrajsek et al. (2015) found that EC CO_2 fluxes over a shallow boreal lake were highest at night and argued that the reason for the nighttime flux increase was water-side convection. Air-water CO_2 concentration gradient may also be higher at night because of the absence of in-lake photosynthesis (Erkkilä et al., 2018), which enhances CO_2 efflux. If EC flux data are sporadic especially at nighttime, the daily average or median EC CO_2 flux may not be representative for the whole day because of the temporal bias.

The CO_2 fluxes obtained with GEMs have been compared with 30-min block-averaged EC CO_2 flux measurements in Lake Kuivajärvi (Erkkilä et al., 2018; Heiskanen et al., 2014; Mammarella et al., 2015). GEMs often tend to more or less underestimate the measured CO_2 flux. Heiskanen et al. (2014) compared the half-hour CO_2 exchange velocities obtained by different GEMs with CO_2 exchange velocities calculated via the EC measurements of CO_2 flux in Lake Kuivajärvi in August–November 2011. In addition to HE, their study included CC, MI, and a surface renewal model by MacIntyre et al. (2010), which closely resembles TE. They concluded that HE and MI performed rather well, the average values of k being about 70% of the value based on the EC measurements, but the average k yielded by CC was approximately half of those yielded by the other GEMs. The surface renewal model yielded the highest values and overestimated the k based on EC measurements, especially during unstratified conditions. The inadequate performance of CC has been shown also in several other studies (e.g., MacIntyre et al., 2010; Mammarella et al., 2015).

Erkkilä et al. (2018) compared the daily medians of the CO_2 flux measured by the EC method in Lake Kuivajärvi during a 16-day period in October 2014 with the corresponding daily median CO_2 fluxes calculated with CC, HE, and TE. In the study, all GEMs tended to give lower CO_2 flux estimates compared to the measurements. The daily median CO_2 fluxes obtained using HE and TE were 60% of the daily median of the measured EC flux, and CC yielded CO_2 fluxes that were half of those obtained with HE and TE. According to Erkkilä et al. (2018), the CO_2 fluxes obtained with TE were most similar to the EC fluxes. However, TE gave the lowest fluxes in the simulations compared to the corresponding calculated values in this work. By contrast, the simulated and calculated CO_2 fluxes agreed best in CC, but CC gave significantly lower fluxes compared to EC measurements in Erkkilä et al. (2018). All in all, none of the GEMs incorporated into MyLake C was highly compatible with CO_2 fluxes obtained by EC measurements, provided that the outcome of the half-hour comparison in Erkkilä et al. (2018) can be extended to a daily scale.

An issue worth noting is that the foregoing comparisons between EC CO_2 fluxes and the corresponding simulated values were based on EC measurements performed at a single site, on the measurement platform, and the measurements may thus not be representative for the whole lake. MyLake C presumes horizontal homogeneity of the water column, and the simulation results can be seen as averages over the lake surface area. However, the EC CO_2 flux measurements do not represent conditions only at a specific point of the lake, either. The source area of the

EC CO_2 flux measurements, the so called footprint area, contributing to 80% of the flux has been estimated to range from 100 to 300 m along the wind direction in Lake Kuivajärvi (Mammarella et al., 2015). Erkkilä et al. (2018) found little spatial variation in manual floating chamber CO_2 flux measurements within the footprint area. Nevertheless, the footprint area is only a small fraction of the lake surface area. There may be considerable spatial variability in near-surface water CO_2 concentration and CO_2 flux in small, shallow boreal lakes (Natchimuthu et al., 2017), which may result in discrepancies in whole-lake CO_2 flux estimates based on EC measurements. In addition, both the calculated and the simulated values of k were determined using the wind speed and other forcing data measured on the platform. Thus, they were suitable for comparison with each other in that regard, but they may not be applicable for the estimation of whole-lake fluxes, either.

In TE, the impact of wind shear on k is high compared to the impact of water-side convection; thus, the performance of TE is strongly dependent on the determination of atmospheric friction velocity $u_{*\mathrm{a}}$. Because MyLake C underestimated $u_{*\mathrm{a}}$ (Fig. 9.5) significantly, the CO_2 flux simulated with TE was low. Also Erkkilä et al. (2018) found that $u_{*\mathrm{a}}$ calculated from wind speed measurements was smaller than the measured $u_{*\mathrm{a}}$ in Lake Kuivajärvi. Wang et al. (2015) showed that bulk models underestimated the turbulent friction velocity over a lake especially when the model parameterization was based on open sea conditions with relatively low surface roughness. This is the case also in MyLake C, in which the Air-Sea Toolbox is used for the calculation of atmospheric forcing. However, again, the observational values for $u_{*\mathrm{a}}$ were obtained from EC measurements on the platform with a footprint of the order of 100 m, and thus they may not be representative for the whole lake. Wind speed and the resultant $u_{*\mathrm{a}}$ over lakes surrounded by forests are lower in sheltered near-shore areas (Markfort et al., 2010). The effect of sheltering on the spatial variation of $u_{*\mathrm{a}}$ is of importance especially in small lakes, such as Lake Kuivajärvi. Also, the calculation of $u_{*\mathrm{a}}$ in the simulations was based on forcing data obtained from the platform in the middle of the lake, and the simulated friction velocity may have been an overestimate of the spatial average. As opposed to wind kinetic energy available for water column mixing, there is no wind sheltering effect applied in the calculation of friction velocity and surface heat fluxes in MyLake.

Heat flux

The performance of the simulation of the effective heat flux Q_{eff} and its components was not very good compared to their measured or calculated counterparts (Figs. 9.3 and 9.5). The model overestimated both latent and sensible latent heat fluxes, which is in line with Stepanenko et al. (2014) who compared the performance of five one-dimensional thermal lake models with EC measurements of sensible and latent heat fluxes over Lake Valkea-Kotinen. All of the models provided higher heat fluxes compared to the measurements. The disparities were in part attributed to an underestimation of the heat fluxes by the EC method, which was also seen in a study on energy balance over Lake Valkea-Kotinen by Nordbo

et al. (2011). However, the EC measurements of sensible and latent heat fluxes around the center of Lake Kuivajärvi, where wind speed is higher than in upwind areas near the surrounding forest, may have yielded higher values compared to the spatial averages of the heat fluxes over the lake. Nevertheless, the effect of the magnitude of water-side convection and thus the value of Q_{eff} on the simulated k was minor or nonexistent in all GEMs but for HE.

More important issues concerning the applicability of the GEMs including water-side convection in a lake model with a daily time step are the accuracy of the calculation of a daily effective heat flux and the applicability of the concept of a daily AML. On a diel scale, Q_{eff} was usually positive on some occasions during daytime because of solar heating and always negative during nighttime. The depth of the AML often increased during nighttime cooling and decreased after the onset of daytime radiative heating. For example, the AML was very shallow under the conditions of strong shortwave radiation and low wind speed around noon, and only a small fraction of the abundant shortwave radiation was trapped within it, which resulted in a low positive or even a negative Q_{eff}. As a consequence, the daily average of the half-hour values of Q_{eff} may have been less positive or more negative than the Q_{eff} calculated using daily average components.

9.2.2 Epilimnetic CO_2 budget

As the more sophisticated GEMs, in comparison to the simple wind-based CC, yielded higher CO_2 losses through efflux from the lake, a higher terrestrial CO_2 loading or a higher in-lake CO_2 production was required to strive to sustain the desired epilimnetic CO_2 concentration in the simulations (Table 9.5). Still, the near-surface CO_2 concentration was underestimated in the simulations (Table 9.1 and Fig. 9.7), which, in part, resulted in low CO_2 fluxes compared to the calculated fluxes (Fig. 9.8). Of course, the simulated CO_2 fluxes could have been made higher by further increasing the values of the organic carbon degradation parameters and thus the epilimnetic CO_2 concentration, but then the metalimnetic and hypolimnetic CO_2 concentrations would have increased too much. Calibrating the model only against the near-surface CO_2 concentration would have resulted in uncontrollable summertime hypolimnetic and wintertime CO_2 dynamics, which would have been disadvantageous in a year-round, vertical model.

The performance of the model regarding epilimnetic CO_2 concentration was largely determined by the degree of success of the simulation of water column temperature and stratification. The measured near-surface CO_2 concentration increased when the epilimnion became thicker, and vice versa, during the stratified period in 2013 (Figs. 9.7 and 9.9). Cooler and more CO_2-rich water entered the epilimnion because of upwelling caused by thermocline tilting and because of entrainment caused by convection during windy and cool days (Heiskanen et al., 2014). Conversely, strong solar radiation during low wind speeds warmed the near-surface water, which resulted in a thin epilimnion. Strong solar radiation also intensified photosynthesis, which increased the uptake of CO_2 (Provenzale et al., 2018).

Overall, the simulations underestimated the near-surface CO_2 concentration (Table 9.3). However, the simulated epilimnion was thicker than the observed epilimnion, for example, in early July 2013. As a result, CO_2 was released from deeper layers because of the thickening of the epilimnion, and a larger epilimnetic volume also enabled sufficient net production in the epilimnion; thus, the simulated near-surface CO_2 concentrations were rather close to the measured concentration during the period. By contrast, the simulated z_{epi} was low and closer to the observed thickness in late June and early August 2013, which resulted in a decline of the simulated near-surface CO_2 concentration close to the atmospheric equilibrium level even in CC. It also resulted in a smaller CO_2 efflux compared to the calculated values (Fig. 9.8). According to temperature measurements, a shallow epilimnion was formed during sunny days with low winds days even in late August and early September 2013. The mixed layer remained shallow also throughout the following nighttime, preventing water-side convection and resulting in a decrease in the near-surface CO_2 concentration. The simulations were not able to reproduce those short-lived episodes of a shallow epilimnion in late summer.

Phytoplankton is an important factor in the in-lake CO_2 budget. Phytoplankton primary production fixes inorganic carbon, and carbon is stored in photosynthetically produced organic matter in the water column or in the sediment until its subsequent mineralization by bacteria. In the model, the phosphate required for phytoplankton growth in the epilimnion is imported via inflow, released from deeper layers as the epilimnion extends deeper, or released through degradation of organic matter in the epilimnion. The rate of nutrient recycling in the epilimnion affects phytoplankton primary production (Essington and Carpenter, 2000). Terrestrial phosphate load was the same in all GEMs, but there were differences in organic matter degradation rates. The death rate of phytoplankton and the degradation rates of autochthonous organic carbon were low in MI, which resulted in more living and dead particulate organic matter sinking into deeper layers and, hence, slowed down the release of phosphate in the epilimnion. The variation in the simulated phytoplankton biomass between the GEMs was notable. However, the total net CO_2 consumption by phytoplankton during the stratified period varied less between models because of the phosphorus limitation of photosynthesis under a higher phytoplankton biomass and because of differences in the length of the active growing season.

There is no data available on Chl *a* concentration in Lake Kuivajärvi in 2013, but in 2011–2012, the Chl *a* concentration at 0–3 m was at maximum 30–50 mg/m^3 in mid-July and declined to less than 2 mg/m^3 in late autumn (Heiskanen et al., 2015). The epilimnetic Chl *a* concentration is usually between 3 and 5 mg/m^3 during the growing season, but diatom peaks may increase the concentration also in spring and in autumn (Provenzale et al., 2018). In the simulations, Chl *a* concentration remained at a rather constant level during the growing season with no distinct peaks apart from growth peaks in spring in CC and TE. Thus, the supposed short-term variation of epilimnetic CO_2 concentration due to seasonal succession of phytoplankton was not captured by any of the GEMs. The GEMs with the lowest open water season average near-surface Chl *a* concentrations, CC and TE, may

have captured the overall level of phytoplankton biomass better than HE and MI. However, as said above, the total net CO_2 consumption by phytoplankton during the stratified period is not only related to the average phytoplankton biomass.

A significant increase in the inflow CO_2 concentration was needed in the GEMs with a higher k to compensate for the high CO_2 efflux (Table 9.2). Scaling of the inflow DIC concentration only during the open water season may have been somewhat contrived, and it may have resulted in rather unnatural inflow CO_2 concentrations especially in TE. However, scaling of the inflow DIC concentration may also be thought as the inclusion of the input of CO_2 via direct groundwater seepage to the lake. If the groundwater CO_2 concentration is high, a high $C_{\mathrm{DI,IN}}$ may be reasonable. The CO_2 concentration in groundwater in southern Finland is around 700–900 $\mathrm{mmol/m^3}$ (Lahermo et al., 1990), which is about tenfold higher than the measured concentration of CO_2 in the inflow of Lake Kuivajärvi as the average of the estimated daily inflow CO_2 concentration time series over the stratified period in 2013 was 86 $\mathrm{mmol/m^3}$. The level of the groundwater CO_2 concentration in Lahermo et al. (1990) agrees rather well with the yearly average of groundwater CO_2 concentration near the shore of a boreal stream measured by Leith et al. (2015). Furthermore, Chmiel et al. (2016) argued that applying groundwater DIC flow as a percentage of stream DIC load may be generally used to estimate groundwater DIC load, which supports the usage of $C_{\mathrm{DI,IN}}$ as a means to include the CO_2 load via groundwater.

There is no information on the volume of inflowing groundwater or its properties in Lake Kuivajärvi. However, because the measured yearly outflow volume is approximately twice the inflowing volume via the main inlet, groundwater seepage may have a notable contribution to the total lake inflow volume. It may be a factor that increases the terrestrial CO_2 loading to the epilimnion during the stratification period, especially in May when the groundwater level is relatively high. The measured near-surface CO_2 concentration decreased at a much slower rate than the simulated concentration after ice-off in May 2013 even in CC, the GEM with the lowest CO_2 efflux (Fig. 9.7). The net gain of CO_2 was thus insufficient in the simulations. Net consumption of CO_2 by phytoplankton was low in the cool epilimnion in May because of the high value of the temperature adjustment coefficient for phytoplankton growth, and CO_2 efflux was low because of a low air-water CO_2 concentration gradient; hence, the simulated sinks of CO_2 were rather small. Labile, autochthonous DOC was absent in the epilimnion, and the degradation of allochthonous DOC was slow under the relatively cool conditions in May. Even though the nonscaled inflow CO_2 concentration was about double the simulated epilimnetic CO_2 concentration and the scaled inflow CO_2 concentrations were even higher, terrestrial CO_2 loading was not capable of restraining the decline of epilimnetic CO_2 concentration in any of the GEMs. However, diatoms, which are abundant in Lake Kuivajärvi (Provenzale et al., 2018), may be a source of easily degradable organic matter also in cool conditions in early spring. Nevertheless, as net primary production consumes CO_2, a diatom spring bloom may not constitute a substantial net CO_2 source. Considering the structure of the model, groundwater loading could be a plausible additional process affecting the epilimnetic CO_2

level in May. This is supported by a study on the carbon budget of a small boreal lake by Chmiel et al. (2016), in which the estimated inorganic carbon gain was not sufficient to equal the inorganic carbon loss and the discrepancy was attributed to a possible underestimation of groundwater inflow.

The issues raised in this work concerning the lake carbon budget can be generalized to a larger scale. The atmospheric exchange of carbon is often calculated using the formula by Cole and Caraco (1998) in empirical studies concerning the determination of the carbon budgets of single boreal or temperate lakes (Chmiel et al., 2016; Einarsdóttir et al., 2017; Sobek et al., 2006; Stets et al., 2009) and in theoretical, large-scale carbon budget studies (Hanson et al., 2004; Humborg et al., 2010; McDonald et al., 2013). Thus, the estimates of CO_2 efflux from lakes may be highly conservative in these studies. The possible underestimation of CO_2 efflux also raises the question of the accuracy of estimates of other components of lake carbon budgets. Estimation of CO_2 efflux from lakes is an important issue also in a global scale. Raymond et al. (2013) estimated the global CO_2 evasion rate from lakes using models that yield relatively small values for the gas exchange velocity especially in small lakes as shown in Dugan et al. (2016). Also, if novel CO_2 exchange models yield higher estimates of CO_2 emissions from inland waters, a higher net terrestrial ecosystem production and a higher carbon flux from land to inland waters is required to close the global carbon budget (Battin et al., 2009). Therefore, research on processes contributing to carbon cycling in boreal waters and on the roles of different allochthonous and autochthonous sources of CO_2 in lakes is sorely needed.

10 Summary and outlook

In this work, two novel vertical process-based coupled physical-biogeochemical lake models of different complexity regarding carbon processes, MyLake DO-DIC and MyLake C, were developed and applied to the simulation of CO_2 dynamics, especially air-water CO_2 flux, in boreal lakes. Good water column temperature simulation performance of the underlying thermal submodel provided a solid base for the development and assessment of the biogeochemical parts of the models. The simpler of the two models, MyLake DO-DIC, was calibrated and validated for the small, humic Lake Valkea-Kotinen. Predictions of ice-off and ice-on dates, onset of stratification, and water column temperature were all in good agreement with observations. However, the model was not fully able to reproduce the high summertime concentrations of chlorophyll *a* in the shallow epilimnion, which could be largely explained by the high abundance of vertically migrating algal species capable of exploiting nutrient resources deeper in the water column. The model described CO_2 accumulation both under ice in winter and in the hypolimnion during the open water season rather well, but the simulated annual CO_2 efflux from the lake to the atmosphere was too high largely because of deficiencies in the simulation of phosphorus-phytoplankton dynamics. The omission of pH simulation may also have simplified the model too much. The more sophisticated model, MyLake C, was calibrated and validated for the humic Lake Kuivajärvi. The performance of CO_2 simulation was significantly improved compared to that of MyLake DO-DIC. However, the differing characteristics of the two lakes, especially the unusual behaviour of the phytoplankton community in Lake Valkea-Kotinen, and different quantities and qualities of measurement data make it difficult to directly compare the performance between the two models.

Further, the applicability of different parameterizations for air-water CO_2 exchange in MyLake C, or gas exchange models (GEMs), was studied. The simpler, wind-based parameterizations of the gas exchange velocity worked better than the more complex GEMs when the results were compared to measurement-based values of the gas exchange velocity for each GEM. All but one of the incorporated gas exchange models yielded clearly too low summertime epilimnetic CO_2 concentrations, which was also reflected by the underestimation of CO_2 fluxes. If a GEM yielded a relatively high general level of CO_2 efflux, MyLake C was incapable of producing enough CO_2 in the water column to compensate for the loss to the atmosphere. The CO_2 flux simulations with the model by Cole and Caraco (1998) (CC), the

simplest of the four models, agreed best with the corresponding calculated fluxes; however, the long and widely used CC model has recently been shown to produce too low CO_2 flux estimates. Hence, none of the four GEMs surpassed the other models in the study because of the complex interplay between the near-surface water CO_2 concentration and air-water CO_2 flux in the simulations. Inclusion of sophisticated and more correct GEMs in lake models is crucial in the accurate assessment of carbon budgets both in single lakes and on a larger scale. However, finding higher estimates for the sources of inorganic carbon in boreal lakes is an important issue if the improved knowledge of the magnitude of CO_2 evasion from lakes is included in future studies on lake carbon budgets.

The effects of climate change, in the forms of higher atmospheric temperature and changes in terrestrial carbon loading, on the CO_2 concentration and air-water CO_2 flux in the presently oversaturated Lake Kuivajärvi between the control period 1980–2009 and the scenario period 2070–2099 were assessed using the MyLake C application. The results implied that boreal lakes may be constantly higher carbon sources to the atmosphere in future climate. Organic matter degradation rates in the water column and in the sediment were higher under warmer conditions, which resulted in a higher water column CO_2 concentration and CO_2 evasion to the atmosphere. Shortening of the ice-covered period and alteration of discharge patterns also modulated the seasonal CO_2 flux dynamics in the scenario period. Increased winter streamflow resulted in a faster buildup of CO_2 under ice, but the maximum under-ice CO_2 concentration and the resulting springtime CO_2 efflux were lower because of an earlier ice-off. Additional increases in either terrestrial inorganic or organic carbon loading resulted in further increases in CO_2 efflux. The effect of an increase in terrestrial dissolved organic carbon (DOC) loading was highest in spring and summer, but not even notable changes in DOC loading did have a high impact on water column CO_2 concentration because of the low degradability of allochthonous organic carbon. On a yearly basis, an increase in inflow CO_2 concentration resulted in a higher water column CO_2 concentration and a higher CO_2 efflux than a corresponding increase in inflow DOC concentration. However, there was not much disparity between the impacts of the most reasonable future inflow concentration increases, 10 to 20% for DOC and about 10% for CO_2, on the total annual air-water CO_2 flux.

The model with a daily time step was not always able to simulate the changes in water column CO_2 concentration and air-water CO_2 flux resulting from short-term physical processes, such as nighttime cooling or simultaneous surface heating and wind mixing. However, a daily temporal resolution is suitable for simulations over long periods of time and for the assessment of CO_2 dynamics on seasonal, yearly, and decadal time scales, especially because of the advantage of a relatively short model execution time. Also, a vertical model does not catch the possible impact of horizontal heterogeneity of air-water heat and CO_2 exchange processes, particularly if also the measurement data used in model calibration and performance assessment are obtained from a single site, thus not being representative for the whole lake. Vertical one-dimensional modeling is, nevertheless, well applicable to studies in which the emphasis is put on the assessment of changes within the lake

instead of correct estimation of the present state.

The simplified scenario analysis in this work was not capable of assessing the whole range of uncertainties in the ecosystem chain extending from the catchment to the lake. Instead, the possible implications of an individual discharge scenario and a small number of hypothetical carbon loading scenarios were estimated, aiming at assessing general trends in the future patterns of lacustrine carbon cycle. Despite the obvious limitations of the applied lake model and the unknown uncertainties associated with the climate change impacts on the catchment-lake continuum, this work gives valuable insight on in-lake mechanisms related to potential changes in carbon cycling. A more comprehensive analysis would be attained using a model chain including also the climate-induced future changes in hydrological and biogeochemical conditions in the catchment. Also, in addition to uncertainties in future forcing and loading data, a biogeochemical lake model has many sources of uncertainty due to lack of knowledge of lake carbon system functioning related to, for example, the characteristics of aquatic organic matter, the elemental composition of phytoplankton, and the composition of sediment in different lakes and under different conditions. Furthermore, large amount of input data and of knowledge on many model parameter values are required for the calibration of a deterministic model and its performance assessment. More comprehensive, long-term measurements of carbon input to lakes both through streamflow and through groundwater along with quantitative studies on carbon-related processes in the water column and in the bottom sediments are needed to improve model performance.

A Formulas in MyLake C

In this appendix, a detailed description of the formulations of the in-lake biochemical inorganic and organic carbon processes implemented in MyLake C, given in Eqs. (4.10) to (4.13), is presented. The parameters for which default values were used in the model application are listed in Table A.1.

Living particulate organic carbon $\mathrm{POC_L}$ is represented in the model by the carbon content in phytoplankton. The concentration of $\mathrm{POC_L}$ in the water column is given by the phytoplankton biomass in carbon units

$$C_{\mathrm{PP}} = \frac{s_{\mathrm{P}}}{y_{\mathrm{c}}} P_{\mathrm{Chl}}, \tag{A.1}$$

where s_{P} is the carbon-to-phosphorus mass ratio in phytoplankton, y_{c} is the phytoplankton yield coefficient (that is, the mass ratio of Chl *a* to phosphorus in phytoplankton), and P_{Chl} is the Chl *a* concentration. Contrary to MyLake DODIC, the ratio of carbon to Chl *a* in phytoplankton is not based on the Redfield ratio but varies with the yield coefficient.

In Mylake C, $\mathrm{CO_2}$ is consumed and DO is produced by phytoplankton through photosynthesis. Following the terminology suggested by Wohlfahrt and Gu (2015), the term apparent photosynthesis is used here to refer to the individual-scale process related to the concept of gross primary production. The rate of apparent photosynthesis is defined as the rate of gross carbon fixation subtracted by the rate of photorespiration. The production of DO in apparent photosynthesis in MyLake C is given by

$$P = \frac{M(\mathrm{O_2})}{M(\mathrm{C})} Q_{\mathrm{p}} \mu C_{\mathrm{PP}}, \tag{A.2}$$

where $M(\mathrm{O_2}) = 32\,\mathrm{g/mol}$ and $M(\mathrm{C}) = 12\,\mathrm{g/mol}$ are the molar masses of oxygen and carbon, respectively, Q_{p} is the photosynthetic quotient, and μ is the specific growth rate of phytoplankton calculated by Eq. (3.16). The photosynthetic quotient expresses the molar ratio of oxygen released to $\mathrm{CO_2}$ assimilated during photosynthesis. It is increased by, for example, photorespiration, and it is larger than unity (Sakshaug et al., 1997). The consumption of $\mathrm{CO_2}$ during apparent

photosynthesis is correspondingly

$$P' = \frac{M(\mathrm{CO_2})}{M(\mathrm{O_2})} \frac{1}{Q_\mathrm{p}} P, \tag{A.3}$$

where $M(\mathrm{CO_2}) = 44.01\,\mathrm{g/mol}$ is the molar mass of $\mathrm{CO_2}$.

The cellular respiration of phytoplankton, also called dark respiration, produces $\mathrm{CO_2}$ and consumes DO. Phytoplankton cellular respiration is found to be linearly related to the growth rate (Geider and Osborne, 1989). In the model, the consumption of DO in phytoplankton cellular respiration is estimated to be

$$R = \frac{M(\mathrm{O_2})}{M(\mathrm{C})} r_\mathrm{PP} \mu C_\mathrm{PP}, \tag{A.4}$$

where r_PP is the phytoplankton cellular respiration fraction, and the production of $\mathrm{CO_2}$ in the process is simply

$$R' = \frac{M(\mathrm{CO_2})}{M(\mathrm{O_2})} R. \tag{A.5}$$

The generation of dead particulate organic carbon, POC, through death of phytoplankton is given by

$$d_\mathrm{Chl} = m C_\mathrm{PP}, \tag{A.6}$$

where m is calculated by Eq. (3.15) and defined as the death rate of phytoplankton instead of the rate of direct remineralization. In addition to the carbon content in dead phytoplankton, denoted as $\mathrm{POC_1}$, dead allochthonous particulate organic carbon, denoted as $\mathrm{POC_2}$, is included in the total water column POC. These two POC pools convert into DOC by fragmentation with different rates $k_\mathrm{POC,1}$ and $k_\mathrm{POC,2}$ for autochthonous and allochthonous POC, respectively, as

$$d_\mathrm{POC} = f_\mathrm{POC} \sum_{i=1}^{2} k_\mathrm{POC,}i C_\mathrm{PO,}i, \tag{A.7}$$

where $C_\mathrm{PO,}i$ is the concentration of the POC pool i and f_DOC is the temperature correction factor for POC fragmentation, given as

$$f_\mathrm{POC} = \begin{cases} \theta_\mathrm{POC}^{T-20} & T \geq 4\,^\circ\mathrm{C}, \\ \theta_\mathrm{POC}^{-16} \theta_\mathrm{c}^{T-4} & T < 4\,^\circ\mathrm{C}, \end{cases} \tag{A.8}$$

where θ_POC is the temperature adjustment coefficient for POC degradation and θ_c is the temperature adjustment coefficient for organic carbon degradation at temperatures below 4 °C. The DOC generated from $\mathrm{POC_1}$ is added to the labile pool, and the DOC generated from $\mathrm{POC_2}$ is divided equally between semilabile and refractory pools (see Section 3.2.3).

A fraction of carbon in phytoplankton is excreted as DOC. The amount of the

extracellular release of organic carbon is found to be proportional to the amount of carbon fixed in phytoplankton through photosynthesis (Baines and Pace, 1991). The excretion of DOC is given in the model by

$$E = r_{\mathrm{ex}} \mu C_{\mathrm{PP}}, \tag{A.9}$$

where r_{ex} is the dimensionless DOC excretion fraction. Phytoplankton exudates are usually easily biodegradable (Bjørnsen, 1998); thus, the excreted DOC is added to the labile pool.

Allochthonous DOC is subject to flocculation, which relocates a portion of DOC into allochthonous POC (von Wachenfeldt and Tranvik, 2008). Flocculation is calculated as

$$F = k_{\mathrm{floc}} \sum_{i=2}^{3} C_{\mathrm{DO},i}, \tag{A.10}$$

where k_{floc} is the flocculation rate and $C_{\mathrm{DO},2}$ and $C_{\mathrm{DO},3}$ are the concentrations of the allochthonous pools DOC_2 and DOC_3, respectively.

The degradation of DOC in the water column is simulated by FOKEMA (Section 3.2.3) with some modifications. The temperature correction of bacterial degradation has been formulated following the convention in other biochemical processes in MyLake. Oxygen limitation has been included through a half-saturation function based on Michaelis–Menten type kinetics. DOC degradation is calculated as

$$d_{\mathrm{DOC}} = \frac{O_{\mathrm{D}}}{O_{\mathrm{D,sat}} + O_{\mathrm{D}}} f_{\mathrm{DOC}} d_{\mathrm{DOC,Tref}} + P_{\mathrm{B}}, \tag{A.11}$$

where O_{D} is the concentration of DO; $O_{\mathrm{D,sat}}$ is the oxygen half-saturation constant; f_{DOC} is the temperature correction factor; $d_{\mathrm{DOC,Tref}}$, Eq. (3.22), is the bacterial DOC degradation at a reference temperature (20 °C); and P_{B}, Eq. (3.24), is the photochemical mineralization of DOC. The temperature correction factor is given as

$$f_{\mathrm{DOC}} = \begin{cases} \theta_{\mathrm{DOC}}^{T-20} & T \geq 4\,^{\circ}\mathrm{C}, \\ \theta_{\mathrm{DOC}}^{-16} \theta_{\mathrm{c}}^{T-4} & T < 4\,^{\circ}\mathrm{C}, \end{cases} \tag{A.12}$$

where θ_{DOC} is the temperature adjustment coefficient for DOC degradation. The degradation of DOC in the water column produces CO_2 and consumes DO. The production of CO_2 through DOC degradation is found by expressing the mineralized carbon in CO_2 mass units:

$$D'_{\mathrm{DOC}} = \frac{M(\mathrm{CO_2})}{M(\mathrm{C})} d_{\mathrm{DOC}}. \tag{A.13}$$

The consumption of DO during the DOC degradation process is obtained analogously to Eq. (A.5) by

$$D_{\mathrm{DOC}} = \frac{M(\mathrm{O_2})}{M(\mathrm{CO_2})} \frac{1}{Q_{\mathrm{r}}} D'_{\mathrm{DOC}}, \tag{A.14}$$

where Q_r is the respiratory quotient, expressing the molar ratio of CO_2 production to DO consumption in bacterial respiration. For humic-rich allochthonous DOC, Q_r is theoretically slightly below 1 (Berggren et al., 2012).

In addition to the variable ν_IM that describes the volume fraction of inorganic matter in the total sediment solids, MyLake C includes explicitly the volume fractions of dead sedimentary particulate organic matter SPOM, ν_DPOM, and living sedimentary particulate organic matter $\mathrm{SPOM_L}$, ν_LPOM. $\mathrm{SPOM_L}$ is represented by the Chl *a* content of sedimentary phytoplankton. In contrast to MyLake v.1.2, the initial mass fraction of Chl *a* in organic sediment particles $s_\mathrm{Chl,sed}$ is given as a constant parameter. The mass fraction is updated along with the net sedimentation of particulate organic matter. Under the assumptions in the biochemical submodel of MyLake v.1.2 (Section 3.2.2) $s_\mathrm{Chl,sed}$ is around 12 g/kg. The concentration of Chl *a* in the total sediment solids is given by

$$P_\mathrm{Chl,sed} = s_\mathrm{Chl,sed}\rho_\mathrm{org}\nu_\mathrm{LPOM}, \tag{A.15}$$

where ρ_org is the density of organic sediment. Correspondingly, the concentration of POC in the total sediment solids is given by

$$C_\mathrm{PO,sed} = s_\mathrm{C}\rho_\mathrm{org}\nu_\mathrm{DPOM}, \tag{A.16}$$

where s_C is the mass fraction of carbon in particulate organic matter.

$\mathrm{SPOM_L}$ degrades directly to inorganic substances. The loss of $\mathrm{SPOM_L}$ is given in Chl *a* units by

$$d_\mathrm{Chl,sed} = k_\mathrm{Chl,sed}\frac{O_\mathrm{D}}{O_\mathrm{D,sat}+O_\mathrm{D}}\theta^{T-20}P_\mathrm{Chl,sed}, \tag{A.17}$$

where $k_\mathrm{Chl,sed}$ is the degradation rate of $\mathrm{SPOM_L}$ and θ is the temperature adjustment coefficient of phytoplankton mineralization in Eq. (3.15). The concentration of DO in the pore water in the active sediment layer is the same as in the corresponding water layer. Also SPOM degrades directly into CO_2, without an intermediate dissolved phase. The degradation of SPOM is calculated as

$$d_\mathrm{POC,sed} = k_\mathrm{POC,sed}\frac{O_\mathrm{D}}{O_\mathrm{D,sat}+O_\mathrm{D}}f_\mathrm{sed}C_\mathrm{PO,sed}, \tag{A.18}$$

where $k_\mathrm{POC,sed}$ is the degradation rate of SPOM and f_sed is the temperature correction factor for sedimentary POC degradation, given by

$$f_\mathrm{sed} = \begin{cases} \theta_\mathrm{sed}^{T-20} & T \geq 4\,^\circ\mathrm{C}, \\ \theta_\mathrm{sed}^{-16}\theta_\mathrm{c}^{T-4} & T < 4\,^\circ\mathrm{C}, \end{cases} \tag{A.19}$$

where θ_sed is the temperature adjustment coefficient for sedimentary POC degradation.

Sedimentary organic matter degradation consumes DO from the corresponding

overlying water column grid layer. The decrease of DO concentration in layer i via living sedimentary POC degradation is

$$D_{\mathrm{Chl,sed},i} = \frac{1}{Q_\mathrm{r}} \frac{M(\mathrm{O_2})}{M(\mathrm{C})} \frac{s_\mathrm{C}}{s_\mathrm{Chl,sed}} \frac{V_{\mathrm{sed},i}}{V_i} d_{\mathrm{Chl,sed},i}, \tag{A.20}$$

where V_i is the volume of layer i and $V_{\mathrm{sed},i}$ is the volume of the active sediment layer below the water layer i. Correspondingly, the DO concentration decrease in layer i via dead sedimentary POC degradation is

$$D_{\mathrm{POC,sed},i} = \frac{1}{Q_\mathrm{r}} \frac{M(\mathrm{O_2})}{M(\mathrm{C})} \frac{V_{\mathrm{sed},i}}{V_i} d_{\mathrm{POC,sed},i}, \tag{A.21}$$

and the total DO consumption through sedimentary organic matter degradation is given by

$$D_\mathrm{sed} = D_\mathrm{Chl,sed} + D_\mathrm{POC,sed}. \tag{A.22}$$

The produced CO_2 is released to the overlying water column grid layer. The increase in water column CO_2 concentration trough sedimentary organic matter degradation is

$$D'_\mathrm{sed} = \frac{M(\mathrm{CO_2})}{M(\mathrm{O_2})} Q_\mathrm{r} D_\mathrm{sed}. \tag{A.23}$$

Table A.1: Default values of parameters incorporated into MyLake C. The remaining new parameters, values of which were obtained through calibration, are presented in Table 8.2. [Modified from Kiuru et al. (2018).]

Parameter	Symbol	Value	Unit	
Mass fraction of carbon in particulate organic matter	s_{C}	0.5×10^6	mg/kg	a
DOC flocculation rate	k_{floc}	1.9×10^{-3}	1/d	b
Living sedimentary particulate organic matter degradation rate	$k_{\mathrm{Chl,sed}}$	4.2×10^{-5}	1/d	c
Oxygen half-saturation constant	$O_{\mathrm{D,sat}}$	15.625	mmol/m^3	d
DOC excretion fraction	r_{ex}	0.1	-	e
Phytoplankton respiration fraction	r_{PP}	0.3	-	f
Phytoplankton carbon-to-phosphorus ratio	s_{P}	50	mg/mg	g
Initial mass fraction of Chl *a* in sedimentary organic matter	s_{Chl}	1.25×10^4	mg/kg	c
Temperature adjustment coefficient for DOC degradation ($4\,^\circ\mathrm{C} \leq T < 10\,^\circ\mathrm{C}$ / $T \geq 10\,^\circ\mathrm{C}$)	θ_{DOC}	1.1/1.047	-	h
Temperature adjustment coefficient for POC fragmentation ($4\,^\circ\mathrm{C} \leq T < 10\,^\circ\mathrm{C}$ / $T \geq 10\,^\circ\mathrm{C}$)	θ_{POC}	1.1/1.072	-	c
Temperature adjustment coefficient for sediment OC degradation ($4\,^\circ\mathrm{C} \leq T < 10\,^\circ\mathrm{C}$ / $T \geq 10\,^\circ\mathrm{C}$)	θ_{sed}	1.1/1.047	-	h

Sources: a, Wetzel (2001); b, von Wachenfeldt and Tranvik (2008); c, Saloranta and Andersen (2007); d, Thomann and Fitzpatrick (1982); e, Baines and Pace (1991); f, Geider and Osborne (1989); g, Meili (1992); h: Stefan and Fang (1994).

Bibliography

Aalto, J., Pirinen, P., and Jylhä, K. (2016). New gridded daily climatology of Finland: Permutation-based uncertainty estimates and temporal trends in climate. *Journal of Geophysical Research: Atmospheres*, 121(8):3807–3823.

Åberg, J., Jansson, M., and Jonsson, A. (2010). Importance of water temperature and thermal stratification dynamics for temporal variation of surface water CO_2 in a boreal lake. *Journal of Geophysical Research: Biogeosciences*, 115:G02024.

Adrian, R., O'Reilly, C. M., Zagarese, H., Baines, S. B., Hessen, D. O., Keller, W., Livingstone, D. M., Sommaruga, R., Straile, D., van Donk, E., Weyhenmeyer, G. A., and Winder, M. (2009). Lakes as sentinels of climate change. *Limnology and Oceanography*, 54(6 part 2):2283–2297.

Ala-aho, P., Rossi, P. M., and Kløve, B. (2013). Interaction of esker groundwater with headwater lakes and streams. *Journal of Hydrology*, 500:144–156.

Algesten, G., Sobek, S., Bergström, A.-K., Jonsson, A., Tranvik, L. J., and Jansson, M. (2005). Contribution of sediment respiration to summer CO_2 emission from low productive boreal and subarctic lakes. *Microbial Ecology*, 50(4):529–535.

Anderson, D. E., Striegl, R. G., Stannard, D. I., Michmerhuizen, C. M., McConnaughey, T. A., and LaBaugh, J. W. (1999). Estimating lake-atmosphere CO_2 exchange. *Limnology and Oceanography*, 44(4):988–1001.

Arhonditsis, G. B., Adams-VanHarn, B. A., Nielsen, L., Stow, C. A., and Reckhow, K. H. (2006). Evaluation of the current state of mechanistic aquatic biogeochemical modeling: Citation analysis and future perspectives. *Environmental Science & Technology*, 40(21):6547–6554.

Arhonditsis, G. B. and Brett, M. T. (2004). Evaluation of the current state of mechanistic aquatic biogeochemical modeling. *Marine Ecology Progress Series*, 271:13–26.

Arhonditsis, G. B., Qian, S. S., Stow, C. A., Lamon, E. C., and Reckhow, K. H. (2007). Eutrophication risk assessment using Bayesian calibration of process-based models: Application to a mesotrophic lake. *Ecological Modelling*, 208(2):215–229.

Arvola, L., George, G., Livingstone, D. M., Järvinen, M., Blenckner, T., Dokulil, M. T., Jennings, E., Aonghusa, C. N., Nõges, P., Nõges, T., and Weyhenmeyer, G. A. (2010). The impact of the changing climate on the thermal characteristics of lakes. In George, G., editor, *The Impact of Climate Change on European Lakes*, pages 85–101. Springer, Dordrecht.

Baines, S. B. and Pace, M. L. (1991). The production of dissolved organic matter by phytoplankton and its importance to bacteria: Patterns across marine and freshwater systems. *Limnology and Oceanography*, 36(6):1078–1090.

Banerjee, S., Scott, D. S., and Rhodes, E. (1968). Mass transfer to falling wavy liquid films in turbulent flow. *Industrial & Engineering Chemistry Fundamentals*, 7(1):22–27.

Bastviken, D., Ejlertsson, J., Sundh, I., and Tranvik, L. (2003). Methane as a source of carbon and energy for lake pelagic food webs. *Ecology*, 84(4):969–981.

Battin, T. J., Luyssaert, S., Kaplan, L. A., Aufdenkampe, A. K., Richter, A., and Tranvik, L. J. (2009). The boundless carbon cycle. *Nature Geoscience*, 2:598–600.

Bengtsson, L. (2012). Ice covered lakes. In Bengtsson, L., Herschy, R. W., and Fairbridge, R. W., editors, *Encyclopedia of Lakes and Reservoirs*, pages 357–360. Springer Netherlands, Dordrecht.

Benner, R. (2002). Chemical composition and reactivity. In Hansell, D. A. and Carlson, C. A., editors, *Biogeochemistry of marine dissolved organic matter*, pages 59–90. Elsevier Science & Technology, San Diego.

Berggren, M., Lapierre, J.-F., and del Giorgio, P. A. (2012). Magnitude and regulation of bacterioplankton respiratory quotient across freshwater environmental gradients. *The Isme Journal*, 6:984–993.

Bergman, T. L., Lavine, A. S., Incropera, F. P., and DeWitt, D. P. (2011). *Fundamentals of heat and mass transfer (7th ed.)*. Wiley, New York.

Bergström, S. (1992). *The HBV model – its structure and applications*. SMHI Reports RH no. 4, Swedish Meteorological and Hydrological Institute, Norrköping.

Beven, K. (2006). A manifesto for the equifinality thesis. *Journal of Hydrology*, 320(1):18–36.

Bjørnsen, P. K. (1998). Phytoplankton exudation of organic matter: Why do healthy cells do it? *Limnology and Oceanography*, 33(1):151–154.

Blenckner, T., Adrian, R., Arvola, L., Järvinen, M., Nõges, P., Nõges, T., Pettersson, K., and Weyhenmeyer, G. A. (2010). The impact of climate change on lakes in northern Europe. In George, G., editor, *The Impact of Climate Change on European Lakes*, pages 339–358. Springer, Dordrecht.

Bowie, G. L., Mills, W. B., Porcella, D. B., Campbell, C. L., Chan, P. W. H.,

and Gherini, S. A. (1985). *Rates, constants, and kinetic formulations in surface water quality modeling*. U.S. Environmental Protection Agency, Athens, Ga.

Bruce, L. C., Hamilton, D., Imberger, J., Gal, G., Gophen, M., Zohary, T., and Hambright, K. D. (2006). A numerical simulation of the role of zooplankton in C, N and P cycling in Lake Kinneret, Israel. *Ecological Modelling*, 193(3):412–436.

Campeau, A. and Giorgio, P. A. (2014). Patterns in CH_4 and CO_2 concentrations across boreal rivers: Major drivers and implications for fluvial greenhouse emissions under climate change scenarios. *Global Change Biology*, 20(4):1075–1088.

Chmiel, H. E., Kokic, J., Denfeld, B. A., Einarsdóttir, K., Wallin, M. B., Koehler, B., Isidorova, A., Bastviken, D., Ferland, M.-È., and Sobek, S. (2016). The role of sediments in the carbon budget of a small boreal lake. *Limnology and Oceanography*, 61(5):1814–1825.

Clark, J. S. (2005). Why environmental scientists are becoming Bayesians. *Ecology Letters*, 8(1):2–14.

Cole, J. J. and Caraco, N. F. (1998). Atmospheric exchange of carbon dioxide in a low-wind oligotrophic lake measured by the addition of SF_6. *Limnology and Oceanography*, 43(4):647–656.

Cole, J. J., Caraco, N. F., Kling, G. W., and Kratz, T. K. (1994). Carbon dioxide supersaturation in the surface waters of lakes. *Science*, 265(5178):1568–1570.

Cole, J. J., Carpenter, S. R., Kitchell, J. F., and Pace, M. L. (2002). Pathways of organic carbon utilization in small lakes: Results from a whole-lake ^{13}C addition and coupled model. *Limnology and Oceanography*, 47(6):1664–1675.

Cole, J. J., Prairie, Y. T., Caraco, N. F., McDowell, W. H., Tranvik, L. J., Striegl, R. G., Duarte, C. M., Kortelainen, P., Downing, J. A., Middelburg, J. J., and Melack, J. (2007). Plumbing the global carbon cycle: Integrating inland waters into the terrestrial carbon budget. *Ecosystems*, 10(1):172–185.

Collins, W. J., Bellouin, N., Doutriaux-Boucher, M., Gedney, N., Halloran, P., Hinton, T., Hughes, J., Jones, C. D., Joshi, M., Liddicoat, S., Martin, G., O'Connor, F., Rae, J., Senior, C., Sitch, S., Totterdell, I., Wiltshire, A., and Woodward, S. (2011). Development and evaluation of an Earth-System model – HadGEM2. *Geoscientific Model Development*, 4(4):1051–1075.

Couture, R.-M., de Wit, H. A., Tominaga, K., Kiuru, P., and Markelov, I. (2015). Oxygen dynamics in a boreal lake responds to long-term changes in climate, ice phenology, and DOC inputs. *Journal of Geophysical Research: Biogeosciences*, 120(11):2441–2456.

Couture, R.-M., Moe, S. J., Lin, Y., Kaste, Ø., Haande, S., and Solheim, A. L. (2018). Simulating water quality and ecological status of Lake Vansjø, Norway, under land-use and climate change by linking process-oriented models with a Bayesian network. *Science of the Total Environment*, 621:713–724.

Couture, R.-M., Tominaga, K., Starrfelt, J., Moe, S. J., Kaste, Ø., and Wright, R. F. (2014). Modelling phosphorus loading and algal blooms in a Nordic agricultural catchment-lake system under changing land-use and climate. *Environmental Science: Processes & Impacts*, 16:1588–1599.

Davidson, T. A., Audet, J., Svenning, J.-C., Lauridsen, T. L., Søndergaard, M., Landkildehus, F., Larsen, S. E., and Jeppesen, E. (2015). Eutrophication effects on greenhouse gas fluxes from shallow-lake mesocosms override those of climate warming. *Global Change Biology*, 21(12):4449–4463.

de Wit, H. A., Couture, R.-M., Jackson-Blake, L., Futter, M. N., Valinia, S., Austnes, K., Guerrero, J.-L., and Lin, Y. (2018). Pipes or chimneys? For carbon cycling in small boreal lakes, precipitation matters most. *Limnology and Oceanography Letters*, 3(3):275–284.

del Giorgio, P. A., Cole, J. J., Caraco, N. F., and Peters, R. H. (1999). Linking planktonic biomass and metabolism to net gas fluxes in northern temperate lakes. *Ecology*, 80(4):1422–1431.

Dibike, Y., Prowse, T., Bonsal, B., de Rham, L., and Saloranta, T. (2012). Simulation of North American lake-ice cover characteristics under contemporary and future climate conditions. *International Journal of Climatology*, 32(5):695–709.

Dinsmore, K. J., Billett, M. F., and Dyson, K. E. (2013a). Temperature and precipitation drive temporal variability in aquatic carbon and GHG concentrations and fluxes in a peatland catchment. *Global Change Biology*, 19(7):2133–2148.

Dinsmore, K. J., Wallin, M. B., Johnson, M. S., Billett, M. F., Bishop, K., Pumpanen, J., and Ojala, A. (2013b). Contrasting CO_2 concentration discharge dynamics in headwater streams: A multi-catchment comparison. *Journal of Geophysical Research: Biogeosciences*, 118(2):445–461.

Doherty, J. and Christensen, S. (2011). Use of paired simple and complex models to reduce predictive bias and quantify uncertainty. *Water Resources Research*, 47(12):W12534.

Downing, J. A., Prairie, Y. T., Cole, J. J., Duarte, C. M., Tranvik, L. J., Striegl, R. G., McDowell, W. H., Kortelainen, P., Caraco, N. F., Melack, J. M., and Middelburg, J. J. (2006). The global abundance and size distribution of lakes, ponds, and impoundments. *Limnology and Oceanography*, 51(5):2388–2397.

Ducharme-Riel, V., Vachon, D., del Giorgio, P. A., and Prairie, Y. T. (2015). The relative contribution of winter under-ice and summer hypolimnetic CO_2 accumulation to the annual CO_2 emissions from northern lakes. *Ecosystems*, 18(4):547–559.

Dugan, H. A., Woolway, R. I., Santoso, A. B., Corman, J. R., Jaimes, A., Nodine, E. R., Patil, V. P., Zwart, J. A., Brentrup, J. A., Hetherington, A. L., Oliver, S. K., Read, J. S., Winters, K. M., Hanson, P. C., Read, E. K., Winslow, L. A., and Weathers, K. C. (2016). Consequences of gas flux model choice on the

interpretation of metabolic balance across 15 lakes. *Inland Waters*, 6(4):581–592.

Einarsdóttir, K., Wallin, M. B., and Sobek, S. (2017). High terrestrial carbon load via groundwater to a boreal lake dominated by surface water inflow. *Journal of Geophysical Research: Biogeosciences*, 122(1):15–29.

Einola, E., Rantakari, M., Kankaala, P., Kortelainen, P., Ojala, A., Pajunen, H., Mäkelä, S., and Arvola, L. (2011). Carbon pools and fluxes in a chain of five boreal lakes: A dry and wet year comparison. *Journal of Geophysical Research: Biogeosciences*, 116:G03009.

Elo, A.-R., Huttula, T., Peltonen, A., and Virta, J. (1998). The effects of climate change on the temperature conditions of lakes. *Boreal Environment Research*, 3(2):137–150.

Erkkilä, K.-M., Ojala, A., Bastviken, D., Biermann, T., Heiskanen, J. J., Lindroth, A., Peltola, O., Rantakari, M., Vesala, T., and Mammarella, I. (2018). Methane and carbon dioxide fluxes over a lake: Comparison between eddy covariance, floating chambers and boundary layer method. *Biogeosciences*, 15(2):429–445.

Essington, T. E. and Carpenter, S. R. (2000). Mini-review: Nutrient cycling in lakes and streams: Insights from a comparative analysis. *Ecosystems*, 3(2):131–143.

Fairall, C. W., Bradley, E. F., Rogers, D. P., Edson, J. B., and Young, G. S. (1996). Bulk parameterization of air-sea fluxes for Tropical Ocean-Global Atmosphere Coupled-Ocean Atmosphere Response Experiment. *Journal of Geophysical Research: Oceans*, 101(C2):3747–3764.

Fang, X. and Stefan, H. G. (2009). Simulations of climate effects on water temperature, dissolved oxygen, and ice and snow covers in lakes of the contiguous U.S. under past and future climate scenarios. *Limnology and Oceanography*, 54(6part2):2359–2370.

Fennel, W. and Neumann, T. (2001). Coupling biology and oceanography in models. *AMBIO: A Journal of the Human Environment*, 30(4-5):232–236.

Gebre, S., Boissy, T., and Alfredsen, K. (2014). Sensitivity of lake ice regimes to climate change in the Nordic region. *The Cryosphere*, 8(4):1589–1605.

Geider, R. J. and Osborne, B. A. (1989). Respiration and microalgal growth: A review of the quantitative relationship between dark respiration and growth. *New Phytologist*, 112(3):327–341.

Granéli, W., Lindell, M., and Tranvik, L. (1996). Photo-oxidative production of dissolved inorganic carbon in lakes of different humic content. *Limnology and Oceanography*, 41(4):698–706.

Gudasz, C., Bastviken, D., Steger, K., Premke, K., Sobek, S., and Tranvik, L. J. (2010). Temperature-controlled organic carbon mineralization in lake sediments. *Nature*, 466:478–481.

Haario, H., Saksman, E., and Tamminen, J. (2001). An adaptive metropolis algorithm. *Bernoulli*, 7(2):223–242.

Hamilton, D. P. and Schladow, S. G. (1997). Prediction of water quality in lakes and reservoirs. Part I—Model description. *Ecological Modelling*, 96(1):91–110.

Han, P. and Bartels, D. M. (1996). Temperature dependence of oxygen diffusion in H_2O and D_2O. *The Journal of Physical Chemistry*, 100(13):5597–5602.

Hanson, P. C., Carpenter, S. R., Armstrong, D. E., Stanley, E. H., and Kratz, T. K. (2006). Lake dissolved inorganic carbon and dissolved oxygen: Changing drivers from days to decades. *Ecological Monographs*, 76(3):343–363.

Hanson, P. C., Carpenter, S. R., Cardille, J. A., Coe, M. T., and Winslow, L. A. (2007). Small lakes dominate a random sample of regional lake characteristics. *Freshwater Biology*, 52(5):814–822.

Hanson, P. C., Pollard, A. I., Bade, D. L., Predick, K., Carpenter, S. R., and Foley, J. A. (2004). A model of carbon evasion and sedimentation in temperate lakes. *Global Change Biology*, 10(8):1285–1298.

Hari, P. and Kulmala, M. (2005). Station for Measuring Ecosystem–Atmosphere Relations (SMEAR II). *Boreal Environment Research*, 10(5):315–322.

Hari, P., Pumpanen, J., Huotari, J., Kolari, P., Grace, J., Vesala, T., and Ojala, A. (2008). High-frequency measurements of productivity of planktonic algae using rugged nondispersive infrared carbon dioxide probes. *Limnology and Oceanography: Methods*, 6(8):347–354.

Hastie, A., Lauerwald, R., Weyhenmeyer, G., Sobek, S., Verpoorter, C., and Regnier, P. (2018). CO_2 evasion from boreal lakes: Revised estimate, drivers of spatial variability, and future projections. *Global Change Biology*, 24(2):711–728.

Heini, A., Puustinen, I., Tikka, M., Jokiniemi, A., Leppäranta, M., and Arvola, L. (2014). Strong dependence between phytoplankton and water chemistry in a large temperate lake: Spatial and temporal perspective. *Hydrobiologia*, 731(1):139–150.

Heiskanen, J. J., Mammarella, I., Haapanala, S., Pumpanen, J., Vesala, T., MacIntyre, S., and Ojala, A. (2014). Effects of cooling and internal wave motions on gas transfer coefficients in a boreal lake. *Tellus B: Chemical and Physical Meteorology*, 66(1):22827.

Heiskanen, J. J., Mammarella, I., Ojala, A., Stepanenko, V., Erkkilä, K.-M., Miettinen, H., Sandström, H., Eugster, W., Leppäranta, M., Järvinen, H., Vesala, T., and Nordbo, A. (2015). Effects of water clarity on lake stratification and lake-atmosphere heat exchange. *Journal of Geophysical Research: Atmospheres*, 120(15):7412–7428.

Herczeg, A. L. and Hesslein, R. H. (1984). Determination of hydrogen ion con-

centration in softwater lakes using carbon dioxide equilibria. *Geochimica et Cosmochimica Acta*, 48(4):837–845.

Hipsey, M. R., Bruce, L. C., and Hamilton, D. P. (2013). *Aquatic Ecodynamics (AED) model library: Science manual*. The University of Western Australia, Perth.

Hipsey, M. R., Bruce, L. C., and Hamilton, D. P. (2014). *GLM—General Lake Model: Model overview and user information*. AED Report #26, The University of Western Australia, Perth.

Holmberg, M., Futter, M. N., Kotamäki, N., Fronzek, S., Forsius, M., Kiuru, P., Pirttioja, N., Rasmus, K., Starr, M., and Vuorenmaa, J. (2014). Effects of changing climate on the hydrology of a boreal catchment and lake DOC—Probabilistic assessment of a dynamic model chain. *Boreal Environment Research*, 19(suppl. A):66–82.

Hondzo, M. and Stefan, H. G. (1992). *Water temperature characteristics of lakes subjected to climate change*. Project Report No. 329, St. Anthony Falls Hydraulic Laboratory, University of Minnesota, Minneapolis.

Hopkinson, C. S., Vallino, J. J., and Nolin, A. (2002). Decomposition of dissolved organic matter from the continental margin. *Deep Sea Research Part II: Topical Studies in Oceanography*, 49(20):4461 –4478.

Houghton, R. (2003). The contemporary carbon cycle. In Holland, H. D. and Turekian, K. K., editors, *Treatise on Geochemistry*, pages 473–513. Pergamon, Oxford.

Humborg, C., Mörth, C.-M., Sundbom, M., Borg, H., Blenckner, T., Giesler, R., and Ittekkot, V. (2010). CO_2 supersaturation along the aquatic conduit in Swedish watersheds as constrained by terrestrial respiration, aquatic respiration and weathering. *Global Change Biology*, 16(7):1966–1978.

Huotari, J., Ojala, A., Peltomaa, E., Pumpanen, J., Hari, P., and Vesala, T. (2009). Temporal variations in surface water CO_2 concentration in a boreal humic lake based on high-frequency measurements. *Boreal Environment Research*, 14(suppl. A):48–60.

Huovinen, P. S., Penttilä, H., and Soimasuo, M. R. (2003). Spectral attenuation of solar ultraviolet radiation in humic lakes in Central Finland. *Chemosphere*, 51(3):205–214.

Huttula, T., Peltonen, A., Bilaletdin, Ä., and Saura, M. (1992). The effects of climatic change on lake ice and water temperature. *Aqua Fennica*, 22(2):129–142.

Huttunen, I., Huttunen, M., Piirainen, V., Korppoo, M., Lepistö, A., Räike, A., Tattari, S., and Vehviläinen, B. (2016). A national-scale nutrient loading model for Finnish watersheds—VEMALA. *Environmental Modeling & Assessment*, 21(1):83–109.

Huttunen, J. T., Väisänen, T. S., Hellsten, S. K., and Martikainen, P. (2006). Methane fluxes at the sediment–water interface in some boreal lakes and reservoirs. *Boreal Environment Research*, 11(1):27–34.

Imberger, J. (1985). The diurnal mixed layer. *Limnology and Oceanography*, 30(4):737–770.

IPCC (2007). In Solomon, S., Qin, D., Manning, M., Chen, Z., Marquis, M., Averyt, K., Tignor, M., and Miller, H., editors, *Climate change 2007: The physical science basis. Contribution of Working Group I to the Fourth Assessment Report of the Intergovernmental Panel on Climate Change*. Cambridge University Press, Cambridge.

IPCC (2014). In Core Writing Team, Pachauri, R., and Meyer, L., editors, *Climate change 2014: Synthesis report. Contribution of Working Groups I, II and III to the Fifth Assessment Report of the Intergovernmental Panel on Climate Change*. IPCC, Geneva.

Jähne, B. and Haußecker, H. (1998). Air-water gas exchange. *Annual Review of Fluid Mechanics*, 30(1):443–468.

Jähne, B., Münnich, K. O., Bösinger, R., Dutzi, A., Huber, W., and Libner, P. (1987). On the parameters influencing air-water gas exchange. *Journal of Geophysical Research: Oceans*, 92(C2):1937–1949.

Jansson, M., Bergström, A.-K., Blomqvist, P., and Drakare, S. (2000). Allochthonous organic carbon and phytoplankton/bacterioplankton production relationships in lakes. *Ecology*, 81(11):3250–3255.

Jansson, M., Hickler, T., Jonsson, A., and Karlsson, J. (2008). Links between terrestrial primary production and bacterial production and respiration in lakes in a climate gradient in subarctic Sweden. *Ecosystems*, 11(3):367–376.

Jennings, E., Järvinen, M., Allott, N., Arvola, L., Moore, K., Naden, P., Aonghusa, C. N., Nõges, T., and Weyhenmeyer, G. A. (2010). Impacts of climate on the flux of dissolved organic carbon from catchments. In George, G., editor, *The Impact of Climate Change on European Lakes*, pages 199–220. Springer, Dordrecht.

Jeppesen, E., Kronvang, B., Meerhoff, M., Søndergaard, M., Hansen, K. M., Andersen, H. E., Lauridsen, T. L., Liboriussen, L., Beklioglu, M., Özen, A., and Olesen, J. E. (2009). Climate change effects on runoff, catchment phosphorus loading and lake ecological state, and potential adaptations. *Journal of Environmental Quality*, 38(5):1930–1941.

Jonsson, A., Åberg, J., Lindroth, A., and Jansson, M. (2008). Gas transfer rate and CO_2 flux between an unproductive lake and the atmosphere in northern Sweden. *Journal of Geophysical Research: Biogeosciences*, 113:G04006.

Jonsson, A., Meili, M., Bergström, A.-K., and Jansson, M. (2001). Whole-lake mineralization of allochthonous and autochthonous organic carbon in a large

humic lake (Örträsket, N. Sweden). *Limnology and Oceanography*, 46(7):1691–1700.

Jylhä, K., Ruosteenoja, K., Räisänen, J., Venäläinen, A., Tuomenvirta, H., Ruokolainen, L., Saku, S., and Seitola, T. (2009). *Arvioita Suomen muuttuvasta ilmastosta sopeutumistutkimuksia varten. ACCLIM-hankkeen raportti 2009 [The changing climate in Finland: Estimates for adaptation studies. ACCLIM project report 2009]*. Reports 2009:4, Finnish Meteorological Institute, Helsinki. ([In Finnish with an abstract, an extended abstract, and captions for figures and tables in English].

Jylhä, K., Tuomenvirta, H., and Ruosteenoja, K. (2004). Climate change projections for Finland during the 21st century. *Boreal Environment Research*, 9(2):127–152.

Jylhä, K., Tuomenvirta, H., Ruosteenoja, K., Niemi-Hugaerts, H., Keisu, K., and Karhu, J. A. (2010). Observed and projected future shifts of climatic zones in europe and their use to visualize climate change information. *Weather, Climate, and Society*, 2(2):148–167.

Kankaala, P., Huotari, J., Tulonen, T., and Ojala, A. (2013). Lake-size dependent physical forcing drives carbon dioxide and methane effluxes from lakes in a boreal landscape. *Limnology and Oceanography*, 58(6):1915–1930.

Kara, E. L., Hanson, P., Hamilton, D., Hipsey, M. R., McMahon, K. D., Read, J. S., Winslow, L., Dedrick, J., Rose, K., Carey, C. C., Bertilsson, S., da Motta Marques, D., Beversdorf, L., Miller, T., Wu, C., Hsieh, Y.-F., Gaiser, E., and Kratz, T. (2012). Time-scale dependence in numerical simulations: Assessment of physical, chemical, and biological predictions in a stratified lake at temporal scales of hours to months. *Environmental Modelling & Software*, 35:104–121.

Karhu, K., Fritze, H., Hämäläinen, K., Vanhala, P., Jungner, H., Oinonen, M., Sonninen, E., Tuomi, M., Spetz, P., Kitunen, V., and Liski, J. (2010). Temperature sensitivity of soil carbon fractions in boreal forest soil. *Ecology*, 91(2):370–376.

Karlsson, J., Giesler, R., Persson, J., and Lundin, E. (2013). High emission of carbon dioxide and methane during ice thaw in high latitude lakes. *Geophysical Research Letters*, 40(6):1123–1127.

Keller, W. (2007). Implications of climate warming for Boreal Shield lakes: A review and synthesis. *Environmental Reviews*, 15(NA):99–112.

Kelly, C. A., Fee, E., Ramlal, P. S., Rudd, J. W. M., Hesslein, R. H., Anema, C., and Schindler, E. U. (2001). Natural variability of carbon dioxide and net epilimnetic production in the surface waters of boreal lakes of different sizes. *Limnology and Oceanography*, 46(5):1054–1064.

Keskitalo, J., Salonen, K., and Holopainen, A.-L. (1998). Long-term fluctuations in environmental conditions, plankton and macrophytes in a humic lake, Valkea-Kotinen. *Boreal Environment Research*, 3(3):251–262.

Kirk, J. T. O. (2011). *Light and Photosynthesis in Aquatic Ecosystems (3rd ed.)*. Cambridge University Press, Cambridge.

Kiuru, P., Ojala, A., Mammarella, I., Heiskanen, J., Kämäräinen, M., Vesala, T., and Huttula, T. (2018). Effects of climate change on CO_2 concentration and efflux in a humic boreal lake: A modeling study. *Journal of Geophysical Research: Biogeosciences*, 123(7):2212–2233.

Köhler, S. J., Buffam, I., Seibert, J., Bishop, K. H., and Laudon, H. (2009). Dynamics of stream water TOC concentrations in a boreal headwater catchment: Controlling factors and implications for climate scenarios. *Journal of Hydrology*, 373(1–2):44–56.

Korhonen, J. and Kuusisto, E. (2010). Long-term changes in the discharge regime in Finland. *Hydrology Research*, 41(3-4):253–268.

Kortelainen, P. (1993). Content of total organic carbon in Finnish lakes and its relationship to catchment characteristics. *Canadian Journal of Fisheries and Aquatic Sciences*, 50(7):1477–1483.

Kortelainen, P. (1999). Occurrence of humic waters. temporal and spatial variability. In Keskitalo, J. and Eloranta, P., editors, *Limnology of Humic Waters*. Backhuys Publishers, Leiden.

Kortelainen, P., Rantakari, M., Huttunen, J. T., Mattsson, T., Alm, J., Juutinen, S., Larmola, T., Silvola, J., and Martikainen, P. J. (2006). Sediment respiration and lake trophic state are important predictors of large CO_2 evasion from small boreal lakes. *Global Change Biology*, 12(8):1554–1567.

Kosten, S., Roland, F., da Motta Marques, D. M. L., van Nes, E. H., Mazzeo, N., Sternberg, L. d. S. L., Scheffer, M., and Cole, J. J. (2010). Climate-dependent CO_2 emissions from lakes. *Global Biogeochemical Cycles*, 24:GB2007.

Kragh, T. and Søndergaard, M. (2004). Production and bioavailability of autochthonous dissolved organic carbon: Effects of mesozooplankton. *Aquatic Microbial Ecology*, 36(1):61–72.

Kratz, T. K., Schindler, J., Hope, D., Riera, J. L., and Bowser, C. J. (1997). Average annual carbon dioxide concentrations in eight neighboring lakes in northern Wisconsin, USA. *Verhandlungen der Internationalen Vereinigung für Theoretische und Angewandte Limnologie*, 26(2):335–338.

Kraus, E. B. and Businger, J. A. (1994). *Atmosphere-Ocean Interaction*. Oxford University Press, New York.

Lahermo, P., Ilmasti, M., Juntunen, R., and Taka, M. (1990). *The geochemical atlas of Finland, Part 1: The hydrogeochemical mapping of Finnish groundwater*. Geological Survey of Finland, Espoo.

Larsen, S., Andersen, T., and Hessen, D. O. (2011). Climate change predicted to cause severe increase of organic carbon in lakes. *Global Change Biology*, 17(2):1186–1192.

Laudon, H., Buttle, J., Carey, S. K., McDonnell, J., McGuire, K., Seibert, J., Shanley, J., Soulsby, C., and Tetzlaff, D. (2012). Cross-regional prediction of long-term trajectory of stream water DOC response to climate change. *Geophysical Research Letters*, 39(18):L18404.

Ledesma, J. L. J., Grabs, T., Bishop, K. H., Schiff, S. L., and Köhler, S. J. (2015). Potential for long-term transfer of dissolved organic carbon from riparian zones to streams in boreal catchments. *Global Change Biology*, 21(8):2963–2979.

Leith, F. I., Dinsmore, K. J., Wallin, M. B., Billett, M. F., Heal, K. V., Laudon, H., Öquist, M. G., and Bishop, K. (2015). Carbon dioxide transport across the hillslope–riparian–stream continuum in a boreal headwater catchment. *Biogeosciences*, 12(6):1881–1892.

López Bellido, J., Tulonen, T., Kankaala, P., and Ojala, A. (2009). CO_2 and CH_4 fluxes during spring and autumn mixing periods in a boreal lake (Pääjärvi, southern Finland). *Journal of Geophysical Research: Biogeosciences*, 114:G04007.

Los, F. and Blaas, M. (2010). Complexity, accuracy and practical applicability of different biogeochemical model versions. *Journal of Marine Systems*, 81(1):44–74.

Maberly, S. (1985). Diel, episodic and seasonal changes in pH and concentrations of inorganic carbon in a productive lake. *Freshwater Biology*, 35(3):579–598.

Maberly, S. C., Barker, P. A., Stott, A. W., and De Ville, M. M. (2013). Catchment productivity controls CO_2 emissions from lakes. *Nature Climate Change*, 3:391–394.

MacIntyre, S., Eugster, W., and Kling, G. W. (2001). The critical importance of buoyancy flux for gas flux across the air-water interface. In Donelan, M. A., Drennan, W. M., Saltzman, E. S., and Wanninkhof, R., editors, *Gas Transfer at Water Surfaces. Geophysical Monograph 127*, pages 135–139. American Geophysical Union.

MacIntyre, S., Jonsson, A., Jansson, M., Åberg, J., Turney, D. E., and Miller, S. D. (2010). Buoyancy flux, turbulence, and the gas transfer coefficient in a stratified lake. *Geophysical Research Letters*, 37:L24604.

MacIntyre, S., Wanninkhof, R., and Chanton, J. (1995). Trace gas exchange across the air–water interface in freshwater and coastal marine environments. In Matson, P. and Harriss, R., editors, *Biogenic trace gases: Measuring emissions from soil and water*, pages 52–97. Wiley-Blackwell, Cambridge, MA.

Magnuson, J. J., Webster, K. E., Assel, R. A., Bowser, C. J., Dillon, P. J., Eaton, J. G., Evans, H. E., Fee, E. J., Hall, R. I., Mortsch, L. R., Schindler, D. W., and Quinn, F. H. (1997). Potential effects of climate changes on aquatic systems: Laurentian Great Lakes and Precambrian shield region. *Hydrological Processes*, 11(8):825–871.

Maharajh, D. M. and Walkley, J. (1973). The temperature dependence of the diffusion coefficients of Ar, CO_2, CH_4, CH_3Cl, CH_3Br, and $CHCl_2F$ in water. *Canadian Journal of Chemistry*, 51(6):944–952.

Mammarella, I., Nordbo, A., Rannik, Ü., Haapanala, S., Levula, J., Laakso, H., Ojala, A., Peltola, O., Heiskanen, J., Pumpanen, J., and Vesala, T. (2015). Carbon dioxide and energy fluxes over a small boreal lake in Southern Finland. *Journal of Geophysical Research: Biogeosciences*, 120(7):1296–1314.

Markfort, C. D., Perez, A. L. S., Thill, J. W., Jaster, D. A., Porté-Agel, F., and Stefan, H. G. (2010). Wind sheltering of a lake by a tree canopy or bluff topography. *Water Resources Research*, 46(3):W03530.

Martin, J. L. and McCutcheon, S. C. (1999). *Hydrodynamics and transport for water quality modeling*. CRC Press, Boca Raton.

Mathias, J. A. and Barica, J. (1980). Factors controlling oxygen depletion in ice-covered lakes. *Canadian Journal of Fisheries and Aquatic Sciences*, 37(2):185–194.

Mattsson, T. (2010). Export of organic matter, sulphate and base cations from boreal headwater catchments downstream to the coast: Impacts of land use and climate. *Monographs of the Boreal Environment Research*, 36:1–45.

Mattsson, T., Kortelainen, P., and Räike, A. (2005). Export of DOM from boreal catchments: Impacts of land use cover and climate. *Biogeochemistry*, 76(2):373–394.

Mattsson, T., Kortelainen, P., Räike, A., Lepistö, A., and Thomas, D. N. (2015). Spatial and temporal variability of organic C and N concentrations and export from 30 boreal rivers induced by land use and climate. *Science of the Total Environment*, 508:145–154.

McDonald, C. P., Stets, E. G., Striegl, R. G., and Butman, D. (2013). Inorganic carbon loading as a primary driver of dissolved carbon dioxide concentrations in the lakes and reservoirs of the contiguous United States. *Global Biogeochemical Cycles*, 27(2):285–295.

Meding, M. E. and Jackson, L. J. (2001). Biological implications of empirical models of winter oxygen depletion. *Canadian Journal of Fisheries and Aquatic Sciences*, 58(9):1727–1736.

Meili, M. (1992). Sources, concentrations and characteristics of organic matter in softwater lakes and streams of the Swedish forest region. *Hydrobiologia*, 229(1):23–41.

Meinshausen, M., Smith, S. J., Calvin, K., Daniel, J. S., Kainuma, M. L. T., Lamarque, J.-F., Matsumoto, K., Montzka, S. A., Raper, S. C. B., Riahi, K., Thomson, A., Velders, G. J. M., and van Vuuren, D. P. P. (2011). The RCP greenhouse gas concentrations and their extensions from 1765 to 2300. *Climatic Change*, 109(1):213–241.

Miettinen, H., Pumpanen, J., Heiskanen, J. J., Aaltonen, H., Mammarella, I., Ojala, A., Levula, J., and Rantakari, M. (2015). Towards a more comprehensive understanding of lacustrine greenhouse gas dynamics—Two-year measurements of concentrations and fluxes of CO_2, CH_4 and N_2O in a typical boreal lake surrounded by managed forests. *Boreal Environment Research*, 20(1):75–89.

Millero, F. J. (1995). Thermodynamics of the carbon dioxide system in the oceans. *Geochimica et Cosmochimica Acta*, 59(4):661–677.

Moriasi, D. N., Arnold, J. G., Liew, M. W. V., Bingner, R. L., Harmel, R. D., and Veith, T. L. (2007). Model evaluation guidelines for systematic quantification of accuracy in watershed simulations. *Transactions of the ASABE*, 50(3):885–900.

Mulholland, P. J. (2003). Large-scale patterns in dissolved organic carbon concentration, flux, and sources. In Findlay, S. E. G. and Sinsabaugh, R. L., editors, *Aquatic Ecosystems: Interactivity of dissolved organic matter*, pages 139–159. Elsevier, New York.

Myhre, G., Shindell, D., Bréon, F.-M., Collins, W., Fuglestvedt, J., Huang, J., Koch, D., Lamarque, J.-F., Lee, D., Mendoza, B., Nakajima, T., Robock, A., Stephens, G., Takemura, T., and Zhang, H. (2013). Anthropogenic and natural radiative forcing. In Stocker, T. F., Qin, D., Plattner, G.-K., Tignor, M., Allen, S. K., Boschung, J., Nauels, A., Xia, Y., Bex, V., and Midgley, P. M., editors, *Climate Change 2013: The physical science basis. Contribution of Working Group I to the Fifth Assessment Report of the Intergovernmental Panel on Climate Change*. Cambridge University Press, Cambridge.

Myrbo, A. (2012). Carbon cycle in lakes. In Bengtsson, L., Herschy, R. W., and Fairbridge, R. W., editors, *Encyclopedia of Lakes and Reservoirs*, pages 121–125. Springer Netherlands, Dordrecht.

Natchimuthu, S., Sundgren, I., Gålfalk, M., Klemedtsson, L., and Bastviken, D. (2017). Spatiotemporal variability of lake pCO_2 and CO_2 fluxes in a hemiboreal catchment. *Journal of Geophysical Research: Biogeosciences*, 122(1):30–49.

Niemi, J. and Raateland, A. (2007). River water quality in the Finnish Eurowaternet. *Boreal Environment Research*, 12(5):571–584.

Nordbo, A., Launiainen, S., Mammarella, I., Leppäranta, M., Huotari, J., Ojala, A., and Vesala, T. (2011). Long-term energy flux measurements and energy balance over a small boreal lake using eddy covariance technique. *Journal of Geophysical Research: Atmospheres*, 116:D02119.

Ojala, A., López Bellido, J., Tulonen, T., Kankaala, P., and Huotari, J. (2011). Carbon gas fluxes from a brown-water and a clear-water lake in the boreal zone during a summer with extreme rain events. *Limnology and Oceanography*, 56(1):61–76.

Omstedt, A., Gustafsson, E., and Wesslander, K. (2009). Modelling the uptake and release of carbon dioxide in the Baltic Sea surface water. *Continental Shelf Research*, 29(7):870–885.

Oni, S. K., Tiwari, T., Ledesma, J. L. J., Ågren, A. M., Teutschbein, C., Schelker, J., Laudon, H., and Futter, M. N. (2015). Local- and landscape-scale impacts of clear-cuts and climate change on surface water dissolved organic carbon in boreal forests. *Journal of Geophysical Research: Biogeosciences*, 120(11):2402–2426.

Oreskes, N., Shrader-Frechette, K., and Belitz, K. (1994). Verification, validation, and confirmation of numerical models in the earth sciences. *Science*, 263(5147):641–646.

Oveisy, A. and Boegman, L. (2014). One-dimensional simulation of lake and ice dynamics during winter. *Journal of Limnology*, 73(3):441–453.

Pajunen, H. (2004). *Järvisedimentit kuiva-aineen ja hiilen varastona [Lake sediments as a store of dry matter and carbon]*. Report of Investigation 160, Geological Survey of Finland, Espoo. [In Finnish with English summary].

Pawlowicz, R. and Bearsley, B. (1999). Air-Sea Toolbox. Retrieved from `https://sea-mat.github.io/sea-mat`.

Peltomaa, E., Ojala, A., Holopainen, A.-L., and Salonen, K. (2013). Changes in phytoplankton in a boreal lake during a 14-year period. *Boreal Environment Research*, 18(5):387–400.

Perroud, M. and Goyette, S. (2010). Impact of warmer climate on Lake Geneva water-temperature profiles. *Boreal Environment Research*, 15(2):255–278.

Pirinen, P., Simola, H., Aalto, J., Kaukoranta, J.-P., Karlsson, P., and Ruuhela, R. (2012). *Climatological statistics of Finland 1981–2010*. Reports 2012:1, Finnish Meteorological Institute, Helsinki.

Podgrajsek, E., Sahlée, E., and Rutgersson, A. (2015). Diel cycle of lake-air CO_2 flux from a shallow lake and the impact of waterside convection on the transfer velocity. *Journal of Geophysical Research: Biogeosciences*, 120(1):29–38.

Portielje, R. and Lijklema, L. (1995). Carbon dioxide fluxes across the air-water interface and its impact on carbon availability in aquatic systems. *Limnology and Oceanography*, 40(4):690–699.

Provenzale, M., Ojala, A., Heiskanen, J., Erkkilä, K.-M., Mammarella, I., Hari, P., and Vesala, T. (2018). High-frequency productivity estimates for a lake from free-water CO_2 concentration measurements. *Biogeosciences*, 15(7):2021–2032.

Prudhomme, C. and Davies, H. (2009). Assessing uncertainties in climate change impact analyses on the river flow regimes in the UK. Part 2: future climate. *Climatic Change*, 93(1–2):197–222.

Pulkkanen, M. and Salonen, K. (2013). Accumulation of low oxygen water in deep waters of ice-covered lakes cooled below 4 °C. *Inland Waters*, 3(1):15–24.

Pumpanen, J., Lindén, A., Miettinen, H., Kolari, P., Ilvesniemi, H., Mammarella, I., Hari, P., Nikinmaa, E., Heinonsalo, J., Bäck, J., Ojala, A., Berninger, F., and

Vesala, T. (2014). Precipitation and net ecosystem exchange are the most important drivers of DOC flux in upland boreal catchments. *Journal of Geophysical Research: Biogeosciences*, 119(9):1861–1878.

Rantakari, M. and Kortelainen, P. (2005). Interannual variation and climatic regulation of the CO_2 emission from large boreal lakes. *Global Change Biology*, 11(8):1368–1380.

Rantakari, M., Mattsson, T., Kortelainen, P., Piirainen, S., Finér, L., and Ahtiainen, M. (2010). Organic and inorganic carbon concentrations and fluxes from managed and unmanaged boreal first-order catchments. *Science of the Total Environment*, 408(7):1649–1658.

Rasilo, T., Ojala, A., Huotari, J., and Pumpanen, J. (2012). Rain induced changes in carbon dioxide concentrations in the soil–lake–brook continuum of a boreal forested catchment. *Vadose Zone Journal*, 11(2).

Rautio, A. and Korkka-Niemi, K. (2015). Chemical and isotopic tracers indicating groundwater/surface-water interaction within a boreal lake catchment in Finland. *Hydrogeology Journal*, 23(4):687–705.

Raymond, P. A., Hartmann, J., Lauerwald, R., Sobek, S., McDonald, C., Hoover, M., Butman, D., Striegl, R., Mayorga, E., Humborg, C., Kortelainen, P., Dürr, H., Meybeck, M., Ciais, P., and Guth, P. (2013). Global carbon dioxide emissions from inland waters. *Nature*, 503:355–359.

Read, J. S., Hamilton, D. P., Desai, A. R., Rose, K. C., MacIntyre, S., Lenters, J. D., Smyth, R. L., Hanson, P. C., Cole, J. J., Staehr, P. A., Rusak, J. A., Pierson, D. C., Brookes, J. D., Laas, A., and Wu, C. H. (2012). Lake-size dependency of wind shear and convection as controls on gas exchange. *Geophysical Research Letters*, 39:L09405.

Read, J. S. and Rose, K. C. (2013). Physical responses of small temperate lakes to variation in dissolved organic carbon concentrations. *Limnology and Oceanography*, 58(3):921–931.

Riley, M. J. and Stefan, H. G. (1988). MINLAKE: A dynamic lake water quality simulation model. *Ecological Modelling*, 43(3):155–182.

Robson, B. J. (2014). When do aquatic systems models provide useful predictions, what is changing, and what is next? *Environmental Modelling & Software*, 61:287 – 296.

Roehm, C. L., Prairie, Y. T., and del Giorgio, P. A. (2009). The pCO_2 dynamics in lakes in the boreal region of northern Québec, Canada. *Global Biogeochemical Cycles*, 23(3):GB3013.

Romarheim, A. T., Tominaga, K., Riise, G., and Andersen, T. (2015). The importance of year-to-year variation in meteorological and runoff forcing for water quality of a temperate, dimictic lake. *Hydrology and Earth System Sciences*, 19(6):2649–2662.

Ruosteenoja, K., Jylhä, K., and Kämäräinen, M. (2016). Climate projections for Finland under the RCP forcing scenarios. *Geophysica*, 51(1):17–50.

Sælthun, N. R. (1996). *The "Nordic" HBV model. Description and documentation of the model version developed for the project Climate Change and Energy Production.* NVE Publication 7, Norwegian Water and Energy Administration, Oslo.

Sakshaug, E., Bricaud, A., Dandonneau, Y., Falkowski, P. G., Kiefer, D. A., Legendre, L., Morel, A., Parslow, J., and Takahashi, M. (1997). Parameters of photosynthesis: Definitions, theory and interpretation of results. *Journal of Plankton Research*, 19(11):1637–1670.

Salonen, K., Arvola, L., and Rask, M. (1984). Autumnal and vernal circulation of small forest lakes in Southern Finland. *Verhandlungen der Internationalen Vereinigung für Theoretische und Angewandte Limnologie*, 22(1):103–107.

Salonen, K. and Rosenberg, M. (2000). Advantages from diel vertical migration can explain the dominance of *Gonyostomum semen* (Raphidophyceae) in a small, steeply-stratified humic lake. *Journal of Plankton Research*, 22(10):1841–1853.

Saloranta, T. M. (2006). Highlighting the model code selection and application process in policy-relevant water quality modelling. *Ecological Modelling*, 194(1):316–327.

Saloranta, T. M. and Andersen, T. (2007). MyLake—A multi-year lake simulation model code suitable for uncertainty and sensitivity analysis simulations. *Ecological Modelling*, 207(1):45 – 60. Uncertainty in Ecological Models.

Saloranta, T. M., Forsius, M., Järvinen, M., and Arvola, L. (2009). Impacts of projected climate change on the thermodynamics of a shallow and a deep lake in Finland: Model simulations and Bayesian uncertainty analysis. *Hydrology Research*, 40(2-3):234.

Saloranta, T. M., Kämäri, J., Rekolainen, S., and Malve, O. (2003). Benchmark criteria: A tool for selecting appropriate models in the field of water management. *Environmental Management*, 32(3):322–333.

Sarkkola, S., Koivusalo, H., Laurén, A., Kortelainen, P., Mattsson, T., Palviainen, M., Piirainen, S., Starr, M., and Finér, L. (2009). Trends in hydrometeorological conditions and stream water organic carbon in boreal forested catchments. *Science of the Total Environment*, 408(1):92–101.

Schiff, S., Aravena, R., Mewhinney, E., Elgood, R., Warner, B., Dillon, P., and Trumbore, S. (1998). Precambrian shield wetlands: Hydrologic control of the sources and export of dissolved organic matter. *Climatic Change*, 40(2):167–188.

Schneider, C., Laizé, C. L. R., Acreman, M. C., and Flörke, M. (2013). How will climate change modify river flow regimes in Europe? *Hydrology and Earth System Sciences*, 17(1):325–339.

Sobek, S., Algesten, G., Bergström, A.-K., Jansson, M., and Tranvik, L. J. (2003). The catchment and climate regulation of pCO_2 in boreal lakes. *Global Change Biology*, 9(4):630–641.

Sobek, S., Durisch-Kaiser, E., Zurbrügg, R., Wongfun, N., Wessels, M., Pasche, N., and Wehrli, B. (2009). Organic carbon burial efficiency in lake sediments controlled by oxygen exposure time and sediment source. *Limnology and Oceanography*, 54(6):2243–2254.

Sobek, S., Söderbäck, B., Karlsson, S., Andersson, E., and Brunberg, A. K. (2006). A carbon budget of a small humic lake: An example of the importance of lakes for organic matter cycling in boreal catchments. *AMBIO: A Journal of the Human Environment*, 35(8):469–475.

Sobek, S., Tranvik, L. J., and Cole, J. J. (2005). Temperature independence of carbon dioxide supersaturation in global lakes. *Global Biogeochemical Cycles*, 19(2):GB2003.

Sobek, S., Tranvik, L. J., Prairie, Y. T., Kortelainen, P., and Cole, J. J. (2007). Patterns and regulation of dissolved organic carbon: An analysis of 7,500 widely distributed lakes. *Limnology and Oceanography*, 52(3).

Solantie, R. (2005). Productivity of boreal forests in relation to climate and vegetation zones. *Boreal Environment Research*, 10(4):275–297.

Søndergaard, M. and Middelboe, M. (1995). A cross-system analysis of labile dissolved organic carbon. *Marine Ecology Progress Series*, 118:283–294.

Stefan, H. G. and Fang, X. (1994). Dissolved oxygen model for regional lake analysis. *Ecological Modelling*, 71(1):37–68.

Stepanenko, V., Jöhnk, K. D., Machulskaya, E., Perroud, M., Subin, Z., Nordbo, A., Mammarella, I., and Mironov, D. (2014). Simulation of surface energy fluxes and stratification of a small boreal lake by a set of one-dimensional models. *Tellus A: Dynamic Meteorology and Oceanography*, 66(1):21389.

Stepanenko, V., Mammarella, I., Ojala, A., Miettinen, H., Lykosov, V., and Vesala, T. (2016). LAKE 2.0: A model for temperature, methane, carbon dioxide and oxygen dynamics in lakes. *Geoscientific Model Development*, 9(5):1977–2006.

Stepanenko, V. M., Machul'skaya, E. E., Glagolev, M. V., and Lykossov, V. N. (2011). Numerical modeling of methane emissions from lakes in the permafrost zone. *Izvestiya, Atmospheric and Oceanic Physics*, 47(2):252–264.

Stepanenko, V. M., Martynov, A., Jöhnk, K. D., Subin, Z. M., Perroud, M., Fang, X., Beyrich, F., Mironov, D., and Goyette, S. (2013). A one-dimensional model intercomparison study of thermal regime of a shallow, turbid midlatitude lake. *Geoscientific Model Development*, 6(4):1337–1352.

Stets, E. G., Striegl, R. G., Aiken, G. R., Rosenberry, D. O., and Winter, T. C. (2009). Hydrologic support of carbon dioxide flux revealed by whole-lake carbon budgets. *Journal of Geophysical Research*, 114:G01008.

Striegl, R. G., Kortelainen, P., Chanton, J. P., Wickland, K. P., Bugna, G. C., and Rantakari, M. (2001). Carbon dioxide partial pressure and ^{13}C content of north temperate and boreal lakes at spring ice melt. *Limnology and Oceanography*, 46(4):941–945.

Striegl, R. G. and Michmerhuizen, C. M. (1998). Hydrologic influence on methane and carbon dioxide dynamics at two north-central Minnesota lakes. *Limnology and Oceanography*, 43(7):1519–1529.

Stumm, W. and Morgan, J. J. (1981). *Aquatic chemistry: An introduction emphasizing chemical equilibria in natural waters (2nd ed.)*. Wiley, New York.

Svensson, U. (1998). *PROBE, Program for boundary layers in the environment. System description and manual*. SMHI RO Report No. 24, Swedish Meteorological and Hydrological Institute, Norrköping.

Tan, Z., Zhuang, Q., Shurpali, N. J., Marushchak, M. E., Biasi, C., Eugster, W., and Walter Anthony, K. (2017). Modeling CO_2 emissions from Arctic lakes: Model development and site-level study. *Journal of Advances in Modeling Earth Systems*, 9(5):2190–2213.

Tedford, E. W., MacIntyre, S., Miller, S. D., and Czikowsky, M. J. (2014). Similarity scaling of turbulence in a temperate lake during fall cooling. *Journal of Geophysical Research: Oceans*, 119(8):4689–4713.

Teutschbein, C., Grabs, T., Karlsen, R. H., Laudon, H., and Bishop, K. (2015). Hydrological response to changing climate conditions: Spatial streamflow variability in the boreal region. *Water Resources Research*, 51(12):9425–9446.

Thomann, R. V. and Fitzpatrick, J. F. (1982). *Calibration and verification of a mathematical model of the eutrophication of the Potomac estuary*. Prepared for Department of Environmental Services, Government of the District of Columbia, Washington, DC.

Thurman, E. (1985). *Organic Geochemistry of Natural Waters*. Kluwer Academic Publishers, Dordrecht.

Tranvik, L. J., Downing, J. A., Cotner, J. B., Loiselle, S. A., Striegl, R. G., Ballatore, T. J., Dillon, P., Finlay, K., Fortino, K., Knoll, L. B., Kortelainen, P. L., Kutser, T., Larsen, S., Laurion, I., Leech, D. M., McCallister, S. L., McKnight, D. M., Melack, J. M., Overholt, E., Porter, J. A., Prairie, Y., Renwick, W. H., Roland, F., Sherman, B. S., Schindler, D. W., Sobek, S., Tremblay, A., Vanni, M. J., Verschoor, A. M., von Wachenfeldt, E., and Weyhenmeyer, G. A. (2009). Lakes and reservoirs as regulators of carbon cycling and climate. *Limnology and Oceanography*, 54(6, part 2):2298–2314.

Tranvik, L. J. and Jansson, M. (2002). Climate change (Communication arising): Terrestrial export of organic carbon. *Nature*, 415:861–862.

Tulonen, T. (1993). Bacterial production in a mesohumic lake estimated from [^{14}C]leucine incorporation rate. *Microbial Ecology*, 26(3):201–217.

Tulonen, T. (2004). *Role of allochthonous and autochthonous dissolved organic matter (DOM) as a carbon source for bacterioplankton in boreal humic lakes*. PhD thesis, University of Helsinki, Helsinki.

Vachon, D., Prairie, Y. T., and Cole, J. J. (2010). The relationship between near-surface turbulence and gas transfer velocity in freshwater systems and its implications for floating chamber measurements of gas exchange. *Limnology and Oceanography*, 55(4):1723–1732.

Vähätalo, A. V., Aarnos, H., and Mäntyniemi, S. (2010). Biodegradability continuum and biodegradation kinetics of natural organic matter described by the beta distribution. *Biogeochemistry*, 100(1):227–240.

Vähätalo, A. V., Salkinoja-Salonen, M., Taalas, P., and Salonen, K. (2000). Spectrum of the quantum yield for photochemical mineralization of dissolved organic carbon in a humic lake. *Limnology and Oceanography*, 45(3):664–676.

Vähätalo, A. V., Salonen, K., Münster, U., Järvinen, M., and Wetzel, R. G. (2003). Photochemical transformation of allochthonous organic matter provides bioavailable nutrients in a humic lake. *Archiv für Hydrobiologie*, 156(3):287–314.

van Vuuren, D. P., Edmonds, J., Kainuma, M., Riahi, K., Thomson, A., Hibbard, K., Hurtt, G. C., Kram, T., Krey, V., Lamarque, J.-F., Masui, T., Meinshausen, M., Nakicenovic, N., Smith, S. J., and Rose, S. K. (2011). The representative concentration pathways: An overview. *Climatic Change*, 109(1):5–31.

Veijalainen, N. (2012). *Estimation of climate change impacts on hydrology and floods in Finland*. PhD thesis, Aalto University, Espoo.

Verpoorter, C., Kutser, T., Seekell, D. A., and Tranvik, L. J. (2014). A global inventory of lakes based on high-resolution satellite imagery. *Geophysical Research Letters*, 41(18):6396–6402.

Vesala, T., Huotari, J., Rannik, Ü., Suni, T., Smolander, S., Sogachev, A., Launiainen, S., and Ojala, A. (2006). Eddy covariance measurements of carbon exchange and latent and sensible heat fluxes over a boreal lake for a full open-water period. *Journal of Geophysical Research: Atmospheres*, 111:D11101.

Virtanen, M. (2009). *Mathematical modelling of flow and transport as link to impacts in multidiscipline environments*. PhD thesis, University of Oulu, Oulu.

von Salzen, K., Scinocca, J. F., McFarlane, N. A., Li, J., Cole, J. N. S., Plummer, D., Verseghy, D., Reader, M. C., Ma, X., Lazare, M., and Solheim, L. (2013). The Canadian fourth generation atmospheric global climate model (CanAM4). Part I: Representation of physical processes. *Atmosphere-Ocean*, 51(1):104–125.

von Wachenfeldt, E., Bastviken, D., and Tranvik, L. J. (2009). Microbially induced flocculation of allochthonous dissolved organic carbon in lakes. *Limnology and Oceanography*, 54(5):1811–1818.

von Wachenfeldt, E. and Tranvik, L. J. (2008). Sedimentation in boreal lakes—

The role of flocculation of allochthonous dissolved organic matter in the water column. *Ecosystems*, 11(5):803–814.

Vuorenmaa, J., Salonen, K., Arvola, L., Mannio, J., Rask, M., and Horppila, P. (2014). Water quality of a small headwater lake reflects long-term variations in deposition, climate and in-lake processes. *Boreal Environment Research*, 19(suppl. A):47–65.

Wang, B., Ma, Y., Chen, X., Ma, W., Su, Z., and Menenti, M. (2015). Observation and simulation of lake-air heat and water transfer processes in a high-altitude shallow lake on the Tibetan Plateau. *Journal of Geophysical Research: Atmospheres*, 120(24):12327–12344.

Wanninkhof, R. (1992). Relationship between wind speed and gas exchange over the ocean. *Journal of Geophysical Research: Oceans*, 97(C5):7373–7382.

Wanninkhof, R. and Knox, M. (1996). Chemical enhancement of CO_2 exchange in natural waters. *Limnology and Oceanography*, 41(4):689–697.

Watanabe, M., Suzuki, T., O'ishi, R., Komuro, Y., Watanabe, S., Emori, S., Takemura, T., Chikira, M., Ogura, T., Sekiguchi, M., Takata, K., Yamazaki, D., Yokohata, T., Nozawa, T., Hasumi, H., Tatebe, H., and Kimoto, M. (2010). Improved climate simulation by MIROC5: Mean states, variability, and climate sensitivity. *Journal of Climate*, 23(23):6312–6335.

Weiss, R. (1970). The solubility of nitrogen, oxygen and argon in water and seawater. *Deep Sea Research and Oceanographic Abstracts*, 17(4):721–735.

Weiss, R. (1974). Carbon dioxide in water and seawater: The solubility of a non-ideal gas. *Marine Chemistry*, 2(3):203–215.

Wetzel, R. G. (2001). *Limnology: Lake and River Ecosystems, 3rd ed.* Academic Press, San Diego, Ca.

Weyhenmeyer, G. A., Kortelainen, P., Sobek, S., Müller, R., and Rantakari, M. (2012). Carbon dioxide in boreal surface waters: A comparison of lakes and streams. *Ecosystems*, 15(8):1295–1307.

Weyhenmeyer, G. A., Kosten, S., Wallin, M. B., Tranvik, L. J., Jeppesen, E., and Roland, F. (2015). Significant fraction of CO_2 emissions from boreal lakes derived from hydrologic inorganic carbon inputs. *Nature Geoscience*, 8(12):933–936.

Wilson, D., Hisdal, H., and Lawrence, D. (2010). Has streamflow changed in the Nordic countries? – Recent trends and comparisons to hydrological projections. *Journal of Hydrology*, 394(3–4):334–346.

Wohlfahrt, G. and Gu, L. (2015). The many meanings of gross photosynthesis and their implication for photosynthesis research from leaf to globe. *Plant, Cell & Environment*, 38(12):2500–2507.

Woo, M.-K., Thorne, R., Szeto, K., and Yang, D. (2008). Streamflow hydrology in the boreal region under the influences of climate and human interference. *Philosophical Transactions of the Royal Society B: Biological Sciences*, 363(1501):2251–2260.

Zappa, C. J., McGillis, W. R., Raymond, P. A., Edson, J. B., Hintsa, E. J., Zemmelink, H. J., Dacey, J. W. H., and Ho, D. T. (2007). Environmental turbulent mixing controls on air-water gas exchange in marine and aquatic systems. *Geophysical Research Letters*, 34(10):L10601.